Feed-forward excitation of interneurons in the cerebellar granule cell layer

Roby Thomas Kanichay

Department of Neuroscience, Physiology and Pharmacology

UCL

April 2008

This is a thesis submitted to the University of London in the Faculty of Life Sciences for the degree of Doctor of Philosophy. I confirm that the work presented is my own. Where information has been derived from other sources it has been indicated.

ProQuest LLC
789 East Eisenhower Parkway
P.O. Box 1346
Ann Arbor, MI 48106-1346

Abstract

The cerebellum is involved in maintenance of posture and balance and coordination of voluntary movements. It has previously been shown that the inhibition of granule cells by Golgi cells, in the input layer of the cerebellar cortex, is important for normal cerebellar function. However, little is known about what determines the firing of spontaneously active Golgi cells and how intrinsic activity interacts with sensory input. In particular, the excitation of the interneuron by mossy fibres, which may mediate feed-forward inhibition of granule cells, has not been characterized.

I have used immuno-histochemistry, patch-clamp recordings and imaging in acute cerebellar slices of rats to study feed-forward mossy fibre input onto Golgi cells and its downstream effects. I confirm that mossy fibres, Golgi cells and granule cells form a functional feed-forward inhibitory circuit. Anatomical analysis of the circuitry suggests that only spatially correlated inputs result in feed-forward inhibition. Activation of the pathway required synchronous activity in 4 out of the approximately 10 mossy fibres contacting a Golgi cell. These inputs can reset the timing of spontaneous Golgi cell firing with remarkably high temporal precision. I found that an interaction between fast EPSC kinetics, electronic compactness and pacemaker conductances allowed precise temporal signaling while integrating only 6 quanta across the dendritic tree of a Golgi cell. Golgi cell mean firing rate was only weakly modulated by mossy fibre input due to dominant pacemaker conductances. These results suggest that the properties of

the feed-forward mossy fibre – Golgi cell – granule cell pathway are tuned to detect and signal coincident synaptic activity with high temporal precision. This provides a likely synaptic basis for precisely timed Golgi cell responses observed *in vivo*, which may signal the onset of sensory stimulation producing spatiotemporally correlated mossy fibre activity. These findings are discussed in the context of current models of granule cell layer processing.

Table of Content

List of Figures

List of Tables

Abbrevations

AMPA = Alpha-amino-3-hydroxy-5-methyl-4-isoxazolepropionic acid

CCD = Charge-coupled device

C_m = Membrane capacitance

CV = Coefficient of variation

DIC = Differential interference contrast

EPSC = Excitatory postsynaptic current

EPSG = Excitatory postsynaptic conductance

EPSP = Excitatory postsynaptic potential

GABA = γ-aminobutyric acid

IPSC = Inhibitory postsynaptic current

IPSG = Inhibitory postsynaptic conductance

LCA = Loose-cell attached

NGS = Neonatal goat serum

NMDA = *N*-methyl-$_D$-aspartic acid

PB = Phosphate-buffer

Q = Quantal size

R_M = Input resistance

Rpm = Rounds per minute

SD = Standard deviation

TBS = Tri-hydroxymethylaminomethane (TRIS) – buffered saline

vGlut1 = Vesicular glutamate transporter-1

V_m = Membrane potential

Acknowledgments

"A searcher requires the virtues of a scholar, teacher and explorer in equal measures to obtain a rare glimpse at the beauty of truth." Sri Aurobindo

First and foremost I would like to thank Prof. Angus Silver for the commitment, patience and ingenuity he showed throughout my PhD training. Working with Angus allowed me to experience what I believe is essential to scientific endeavor: The need to understand an issue in its entirety, the courage and skill to realize innovative ideas and openness to criticism. His relentless sharp eye for detail and consistency often enough caused me embarrassment, but "cutting the rank growth promotes development" Khalid Gibran. Angus's fun and fascination for neuroscience, his generosity and drive were inspiring and motivating. For this I want to express my deep gratitude.

Through my work in Angus' lab I also assimilated some knowledge of neuroscience, in particular synaptic physiology, neuronal signal processing, electrophysiology, cellular imaging and computational modeling. This was helped by the Single Ion Channel Analysis Course (2004) lectured by David Colquhoun, The Plymouth Course in Advanced Optical Imaging (2004) run by Brad Amos and the FIAS Summer School of Computational Neuroscience (2006) in Frankfurt organized by Juergen Triesch and Wolf Singer.

The work on this thesis was greatly facilitated by practical advice from and discussions with my coworkers who taught me about computational modeling and quantitative data analysis (Volker Steuber, Ingo Kleppe), slice electrophysiology (David DiGregorio and Chiara Saviane) and optics (Tomas Fernandez, Paul Kirby and Srinivas Nadella). Particular credit is due to Jason Rothmann for his help on data analysis and programming in Neuromatic, which saved me months of manual data analysis and Zoltan Nusser, who taught me the basics of immuno-histochemistry. Izumi Harako and the members of the Physiology Staff have been very helpful in my scientific endeavors in administrative and practical matters. Daniel Ward, Padraig Gleeson, Federico Minneci and Koen Vervaeke I want to thank for useful comments on this manuscript.

I would also like to thank my second supervisor Trevor Smart for his support and advice throughout my Ph.D. and my examiners Ole Paulsen and Mark Farrant for their kindness to read and scrutinize my thesis.

I am indebted to the Wellcome Trust and Prof. David Attwell for giving me the opportunity to do my Ph.D. at UCL - a stimulating place with a great tradition to do biophysical neuroscience.

I owe much to my fellow Wellcomes - Velia, Izumi, Benedetto, Alex – for making my time in London so enjoyable. My girlfriend Elvira and my family, I want to thank for continued and generous support giving me the drive and energy to pursue my career and scientific interests.

Chapter One

1 General Introduction

1.1 The brain and network dynamics

The main task of the brain is to integrate sensory information about the environment and body to produce an output that leads to a behavioural response. It achieves this by the concerted computations of functionally specialized brain areas. Computations are thought to be embedded in the dynamics of neural networks in these specialized areas and are shaped by the anatomical, synaptic and cellular properties of the network. Hence a fundamental step towards understanding the brain is to understand the dynamics of neural networks, their origins and purpose. Recent work on cortical signal processing *in vivo* has shown that activity intrinsic to neural networks is essential to sensory perception since it powerfully modulates stimulus evoked activity (Arieli *et al.*, 1996; Tsodyks *et al.*, 1999; Kenet *et al.*, 2003). Sensory stimulation of the visual cortex with natural scenes, for example, only produced a 20% increase in the overall network activity from spontaneous levels (Petersen *et al.*, 2003; Fiser *et al.*, 2004). In this case, information processing seems to be largely based on small changes in network dynamics. But the interaction of intrinsic activity and stimulus evoked activity is poorly understood. However, it is clear that interneurons, neurons with a locally projecting, typically inhibitory output, play a pivotal role in shaping the intrinsic and stimulus evoked activity and thus the dynamics in a neuronal network.

1.2 Roles of interneurons in neuronal computations

GABA receptors and control of neural excitability

The large neurochemical and anatomical diversity of inhibitory interneurons reflects the wide range of functional roles they play in network computations. Inhibitory interneurons typically release γ-aminobutyric acid (GABA), which is the main inhibitory neurotransmitter in the central nervous system, or glycine – the main inhibitory neurotransmitter in the peripheral nervous system, onto postsynaptic targets. GABA activates ionotropic $GABA_A$ or metabotropic $GABA_B$ receptors whereas glycine activates ionotropic glycine receptors. $GABA_B$ receptors are G-Protein coupled receptors, which upon activation initiate an intracellular signal cascade that can lead to the modulation of e.g. calcium and potassium channels (for review see Emson, 2007). $GABA_A$ and glycine receptors preferentially conduct chloride ions upon activation[1]. The subunit composition of the ligand-gated channel[2] determines ligand affinity, single channel opening time and frequency and channel conductance and thus amplitude and kinetics of the macroscopic current. In mammals 19 genes express protein isoforms which can assemble to pentameric $GABA_A$ receptors (Korpi & Sinkkonen, 2006). This gives rise to a vast number of subunit compositions with different kinetics and conductance (Mody & Pearce, 2004; Korpi & Sinkkonen, 2006). The direction of the evoked chloride flux is determined by the driving force for chloride ions, which results from the difference in chloride equilibrium potential and the membrane potential. Since both parameters can change, for example during

[1] and HCO_3^- to a lesser extent ($V_{reversal}$ = +20mV).
[2] $GABA_A$ and glycine receptors belong, along with ionotropic acetylcholine and serotonin receptors, to the group of structurally related pentameric cysteine-loop receptors.

development (Ben-Ari, 2002), activation of $GABA_A$ receptors in early development has a depolarising effect (membrane potential < chloride reversal potential), whereas in adulthood GABA and glycine usually mediate hyperpolarising (membrane potential > chloride reversal potential) and shunting inhibition (membrane potential = chloride reversal potential). When the GABA reversal potential is positive to the membrane potential GABA release from interneurons can act to enhance and synchronize the firing of target cells (Marty & Llano, 2005; Vida *et al.*, 2006). When GABA acts by hyperpolarizing or shunting it generally reduces firing but also can entrain action potentials (Lytton & Sejnowski, 1991; Cobb *et al.*, 1995; Bartos *et al.*, 2001) and shape the time window for spike generation and coincidence detection (Pouille & Scanziani, 2004). The GABA-induced hyperpolarisation may also interact with intrinsic voltage-gated channels, such as HCN channels mediating hyperpolarisation-activated depolarization. Such interactions result in "rebound" depolarization, which can influence and control target cell spiking (Llinas & Muhlethaler, 1988; Cobb *et al.*, 1995). So the balance and timing of excitation and inhibition is clearly important in determining the input-output relationship of a single cell, and in consequence of the network. In the following sections I will give some examples demonstrating the different functional roles interneurons can fulfill based on their varied molecular, anatomical and electrophysiological properties.

Feed-forward inhibition

The effect of inhibitory interneurons on their target cells depends on their exact wiring. In the case of feed-forward inhibition, interneuron and target cell receive the same excitatory input, thus the target cell receives inhibition depending on its

excitatory drive. Pouille and Scanziani demonstrated elegantly how anatomical, cellular and synaptic properties contribute to a feed-forward inhibitory network that can control spike timing of hippocampal pyramidal cell (Pouille & Scanziani, 2001; Jonas *et al.*, 2004). Firstly, the integrative properties of basket cells, with rapid membrane time constant and ionotropic glutamate receptors with fast kinetics are tuned to detect coincident activity in the excitatory synaptic input. Secondly, excitatory synapses onto basket cells typically depress (Losonczy *et al.*, 2002). Thus only the onset of a stimulus train is reliably transmitted across the synaptic connection. Thirdly, basket cells innervate pyramidal cells (peri-) somatically and activation of (peri-) somatic GABA receptors leads to a large, fast rising and decaying inhibitory conductance in pyramidal cells, thereby powerfully controlling excitatory drive. Together these synaptic, cellular and anatomical properties result in a reduction of the integration time window of pyramidal cells on the onset of a stimulus train, so that pyramidal cell spike timing precision is enhanced.

Lateral inhibition

Lateral inhibition, also called surround inhibition, is a special form of feed-forward inhibition in that the interneuron does not inhibit target neurons receiving the same input but adjacent neurons receiving similar input. In the somatosensory cortex of mammals, for example, some cortical pyramidal cells respond to the tactile stimulation of a particular body region - their receptive field - with an increase in firing rate. Pyramidal cells are organized in a somatosensory map, i.e. neighbouring patches in the somatosensory cortex are responsive to neighbouring patches of skin. Firing of a neuron within that map

gives information on the location of a tactile stimulus. But receptive fields of touch sensitive neurons overlap, which makes stimulus localization ambiguous. Inhibitory interneurons which also receive excitation upon tactile stimulation cause inhibition in neighbouring pyramidal cells proportional to the excitatory drive they receive. This way, only pyramidal cells with the strongest excitation, the ones where the stimulus is in the centre of their receptive field, can increase their firing. As a result lateral inhibition shapes the receptive field properties of neurons to increase the resolution of tactile perception (Mountcastle & Powell, 1959a, 1959b; Nicholls, 2001). Such sharpening of receptive field properties via lateral inhibition also occurs in visual processing in the retina to enhance the contrast of edges in an image and in auditory processing to narrow the frequency tuning curve of sound sensitive neurons (Arthur *et al.*, 1971; Nicholls, 2001).

A specialized form of lateral inhibition is reciprocal inhibition employed in muscular control. Coordinated movement requires an ensemble of muscles to act in an orchestrated fashion. To bend ones elbow joint, for example, the flexion of the biceps (agonist) muscle and relaxation of the triceps (antagonist) muscle has to be coordinated (see **Figure 1-1a**). Both muscles are innervated by different motoneurons originating in the spinal cord which in turn are excited by neurons originating in higher processing areas in the brain stem (descending pathway). The action of motoneurons is controlled and coordinated by glycinergic inhibition mediated by interneurons in the spinal cord.

Eccles and coworkers, facilitated by the advancement of electrophysiological and anatomical techniques, elucidated the mechanisms underlying motoneuron

control through interneurons in the 1940s. Group Ia interneurons, for example, receive excitatory input via the descending pathway and project their inhibitory output on the motoneuron innervating the antagonistic muscle (**Figure 1-1a**). Therefore excitation and subsequent flexion of the agonist leads to reciprocal inhibition and thus relaxation of the antagonist.

Feedback inhibition

The term feedback inhibition is used when an interneuron is inhibiting cells it receives input from. Eccles and coworkers demonstrated the benefit of feed-forward inhibition in the spinal cord preparation. Motoneurons not only innervate their respective muscles but also inhibitory interneurons called Renshaw cells (see **Figure 1-1a**). Renshaw cells provide continuous glycinergic inhibition to the motoneurons they receive excitation from. This inhibition is modulated by Renshaw cell firing which, in turn, is dependent on the excitatory drive from motoneurons. Effectively the circuitry dampens the firing of motoneurons and prevents large increases or drops in motoneuron firing rate. This way, sudden jerks are avoided and movements are executed smoothly. The action of Renshaw cells can be modulated by descending pathways to confer flexibility to this mechanism.

Pouille and Scanziani (2004) have demonstrated how feedback inhibition controls pyramidal cell firing rate in the hippocampus. Again, synaptic, cellular and anatomical properties of interneurons mediating feedback inhibition were well suited for such a function. Interneurons innervating the dendritic compartment of pyramidal cells received slow, small amplitude excitation from

the same pyramidal cells they innervated. Summation of excitatory postsynaptic potentials (EPSPs) was required to drive the interneuron membrane potential beyond threshold. Interneuron firing activated GABA receptors with slow kinetics, so that dendritic integration of pyramidal cell inputs could be regulated based on the overall network output.

Role of interneurons in network oscillations and spike synchronization

Evidence for synchronization of neuronal firing and resulting oscillations is found in the brain on multiple levels. Electroencephalogram (EEG) oscillations are believed to show the concerted action of several functionally specialized areas of the brain. Oscillations are also found in recordings with local field potential electrodes in a particular brain structure indicating synchronized firing of local populations of neurons. On a single cell level sub-threshold oscillations have been observed in the inferior olive (Llinas & Yarom, 1986), the olfactory bulb (Desmaisons *et al.*, 1999), neocortical and hippocampal neurons (Alonso & Llinas, 1989; Dickson *et al.*, 2000). Oscillations and the associated synchronized neuronal activities across brain areas, within a neuronal network or on a single cell level are thought to be essential for brain function as they may play a role in perceptual binding of stimulus features (Gray *et al.*, 1989) and neural coding strategies (O'Keefe & Recce, 1993; Hopfield, 1995). In support of this, network oscillations vary with the behavioral state of the animal and abnormalities in the oscillatory EEG pattern occur in patients with neurological diseases like schizophrenia, autism and Parkinson's disease (Uhlhaas & Singer, 2006). This is

particularly obvious in the case of epilepsy which is characterized by excessive neuronal synchronization.

Synchronized activity and oscillations are generated by the action of networks of various GABAergic interneurons. This has been particularly well elucidated in the hippocampus where the synaptic, cellular and anatomical properties of interneurons and the resulting firing patterns are well correlated with certain frequency bands of hippocampal network oscillations (for review see (Somogyi & Klausberger, 2005; Mann & Paulsen, 2007). For example, the hippocampal theta-rhythm in the CA1 region is generated by the concerted action of interneurons of the axo-axonic type, parvalbumin-positive basket cells and bistratified cells releasing GABA to synchronize pyramidal cell firing. Parvalbumin-positive basket cells are electronically coupled via gap-junctions and form autapses which ensure spiking precision and synchronization (Cobb *et al.*, 1997; Tamas *et al.*, 2000). They make synapses on the perisomatic compartment of many pyramidal cells and fire together with axo-axonic interneurons, which contact the initial segment of pyramidal cells, on the peak or descending phase of the theta-oscillation (**Figure 1-1b**). This will powerfully reduce pyramidal cell excitability and synchronize subsequent pyramidal population firing (Cobb *et al.*, 1997). The inhibitory action of parvalbumin-positive basket cells is temporally limited by the firing of bistratified interneurons which inhibit basket cells at the trough of the theta-rhythm leading to disinhibition of pyramidal cells (**Figure 1-1b**). Thus the concerted action of three interneuron types, with specialized synaptic, cellular and anatomical properties creates and controls the network dynamics of pyramidal cells in the

hippocampus.[3] Local connectivity of the network and the synaptic and cellular properties of participating interneurons confer the ability to generate oscillatory behaviour in neuronal networks of various frequencies from 5-10 (theta- rhythm) to 200 Hz (fast ripples). The functional importance of such dynamics has been highlighted by O'Keefe, McNaughton, Buzsaki and colleagues. Their *in vivo* recordings of hippocampal pyramidal cells (place cells) in freely moving rats showed that the phase relationship of place cell firing to the underlying theta-oscillation can predict the position of the animal in the place field (O'Keefe & Recce, 1993).

[3] Other interneuron cell types participating in the generation of network oscillation are left out for simplification

Figure 1-1 Role of interneurons in neural networks *a)* Feed-forward and feedback inhibition of motoneurons in the spinal cord: Illustrated is a horizontal cut through spinal cord with corticospinal afferents (descending pathways) and efferents to skeletal muscles. Neurons and fibres in black are inhibitory; those in white excitatory. Motoneurons excite flexor and extensor muscles which evokes flexion. Motoneurons are excited by corticospinal afferents and inhibited by interneurons (Ia inhibitory interneuron and Renshaw cell). Ia inhibitory interneurons receive excitation from corticospinal afferents, which innervate the antagonistic motoneurons, whereas Renshaw cells receive excitation from agonistic motoneurons. Thereby the circuitry allows for lateral feed-forward and feedback inhibition of motoneurons via Ia inhibitory and Renshaw interneurons, respectively. Both inhibitory pathways can be controlled by descending inputs modulating interneuron excitability (adapted from Kandel; 2000). *b)* Contribution of interneurons to generation of network oscillations. Relationship between local field potential oscillation in the theta-frequency range (first trace,

top panel) with firing pattern of parvalbumin positive (PV+) basket cell (second trace, top panel). Same for axo-axonic cell (middle panels) and bistratified cell (bottom panels). Scales: 0.2 mV, 0.3 s (taken from Somogyi & Klausberger; 2005)

1.3 Why study the cerebellum?

The cerebellar network is in several ways an excellent model system to study the general operating principles of the brain. It has a relatively simple anatomy with defined cell types, which offers the opportunity to perform targeted cell type specific genetic manipulations (Watanabe *et al.*, 1998; Hansel *et al.*, 2001; Wada *et al.*, 2007; Wulff *et al.*, 2007) and test the function of different network components in cerebellar processing. Cerebellar processing capabilities can be accessed quantitatively through cerebellum-dependent behavioural paradigms like pavlovian eye-blink conditioning, vestibular-ocular reflex adaptation or rotorod performance. Consequently the cerebellum is an ideal preparation to study to role of interneurons in network computations.

Macroscopically, the cerebellum is part of the hindbrain, located dorso-caudal to the brain stem (**Figure 1-2a**). The cerebellar surface shows parallel transverse convolutions (lobes and lobules) that are separated by fissures. The primary fissure divides anterior from posterior lobe and the posterior fissure separates the flocculonodular lobe (**Figure 1-2b**), the lobes are subdivided to 10 lobules. In a sagittal section (**Figure 1-2c**) lobes and lobules appear like branches arising from common trunk of white matter. Each white matter branch gives rise to an easily discernable structure containing granule cell and molecular layer, termed "folium". Folia run in the parallel transverse axis to give rise to the convoluted structure of the cerebellum. In the longitudinal or sagittal axis the cerebellum can be divided into vermis, the central part, left and right hemisphere and, most laterally, the paraflocculi (**Figure 1-2a**). Santiago Ramon y Cajal and Camillo Golgi were the first to use the Golgi stain method to study the cerebellar anatomy

in detail. These studies marked the beginning of modern neuroscience. They described a layered anatomy with easily distinguishable cell types. The cerebellar cortex consists of four layers: (1) the white matter tract composed mainly of myelinated axon fibres transporting the input and output of the cortex (2) the granule cell layer, which can be considered the input layer of the cortex containing an abundant number of granule cells (3) the Purkinje cell layer and (4) the molecular layer which comprises parallel fibres (bifurcating granule cell axons) and molecular layer interneurons.

As shown in **Figure 1-3a** the cerebellum receives somatosensory information via mossy fibres which originate from various extracerebellar sources (e.g. different brainstem nuclei conveying spinal cord, neocortical and vestibular information) and reach the cerebellum via cerebellar peduncles. They contribute approximately 2/3 of the fibres in the white matter tract (Palkovits *et al.*, 1972). Mossy fibres synapse onto granule cells within the granule cell layer. Granule cells transform the information carried by mossy fibres and relay it via parallel fibres onto Purkinje cells. For this signal transformation the inhibition of granule cells by Golgi is thought to be important (Marr, 1969; Albus, 1971; Watanabe *et al.*, 1998). Purkinje cells integrate parallel fibre input with a second sensory input carried by climbing fibres to produce the sole output of the cerebellar cortex. Purkinje cell axons project through the white matter tract and cerebellar peduncles onto deep cerebellar nuclei cells, which in turn project to various extracerebellar brain regions, particularly centres of motor control in the brain stem.

Lesion studies have shown that the cerebellum is involved in motor coordination and maintenance of posture and balance (Fluorens 1824 in Palay & Chan-Palay, 1974). However, the cerebellum is not an initiator or activator of movement, but modulates motor commands. Its purpose is to combine information on the environment and body position from sensory receptors with a desired motor output to modulate a command signal to deal with environmental variability and make movements smooth and accurate. In agreement with this notion impairment of cerebellar function in humans, e.g. through stroke or encephalitis causes ataxia with symptoms of disturbed stance, ataxic gait, kinetic tremors, dizziness and double vision. Recent work also implicates the cerebellum in several cognitive tasks and cerebellar disorders have been associated with schizophrenia and autism (Ito, 2006). The computational task the cerebellum performs requires the accurate prediction of an outcome in time and space and is comparable to challenges for multivariable control system in modern control theory.

Already Cajal and Golgi suggested that the cerebellum is built from a repetitive arrangement of a basic microcircuit, a microcomplex involving mossy fibres, granule and Golgi cells, Purkinje cells, molecular layer interneurons and deep cerebellar nuclei neurons. This suggests that the cerebellum is executing a single characteristic computation that can be deployed to address a variety of behavioural tasks due to differences in downstream targets and nature of inputs (Medina & Mauk, 2000). Jansen and Brodal (1962) discovered that efferents of cerebellar sagittal patches are connected to distinct parts of deep cerebellar nuclei controlling different body movements, thereby dividing the cerebellum into functional sagittal subdivisions. The hope is that by elucidating the anatomical,

synaptic and cellular properties of this relatively simple microcircuit we can understand its operating principles and extrapolate them to the entire cerebellum.

Figure 1-2 The structure of the brain with cerebellum *a)* Top view (left) onto a rat brain with olfactory bulb, neocortex, cerebellum and spinal cord clearly visible. The cerebellum can be divided into v = vermis, h = hemispheres, p = paraflocculus in the sagittal plane. In the bottom view (right) the p = paraflocculi are clearly discernible. Inset: side view onto cerebellum with brain stem and spinal cord (rest of brain is removed). Paraflocculus and hemispheres are visible (taken from Palay & Chan-Palay 1974). *b)* Lobular structure of the cerebellum: The cerebellum is a curved and folded structure. Unfolding the cerebellum reveals distinct lobes separated by fissures. Anterior lobe and posterior lobe are separated by primary fissure and floccunodular lobe is separated by the posterior fissure. Uvula and Culmen are posterior and anterior parts of the vermis, respectively (adapted from http://en.wikipedia.org/wiki/Cerebellum). *c)* Toluidine blue epoxy staining of a sagittal slice of vermal rat cerebellum. Tissue with most intense staining is white matter, followed by the granule cell layer. The molecular layer is stained least (taken from Palay & Chan-Palay 1974).

Figure 1-3 The cerebellar circuitry *a)* Schematic drawing of a simplified cerebellar circuitry in the sagittal and transverse perspective: On the left the boundaries and layers of the cerebellar cortex are indicated: Pia, mol = molecular layer, PC = Purkinje cell layer, gr = granule cell layer, wm = white matter. Granule cells have ascending axons which bifurcate like a "T" to form parallel fibres in the transverse axis. PCs with their planar sagittal dendritic tree in the molecular layer are inhibited by molecular layer interneurons (B = basket and S = stellate cells, also with planar sagittal dendritic tree). Lugaro cells, located below the Purkinje cell layer, have long dendrites in the transverse axis. Golgi cells (GC), interneurons in the granule cell layer have basolateral dendrites within the granule cell layer and ascending dendrites in the molecular layer and innervate granule cells. The afferent MF = mossy fibre and CF = climbing fibre inputs (in red) enter the cerebellar cortex to synapse onto granule and Golgi cells and Purkinje cells, respectively. They also project to neurons in deep cerebellar nuclei. Taken from Palay & Chan-Palay 1974. *bi)* Drawing of granule cell layer circuitry. Golgi cell (GoC) with basolateral and ascending dendrites has large axonal arbour and inhibits granule cells (grc in green). Granule cells each have 4 dendrites and project an axon into the molecular layer where it bifurcates to contact ascending dendrites of Golgi cells and Purkinje cells (PC). Golgi and granule cells receive input from mossy fibres (mf). Taken and modified from Eccles et al. (1967) *bii)* simplified schematic drawing of granule cell layer circuitry. Golgi cell (GoC) inhibits granule cell (grc). Both cells receive excitatory mossy fibre input (mf). This allows for feed-forward inhibition of granule cells. Granule cells excite Golgi cells via parallel fibres (pf) as part of a feedback inhibitory circuit.

1.4 Structure and properties of the granule cell layer

The granule cell layer is the input layer of the cerebellar cortex. Here somatosensory information conveyed by mossy fibres is transformed by granule cells before relayed to Purkinje cells (**Figure 1-3bi**). According to an influential theory of cerebellar processing developed by Marr (1969) and Albus (1971) the cerebellum works as a pattern discriminator and the granule cell layer performs the task of separating pattern of mossy fibre input.

Mossy fibres

To understand the signal transformations the granule cell layer performs it is useful to consider the properties of mossy fibre input into this structure. Mossy fibres represent the sole source of excitation to granule cells. They originate from several extracerebellar sources and convey, via various brain stem nuclei[4] (e.g. pons, trigeminal nucleus), somatosensory information from the spinal cord, neocortex and cranial nerves to the cerebellar cortex (and deep cerebellar nuclei). Each mossy fibre sends collaterals into several cerebellar lobules, but within a lobule it forms distinct regional ramifications of ~15-25 terminal structures which cluster in the sagittal plane (Garwicz *et al.*, 1998; Wu *et al.*, 1999). The projections occur in a way that a fractured somatotopic map arises. This means that small sagittal patches (~200 μm diameter in cat) of granule cell layer, called "microzones", receive somatosensory information of a particular body part, but neighbouring patches do not represent neighbouring body parts (**Figure 1-4a;** Shambes *et al.*, 1978). Interestingly, the somatotopic organization of the mossy

[4] An important exceptions is the primary vestibular nerve which can give rise to direct mossy fibres

fibre input is well matched by the projection pattern of climbing fibres (Garwicz *et al.*, 1998), which implies that a sagittal patch of cerebellar cortex receives climbing fibre and mossy fibre input with the similar somatotopic origin. Mossy fibres carry information on different sensory modalities like joint angle (Van Kan *et al.*, 1993), touch (Jorntell & Ekerot, 2006), whisker deflection (Chadderton *et al.*, 2004) and can be multimodal (Van Kan *et al.*, 1993; Garwicz *et al.*, 1998). They code for different features of a stimulus, for example phasic and/or tonic components of arm movement with different sensitivity and can achieve firing rates up to 700 Hz during whisker stimulation (Rancz *et al.*, 2007). Studies of mossy fibre synaptic physiology suggest that vesicular release can keep up with such high firing rates due to a large vesicle pool and rapid vesicle reloading of release sites (Saviane & Silver, 2006).

Figure 1-4 Granule cell layer input mapping *a)* Fractured somatotopic map in the cerebellar granule cell layer of lobule CrusII in cat. Extracellular recordings of granule cell activity *in vivo* in response to sensory stimulation reveal receptive fields. Different body parts are represented multiple times in various parts of the lobule (Shambes *et al.*, 1978). Illustration taken from Kandel (2000) *b)* Microscopic structure of the glomerulus: Schematic drawing of a simple glomerulus with mossy fibre terminal (blue) contacting a number of granule cell dendrites each of which has several digits (red) and a Golgi cell dendrite (green). Contacts between Golgi cell axons and granule cell dendrites (yellow) are located on the periphery of the glomerular structure which is enclosed in a glial sheet (grey). Taken from Eccles et al. (1967).

Granule cells

Cerebellar granule cells are the most numerous neuronal cell type in the brain. They make up about half of the neurons of the brain (~10^{11}) and are an ideal model system to study synaptic physiology and synaptic integration with electrophysiological methods, due to their electronic compactness (Silver *et al.*, 1992). Granule cells receive excitatory input from on average four mossy fibres (Eccles *et al.*, 1967) and inhibitory input from Golgi cells. Both synaptic connections are made within a specialised synaptic structure called the glomerulus (**Figure 1-4b**). Although the shape and size of glomerli varies greatly[5] the average diameter of a glomerulus is ~10 μm (in rat, Wu *et al.*, 1999) and the glomerular density appears uniform throughout a folium (Palkovits *et al.*, 1972). An electronmicroscopic (EM) study of glomeruli in rats showed that 34% of the glomerular volume, particularly the core, was inhabited by the mossy fibre rosette, 53% by granule cell dendrites and 13%, mostly in the periphery, was occupied by Golgi cell axons (Jakab & Hámori, 1988). A rosette, which can originate from en-passant or terminal mossy fibre structures, is contacted by 20-100 granule cell dendrites[6]. Each granule cell dendrite gave rise to around 4 dendritic protrusions, named digits that were postsynaptic targets for either synapses with the mossy fibre or contacts with Golgi cell axons[7].

[5] A coarse anatomical distinction can be made between complex and simple glomeruli; however complex structures appear to be simply a conglomerate of simple glomeruli (Hamori, 1983).
[6] Estimates in the literature vary. Fox and colleagues (1967) estimated ~20 granule dendrites contacting a glomerulus based on light microscopic studies of cat tissue. Palkovits and colleagues (1972) calculated ~100 mossy fibre-granule cell contacts in a glomerulus from mean data on the cerebellar anatomy in cat and Jakab and Hamori (1988) measured ~50 granule cell dendrites contacting a glomerulus in rat .
[7] Only 8% of digits receive both excitatory input from mossy fibres and inhibitory input from Golgi cell axons.

This arrangement results in, on average, 5 synaptic release sites from a mossy fibre onto a granule cell dendrite distributed onto its digits (Sargent *et al.*, 2005). The compactness of synaptic structure and close proximity of mossy fibre release sites onto granule cells results in the phenomenon of neurotransmitter spillover, which means that glutamate can easily diffuse to postsynaptic ionotropic glutamate receptors on neighbouring granule cell digits and give rise to spillover currents (DiGregorio *et al.*, 2002). Spillover currents prolong the decay time course and reduce the variability of currents evoked in postsynaptic cells (DiGregorio *et al.*, 2002; Sargent *et al.*, 2005). Also, glutamate spilling onto presynaptic metabotropic glutamate receptors, located presynaptically on Golgi cell axons, leads to a reduction in GABA release from these axons (Mitchell & Silver, 2000b). Spillover effects are sensitive to the glomerular morphology, and developmental changes can lead to significant alterations in the kinetics of receptor activation (Cathala *et al.*, 2005).

Glutamate released from mossy fibres onto granule cells activates AMPA and NMDA receptors. Granule cell AMPA receptor mediated currents are characterized by fast rise and decay kinetics (Silver *et al.*, 1992; Cathala *et al.*, 2003) and experience only moderate desensitization (DiGregorio *et al.*, 2007). Thus AMPA receptors can mediate fast EPSCs in response to synaptic glutamate release during high frequency transmission, while mediating a tonic current component activated by residual glutamate built-up in the synaptic cleft (Saviane & Silver, 2006, DiGregorio, 2007). These AMPA receptor properties (DiGregorio *et al.*, 2007) in combination with the vast vesicle pool, rapid vesicle reloading in the presynaptic terminal (Saviane & Silver, 2006) and the synaptic

morphology (DiGregorio *et al.*, 2002; Nielsen *et al.*, 2004; Cathala *et al.*, 2005) allows the broad bandwidth transmission of rate-coded information at the mossy fibre-granule cell synapse.

NMDA receptors contribute substantially to the synaptic charge transfer in developing cerebellum due to the incorporation of the NR2B subunit in the receptor complex. But the contribution of NMDA receptors to the synaptic charge is greatly reduced in mature granule cells (Cathala *et al.*, 2003), due to a developmental switch to the NR2A and later NR2C subunit (Cathala *et al.*, 2000) and localization of receptors at extrasynaptic sites (Yamada *et al.*, 2001). However, NMDA receptors may play an important physiological role in regulating long term plasticity at the mossy fibre – granule cell synapse (D'Angelo *et al.*, 1999; Gall *et al.*, 2005). Long term potentiation (LTP) is induced by repetitive bursts of mossy fibre activity (e.g. theta burst) which activate NMDA, metabotropic glutamate receptors (mGluR) and voltage-gated Ca^{2+}-channels to elevate the intracellular calcium concentration. This increases intrinsic granule cell excitability (Armano *et al.*, 2000) and triggers the production of nitric oxide (NO), which diffuses to the presynaptic terminal to augment release probability (Maffei *et al.*, 2003). However, if synaptic stimulation is weak the lower Ca^{2+} influx leads to long term depression (Gall *et al.*, 2005).

Granule cells usually require the summation of multiple EPSPs to reach spike threshold (Gabbiani *et al.*, 1994, Cathala, 2003; D'Angelo *et al.*, 1995; Chadderton *et al.*, 2004; Jorntell & Ekerot, 2006; Rancz *et al.*, 2007) and

typically responds with a high frequency burst of action potentials to electrical stimulation of mossy fibres (Eccles *et al.*, 1967) as well as peripheral sensory stimulation (Chadderton *et al.*, 2004; Jorntell & Ekerot, 2006; Rancz *et al.*, 2007).

1.5 Interneurons of the granule cell layer

Camillo Golgi, in his first account on the cerebellar cytoarchitecture (Golgi, 1886) recognized 2 large nerve cells types within the granule cell layer. One type he described as a fusiform cell typically located below the Purkinje cell layer extending dendrites horizontally along the Purkinje cell layer. The second type was located in the granule cell layer had a polygonal soma and extended dendrites vertically into the molecular layer. Retzius named the latter cell type after their discoverer Golgi (in Palay & Chan-Palay, 1974). Cajal noted that there was some anatomical differentiation within the group of granular layer Golgi cells (Cajal, 1911). He distinguished Golgi cells (large and small) with dendrites ascending into the molecular layer and an axon spanning large parts of the granular layer from two atypical groups, globular cells with their axons projecting across the white matter tract to the opposite granule cell layer and cells with a thin axonal plexus. A differentiation based on internal cellular organelles revealed by Nissl staining also led to the classification of Golgi cells and globular cells. A classification based on anatomy, biochemical markers and physiological behaviour lead to the recognition of three interneuron types (Geurts *et al.*, 2003; Simat *et al.*, 2007). This classification gave rise to three main interneuron types in the granule cell layer (1) the most abundant interneuron the

Golgi cell, (2) the Lugaro cell and (3) the unipolar brush cell, which is almost exclusively found in the vestibular cerebellum of mammals.

Lugaro cell

More recent attempts of biochemical and anatomical cell type classification show a clear distinction between the first nerve cell type described by Camillo Golgi, later named the Lugaro cell and the second cell type, the Golgi cell. Lugaro cell somata have an elongated shape and typically lie just below the Purkinje cell layer and give rise to horizontal dendrites that extend short branches into the molecular and granular layer. Their axons are myelinated and run for long distances (>1 mm) along the parallel fibre axis. They bifurcate extensively in the molecular layer to contact basket, stellate and Golgi cell dendrites (Palay & Chan-Palay, 1974; Simat *et al.*, 2007). In some cases the axon can be traced in an almost linear trajectory to the white matter tract. Lugaro cells contain monoamine neurotransmitters, GABA and glycine and express the calcium binding protein calretinin. The importance of calretinin has been emphasized by a study showing deficits in motor coordination in mice lacking calretinin (Schiffmann *et al.*, 1999). Golgi cells do not show calretinin immunoreactivity and characteristically express the metabotropic glutamate receptor 2 (mGluR2). Recent anatomical studies have revealed cells in deeper parts of the granular layer with globular cell body and a Golgi cell-like dendritic arbourisation which project axons to contact molecular layer interneurons. These cells are also calretinin positive and named deep Lugaro cells (Laine & Axelrad, 2002; Simat *et al.*, 2007). They amount, together with classical Lugaro cells, to about 33% of granule cell layer interneurons (16 and 17% respectively). Although anatomically

and biochemically well characterized much less is known about Lugaro cell physiology and their synaptic inputs. Anatomical data suggests that Lugaro cells receive excitatory input from mossy fibres and climbing fibre collaterals (Palay & Chan-Palay, 1974) and inhibitory input from Purkinje cell collaterals. But no physiological demonstration has been published. Lugaro cells could be selectively activated by the neuromodulator serotonin in cerebellar slices (Dieudonne & Dumoulin, 2000). Serotonin application turned otherwise silent Lugaro cells into rhythmically firing cells.

Unipolar brush cell

Unipolar brush cells, discovered by Mugnaini (Mugnaini & Floris, 1994), also express calretinin and are predominantly found in the vestibular cerebellum (floccularnodular lobe) of mammals. They are excitatory interneurons typically smaller than Lugaro and Golgi cells. Unipolar brush cells extend a single dendritic brush to contact a mossy fibre rosette and form a giant glutamatergic synapse. Mossy fibre-evoked EPSCs in unipolar brush cells exhibit much slower kinetics compared to granule cell EPSCs. This is most likely due to a larger synaptic apposition and the activation of NMDA receptors (Rossi *et al.*, 1995). The slow EPSC results in a large and slowly decaying EPSP which triggers a burst of action potentials (Rossi *et al.*, 1995). The unipolar brush cell axon gives rise to several collaterals to form intrinsic glomeruli contacting granule cells and other unipolar brush cells (Dino *et al.*, 2000). Thus unipolar brush cells have been proposed to be a cellular amplifier of mossy fibre signals.

1.6 The Golgi cell

Approximately 2/3 of the interneurons of the cerebellar granule cell layer can be classified as Golgi cells. Golgi cells are characterized by a large polymorph cell body (10-30 μm in diameter), a large ascending dendritic tree, reaching into the molecular layer, and basolateral dendrites as well as a large axonal arbour restricted to the granule cell layer. This description holds true for small and large Golgi cells described by Camillo Golgi. Biochemically, Golgi cells show some diversity. Approximately 90% of them are immunopositive for mGluR2, but a small proportion stains positive for the neuropeptide somatostatin and the calcium binding protein neurogranin (Geurts *et al.*, 2003; Simat *et al.*, 2007).

Synaptic inputs to Golgi cells

Anatomical evidence suggests that Golgi cell receive excitatory input from parallel fibres, mossy fibres and climbing fibres. Inhibitory input is provided by Lugaro cells, molecular layer interneurons and Purkinje cell axon collaterals (Palay & Chan-Palay, 1974). Because fibre pathways intermingle and make unambiguous fibre stimulation difficult (Misra *et al.*, 2000), only the parallel fibre input has been characterized so far (Dieudonne, 1998). Glutamate released by parallel fibres onto Golgi cells is sensed by AMPA receptors with fast kinetics (Dieudonne, 1998), synaptic NMDA (Misra *et al.*, 2000) and kainate receptors (Bureau *et al.*, 2000). Extensive parallel fibre input also activates mGluR2 on ascending dendrites which leads to a silencing of Golgi cell firing induced by the activation of GIRK channels hyperpolarsing the cell (Watanabe *et al.*, 1998). Excitatory postsynaptic currents (EPSCs) in response to trains of parallel fibre activation facilitate, likely due to residual presynaptic calcium (Chen & Regehr,

1999). In contrast to parallel fibre-Purkinje cell transmission, Golgi cells cannot counteract post-tetanic potentiation with retrograde endocannabinoid mediated down-regulation of release probability (Beierlein *et al.*, 2007). Parallel fibre to Golgi cell transmission has a low quantal content and the presumed temporal dispersion of parallel fibre activity implies a low efficacy in driving Golgi cell firing (Dieudonne, 1998). Anatomical data suggests that Golgi cells also receive excitatory input from mossy fibres. Already Ramon y Cajal noted that Golgi cell dendrites also participate in glomerular structures. This was confirmed by EM studies demonstrating synaptic contacts between mossy fibre rosettes and Golgi cell dendrites (Hamori & Szentagothai, 1966). These synaptic connections appear infrequent and distinguish themselves structurally by postsynaptic protrusions which seem to separate the 2-4 synaptic specializations. However a electrophysiological demonstration of the synaptic input and its effect is missing. Also, controversy as to whether mossy fibres synapse onto Golgi cell descending dendrites (Hamori & Szentagothai, 1966) or onto the soma (Palay & Chan-Palay, 1974) and about the number of connections remains. Climbing fibre collaterals synapsing onto Golgi cell somata are thought to be a third excitatory input. But little electrophysiological and anatomical evidence exists, maybe due to the scarceness of climbing fibre collaterals (Palay & Chan-Palay, 1974; Ekerot & Jorntell, 2001). Golgi cell ascending dendrites receive GABAergic and glycinergic inhibitory input from molecular layer interneurons and Lugaro cells, respectively[8]. Serotonin application, preferentially activating Lugaro cells, did not change spontaneous Golgi cell firing rate in parasagittal slices suggesting that the effect of individual Lugaro cells is small (Dieudonne & Dumoulin, 2000).

[8] In fact, Lugaro cells corelease GABA and glycine onto Golgi cells (Dumoulin et al. 2001).

But due to their large axonal arbourization it is possible that several Lugaro cell axons converge onto a Golgi cell to synchronize interneuron firing along a parallel fibre beam. An inhibitory synapse by Purkinje cell collaterals to Golgi cells has been proposed (Palay & Chan-Palay, 1974) but is questionable (Larramendi & Lemkey-Johnston, 1970).

Golgi cell inhibition of granule cells

Golgi cells provide the sole source of inhibition for granule cells. The Golgi cell axon bifurcates extensively and covers a large volume within the granule cell layer. It makes inhibitory synapses onto granule cell and unipolar brush cell dendritic digits within glomeruli. EM data suggests that only approximately 60% of granule cell dendrites receive inhibitory input (Jakab & Hámori, 1988). Within a glomerulus there were about 20 Golgi cell axon varicosities, each of which made 4-5 anatomically identified synaptic specialization onto a digit. Whether the inhibitory synapses are formed by one or multiple Golgi cell axons is unknown. It is assumed that a Golgi cell inhibits over 5000 granule cells within its axonal arbour (Tyrrell & Willshaw, 1992). GABA and glycine are co-released onto postsynaptic targets, but since granule cells express GABA receptors and unipolar brush cells glycine receptors the action of respective neurotransmitters is selective (Dugue *et al.*, 2005). GABAergic inhibition of granule cells takes two forms. (1) Tonic inhibition mediated by α_6 and δ-subunit containing high affinity extrasynaptic $GABA_A$ receptors (Brickley *et al.*, 1996; Nusser *et al.*, 1998) activated by ambient GABA (2) action potential-dependent phasic inhibition mediated by synaptic $GABA_A$ receptors containing the γ_2-subunit. The chloride reversal potential in young rats (P7) is -25mV which makes the action of

GABA depolarizing from a resting membrane potential of -55mV (Brickley *et al.*, 1996). At P21 the reversal potential and the resting membrane potential have shifted to -63mV and -71mV, respectively (Brickley *et al.*, 1996) which makes $GABA_A$ receptor mediated inhibition shunting. Action potential-dependent inhibition also has a spillover component which adds to tonic inhibition in young (Rossi & Hamann, 1998) and adult rats (Carta *et al.*, 2004). A developmental switch occurs from pure phasic inhibition at juvenile age (P7 rats, (Wall & Usowicz, 1997) to a dominant tonic inhibition at P21. At older ages the tonic component carries 99% of the total inhibitory charge at rest (Brickley *et al.*, 1996). The inhibition is partially maintained by action potential-independent GABA release and can be modulated by GABA transporters and neuromodulators – most prominently acetylcholine, which induces vesicular GABA release via activation of nicotinic receptors (Rossi *et al.*, 2003). Tonic inhibition decreases granule cell excitability (Brickley *et al.*, 1996; Rossi & Hamann, 1998) and has been implicated in gain control of granule cells (Marr, 1969; Tyrrell & Willshaw, 1992; Mitchell & Silver, 2003). α_6-knockout mice have disrupted tonic inhibition and compensate this with an up-regulation of leak potassium channels to reduce granule cell excitability (Brickley *et al.*, 2001). In agreement with the importance of tonic inhibition for cerebellar function, α_6 subunit-containing GABA receptors in granule cells seem to be the molecular target for alcohol induced motor impairment (Carta *et al.*, 2004; Hanchar *et al.*, 2005). A single nucleotide mutation in the gene coding for the α_6-subunit appears to increase the sensitivity of $\alpha_6\beta_3\delta$ receptors in granule cells to ethanol. The potentiation makes rats with this mutation more prone to alcohol induced motor deficits (Hanchar *et al.*, 2005). But these findings have subsequently been

challenged (Botta *et al.*, 2007). Watanabe et al. (1998) showed that pharmacological ablation of Golgi cell led to severe motor deficits followed by a partial recovery due to a developmental down-regulation of NMDA receptors in granule cells to reduce excitability and presumably offset the effects of reduced tonic inhibition. But the recovery was only partial and deficits prevailed for sophisticated motor tasks suggesting that phasic inhibition is also important in granule cell layer processing.

The glomerular architecture also allows GABA released from Golgi cell axons to spill over onto presynaptic metabotropic $GABA_B$ receptors on mossy fibres. $GABA_B$ receptor activation leads to a reduction in the mossy fibre release probability (Mitchell & Silver, 2000a).

Golgi cell firing behaviour in vivo

Single unit recordings from Golgi cells in rats, cats and monkeys show that Golgi cells are spontaneously firing with varying regularity (Edgley & Lidierth, 1987; Van Kan *et al.*, 1993; Vos *et al.*, 1999b). The interneuron responds in several ways to sensory stimulation in its receptive field. The majority of cells in anesthetized rats exhibit a suppression of spontaneous activity in response to tactile stimulation of a very large, often bilateral receptive field (Holtzman *et al.*, 2006). This depression lasted for hundreds of milliseconds and, in a subset of cells, was preceded by a sharp increase in instantaneous firing rate (Holtzman *et al.*, 2006). This short latency response could have multiple peaks in the peri-stimulus time histogram and varied considerably depending on the stimulus location. The increase in instantaneous firing rate was not dependent on the

stimulus amplitude and over larger time scales (hundreds of milliseconds) the mean Golgi firing rate was only weakly modulated (De Schutter *et al.*, 2000). *In vivo* measurements performed by Vos et al. (1999) in anesthetized rats indicated that short latency responses occur to a more restricted receptive field compared to the long lasting depression and that the earliest response occurring with sub-millisecond spike precision has the narrowest receptive field. Based on the combined *in vivo* data it has been proposed that the multiple peaks in the peri-stimulus time histogram occurring at (1) 2-4 ms, (2) 7-11 ms and (3) 12-20 ms are due to spinocerebellar mossy fibres, parallel fibres and cerebrocerebellar mossy fibres, respectively (De Schutter *et al.*, 2000). But this remains speculative. It is noteworthy that the pronounced silent period after the short latency response observed in rodent Golgi cells is not observed in cats (Edgley & Lidierth, 1987) or monkeys (Van Kan *et al.*, 1993), which might be because these studies were performed in awake behaving animals. Contrary to tactile stimulation of face (trigeminal input) and forelimbs, vestibular input and joint displacement induces a slow modulation of tonic Golgi cells firing rate (Edgley & Lidierth, 1987; Van Kan *et al.*, 1993; Barmack & Yakhnitsa, 2008). In conclusion, Golgi cell firing behaviour *in vivo* is variable and strongly depends on the stimulus paradigm used and the receptive field stimulated.

Elucidating the role of Golgi cells in granule cell layer processing

In an influential theory on cerebellar processing Marr (1969) proposed that the cerebellar cortex works as a pattern recognition device in which the granule cell layer performs an input transformation that increases pattern separability and

prevents over-excitation of the network. In this model parallel fibre input provides Golgi cells with slow global sampling of the network activity whereas mossy fibre input provides local fast sampling of the feed-forward excitation. This allows Golgi cells to set granule cell gain according to predicted and current network activity. But *in vivo* data suggests that Golgi cells are a bad predictor of mean input drive and Golgi cell firing is not suitable for gain modulation. Consequently, new models of granule cell layer processing have been developed (Fujita, 1982; De Schutter *et al.*, 2000; Medina & Mauk, 2000; Isope *et al.*, 2002; Yamazaki & Tanaka, 2007a). However, due to the lack of experimental data on the anatomical and biophysical properties of certain aspects of the network, particularly the feed-forward excitation of Golgi cells, these models are poorly constrained and have limited predictive power. I have examined the anatomical and synaptic properties of mossy fibre input onto Golgi cells and studied how it interacts with intrinsic Golgi cell activity to produce inhibition relevant to granule cell processing. I will discuss how the anatomical, synaptic and cellular properties of this connection give a mechanistic insight into neuronal firing behaviour observed *in vivo* and re-evaluate proposed models of granule cell layer network dynamics and signal processing in light of new experimental data on the mossy fibre - Golgi cell - granule cell circuit presented in this thesis.

Chapter Two

2 Materials and Methods

2.1 Solutions

Electrophysiology

Unless otherwise indicated chemicals were obtained from Sigma-Aldrich (www.sigmaaldrich.com) or Tocris (www.tocris.com). All concentrations in mM unless stated otherwise.

artificial cerebro-spinal fluid (ACSF): 125 NaCl

2.5 KCl

2 $CaCl_2$

1 $MgCl_2$

1.25 NaH_2PO_4

26 $NaHCO_3$

25 glucose

pH=7.3 with 95%O_2/5%CO_2

potassium-gluconate slicing solution: 130 K-gluconate

15 KCl

0.05 EGTA

20 HEPES

25 glucose

pH=7.4 with NaOH

intracellular solution (Golgi cell):

5 Na-$MeSO_3$

130 K-$MeSO_3$

10 HEPES

5 $MgCl_2$

0.1 EGTA

0.3 NaGTP

4 NaATP

pH=7.3 with 5N KOH

intracellular solution was made up from 160 µl (1.25x stock) + 20 µl 40 mM NaATP, 3 mM NaGTP stock in 10 mM HEPES + 20 µl additives; final Osmolarity 280-290 mOsm

additives:

1. 2 µl 10 mM Alexa488 or Alexa594 (Molecular Probes; final conc. 100 µM)

   18 µl H_2O
2. 2 µl 10 mM Alexa488 or Alexa594

   9 µl 350 mM TEA (final conc. 17.5 mM)

   9 µl 100 mM QX314 (final conc. 5 mM)
3. 4 µl 10 mM Oregon BAPTA 1 (Molecular Probes; final conc. 200 µM)

   16 µl H_2O
4. 4 µl 10 mM OGB-1

8 µl 350 mM TEA (final conc. 17.5 mM)

8 µl 100 mM QX314 (final conc. 5 mM)

5. 0.4 mg biocytin (Invitrogen)

20 µl H_2O

intracellular solution (granule cell): 110 K-$MeSO_3$

40 HEPES

6 NaOH

3 $MgCl_2$

0.02 $CaCl_2$

0.15 BAPTA

0.3 NaGTP

4 NaATP

pH=7.3 with 5N KOH

intracellular solution was made up from 160 µl (1.25x stock) + 20 µl 40 mM NaATP, 3 mM NaGTP stock in 40 mM HEPES + 20 µl additives; final Osmolarity 280 mOsm

additives: 1. 3 µl 0.01M BAPTA

17 µl H_2O

Table 1 List of drugs

Drug	final conc.	solvent	stock conc	dilution	Source
SR95531 (Gabazine)	10 μM	H_2O	10 mM	1:1000	Tocris
Strychnine	0.3 μM	H_2O	0.5 mM	1:3333	Tocris
NBQX[9]	100 μM	H_2O	20 mM	1:200	Tocris
AP5[10]	10 μM	H_2O	10 mM	1:1000	Tocris
$NiCl_2$	100 μM	H_2O	10 mM	1:100	Sigma
E4CPG[11]	500 μM	0.5M NaOH	50 mM	1:100	Tocris
CPPG[12]	200 μM	0.5M NaOH	20 mM	1:100	Tocris
Baclofen	100 μM	1 M NaOH	20 mM	1:100	Tocris
GYKI 52466[13]	100 μM	0.1 M HCl	5 mM	1:50	Tocris
ZD 7288[14]	50 μM	H_2O	50 mM	1:1000	Tocris
Kynurenic acid	1 mM	DMSO	50 mM	1:50	Tocris

Immunohistochemistry

0.2M Phosphate buffer (PB): 23.373g Na_2HPO_4 (Molecular Weight 142g/mol)

(pH = 7.4) 4.236g Na H_2PO_4 (Molecular Weight 120g/mol)

1000 ml H_2O

0.1 M PB: 500 ml 0.2M PB

500 ml H_2O

[9] 2,3dioxo-6-nitro-1.2.3.4-tetrahydrobenzo quinoxaline-7-sulfonamide
[10] D-(-)-amino-5-phosphonopentanoic acid
[11] (RS)-a-ethyl-4-carboxy phenyl glycine
[12] (RS)-a-cyclopropyl-4-phosphono phenyl glycine
[13] 4-(8-Methyl-9H-1,3-dioxolo[4,5-h][2,3]benzodiazepin-5-y l)-benzenamine hydrochloride
[14] 4-Ethylphenylamino-1,2-dimethyl-6-methylaminopyrimidinium chloride

Materials and Methods

4% paraformaldehyde (100 ml): 4 g paraformaldehyde was dissolved in 50 ml 60°C H_2O with a few drops NaOH under continuous shaking. After 50 ml 0.2 M PB was added the fixative filtered and the pH measured (=7.3)

(when tissue was fixated for electron-microscopic analysis 2 ml 25% glutaraldehyde (GA) was added just before use; final conc. 0.05%)

Tris buffered Saline (TBS): 6.61 g Trizma HCl
(pH = 7.4) 0.97 g Trizma Base
1000 ml H_2O

Na-azide was added to 4% paraformaldehyde, TBS and PB (final conc. 0.05%) to preserve solutions over longer periods

blocking solution: 10% neonatal goat serum (NGS from Invitrogen) in TBS

incubation solution: 2% NGS and 0.05% Triton in TBS
Triton was dissolved in TBS on a slowly rotating stirrer (care was taken not to shake the solution)

Primary antibody: anti-vGlut-1 = polyclonal IgG antibody raised in rabbit against mammalian vesicular glutamate transporter 1 (antigen: rat vGlut-1 amino acid residues 456-560) was used in 1:1000 dilution in incubation solution (obtained from Synaptic Systems GmbH, Goettingen Germany, Catalog No. 135 302)

Secondary antibodies: anti-rabbit = polyclonal antibody raised in goat against epitope in IgG of rabbit and coupled to Alexa488 was used in 1:500 dilution in incubation solution (www.products.invitrogen.com; Catalog No. A-11008)

streptavidin = biocytin binding protein coupled to Alexa594 was used in 1:1000 dilution in incubation solution (www.products.invitrogen.com; Catalog No. 32356)

2.2 Slice preparation

Parasagital slices of rat cerebellum were prepared in accordance with Home Office regulations in the following way: 25-day old (P25) Sprague Dawley rats were decapitated with scissors or guillotine. The brain was removed from the head in ice-cold ACSF by first removing the fur to the front brow and making two lateral cuts in the cranium with fine scissors just above the ear line leading to the forehead. This allowed opening of the skull and preparation of the whole brain. The brain was mounted with fine needles on a pre-cooled petri dish, with 2-3 mm 5% Sylgard in the bottom, filled with ice-cold ACSF. The meningis was

removed from the cerebellum with fine forceps. The cerebellum was separated by a coronal cut and the cerebellar vermis (central part of the cereballar cortex) isolated with two parasagital cuts. The vermis was glued onto the slicing platform with Loctite SuperGlue (Loctite Henkel), submerged in ice-cold slicing solution or ACSF and cut into 200 to 220 μm thick slices using a vibratome (Campden Integraslice 7550 PSDS from Campden Instuments or Leica VT 1000S form Leica both used with ceramic blades (part# 7550/I/C) from Campden Instruments. Blades were changed after 5-7 times use). The tissue was thereafter stored at 30-32 °C ACSF for 45-60 minutes. On some occasions 10 μM AP5 or 1 mM kyurenic acid was added to the solutions in the slicing and incubation chamber to reduce ischemic neurotoxicity. Slices could then be stored for up to 6 hours at room temperature before use.

2.3 Electrophysiological Recording Conditions

For electrophysiological recordings cerebellar slices were transferred to a recording chamber under an Olympus BX50WI microscope. Here, brain slices were placed between a stainless steel washer covered with thin nylon threads that formed a net and a flattened platinum wire with attached nylon strings to immobilize the tissue and allow the continuous perfusion of oxygenated and carbonated ACSF heated to 34-36°C. The gravity-fed perfusion achieved a flow rate of 3-5 ml/min. Pharmacological agents were added to the solution when mentioned. Tissue was visualized under a ×60 (NA=0.9) water-immersion objective with infrared differential interference contrast optics and a CCD camera. The contrast was further enhanced with an electronic contrast enhancement box (C2400 Camera Controller, Hamamatsu). For targeted patching

of cells the magnification was enhanced to ×96 by separate magnifying lenses in the light path. Fire-polished patch pipettes were produced from borosillicate glass capillaries (from Sutter Instrument, Novato, CA, USA; O.D. = 1.5 mm, I.D. = 0.75 mm, 10 cm length with filament) with a Sutter P97 horizontal Puller (Sutter Instruments, Novato, CA, USA) and attached to a headstage. Positive pressure was applied to the pipette to keep the tip free of debris when penetrating the tissue. The pipette was positioned with the help of micromanipulators (Luigs&Neumann SM1) above a targeted cell so that the outflow at the tip produced a "dimple" on the membrane surface.

Loose cell-attached recordings

For loose cell-attached recordings (LCA) recordings the pipette filled with ACSF (7-10 MΩ pipette resistance) was slightly retracted before releasing the pressure. Occasionally light suction was applied, to help achieve patch resistances of 50-200MΩ. This configuration allowed monitoring of cell firing without perturbation of the cell's internal milieu. Action potentials were identified based on prominent upward and inward deflections in the current trace (Vos *et al.*, 1999b). Recording stability was monitored by observing the action potential shape.

Whole-cell recordings

For whole-cell recordings the pressure was released to form a GΩ-seal (cell-attached configuration) which was then broken by applying gentle negative pressure or a short (5μs) "zap" current pulse to obtain the whole-cell configuration. The holding potential in voltage-clamp recordings was -60 and -70

mV for Golgi cells and granule cells, respectively. Recording electrodes were filled with the respective intracellular solution for Golgi and granule cells (5-7MΩ). Input and series resistance was monitored throughout the recording by measuring the maximal and steady state current of a transient in response to a 5mV voltage step. Only recordings with series resistances < 35 MΩ (before compensation) were analyzed. Recording stability was accessed with a Spearman's rank correlation test on the transient peak or in case of current-clamp recordings on the average membrane potential in a 5 ms time window before stimulation. During recordings of Golgi cells, which had an apparent capacitance of 37±14 pF (n=58) series resistance compensation (50-70%, lag 10μs) was utilized. This resulted in an effective RC filtering ($1/2\pi R_s C_m$) of approximately 1 kHz for Golgi and granule cells. Voltage-clamp recordings of Golgi and granule cells were not corrected for the 8mV (calculated) and 6.3mV (measured, DiGregorio et al. 2007) liquid junction potential, respectively. Since the Axopatch 200B amplifier circuitry was not fast enough to accurately resolve Golgi cell action potentials even in "I-clamp fast" mode we used the Axoclamp2B for current-clamp recordings of Golgi cells. Current-clamp recordings were made after obtaining the whole-cell voltage-clamp configuration (in continuous Single Electrode Voltage Clamp mode). The bridge (continuous current-clamp) mode allowed recording of (fast changing) membrane potential with little distortion and injection of currents after balancing the series resistance. In the absence of current injection spontaneous Golgi cell firing was variable over time. Since the whole-cell configuration appeared to affect spontaneous firing in an unpredictable fashion (Forti *et al.*, 2006) I injected hyper- or

depolarising currents, typically -50 to +40 pA, to match the spontaneous firing frequency observed in LCA recordings.

Synaptic stimulation

Axons were stimulated with an ACSF-filled glass pipette with a relatively large tip size and low resistance (< 5 MΩ placed in the white matter tract, typically 100-200 μm away from the recording site, to stimulate mossy fibres, or in the upper granular layer or molecular layer to stimulate parallel fibres. The stimulation consisted of a 20-200 μs 5-100 V voltage pulse generated by an isolated stimulator (DS2A, Digitimer Ltd). Stimulus location has profound influence on type and number of fibres stimulated, the recorded stimulus artefact as well as the transmission latency (Action potential propagation speed ~5 m/s; Kole *et al.*, 2007). Therefore after establishing LCA, cell-attached or whole-cell configuration the stimulus electrode was moved until a stimulus location was found that reliably produced a response that was well separated from the stimulus artefact. To avoid accumulation of receptor desensitization during repetitive stimulation of synaptic inputs the mean stimulation frequency was set to < 1 Hz. The synaptic release probability was manipulated with different Ca^{2+}/Mg^{2+} ratios. The 2 mM Ca^{2+}/ 1 mM Mg^{2+} ratio in control conditions was reduced to 1/5 to diminish release probability and increased to 4/1 or 6/1 to augment release probability. The change in the divalent ion concentration in the perfusion solution was accompanied by an alteration in the stimulation threshold for fibre activation. Low external calcium concentrations lower the threshold whereas high calcium concentrations increase the voltage threshold for fibre stimulation. Similarly, high frequency stimulation increases in the stimulus threshold for later

events in a train. These threshold changes were compensated by changing the stimulus intensity appropriately.

2.4 Electrophysiological Data Acquisition

Electrophysiological experiments were performed with a Axopatch 200B amplifier (Molecular Devices, Sunnyvale, CA, USA) attached to a CV203BU headstage for voltage-clamp recordings or a Axoclamp 2B (Molecular Devices, Sunnyvale, CA, USA) attached to a HS2A (Gain x0.1) headstage for current-clamp recordings. LCA recordings were made with both types of amplifier. Data was low pass filtered at 10-30 kHz and digitized at 50-100 kHz using the following D/A converters National Instrument BNC-2090 connected to National Instrument PCI 6052E 16bit board and National Instrument BNC-2110 connected to National Instrument PCI 6713 12bit board. Recordings were acquired and analyzed with IgorPro (Wavematrics) using NeuroMatic (http://physiol.ucl.ac.uk/research/silver_a/neuromatic/) run on a Pentium IV with 256MB RAM. All traces displayed in figures were further digitally filtered using a binomial smoothing function (Smooth = 6) in IgorPro resulting in a frequency of 3.5–7 kHz.

2.5 Electrophysiological Data Analysis

Loose cell-attached recordings

In LCA recordings the action potential latency was defined as 50% time point of the inward deflection.

The relationship between the timing and the effect of mossy fibre stimulation on rhythmically active GoCs was assessed with a phase-response curve (Rinzel & Ermentrout, 1998), which determines the normalised difference between the expected interspike interval (T_0) and the observed interspike interval (T_n) as a function of stimulus phase (θ; time difference between spontaneous action potential before stimulation and time point of stimulation normalised by T_0).

$$\Delta\theta = \frac{T_0 - T_n(\theta)}{T_0} \qquad \text{(Equation 1)},$$

$\Delta\theta$ = phase-response, T_0 = median of interspike-interval (ISI) before stimulation, T_n = ISI between action potentials of interest (see **Figure 5-1a**).

Whole-cell recordings

The spike threshold was determined by computing the first derivative of the membrane voltage (dV/dt) and determining a dV/dt that was 5 SDs above the mean rate of change of sub-threshold regions. This gave a threshold criterion of approximately 5 mV/ms, see also Forti *et al.*, 2006, which reliably identified the rising phase of action potentials and corresponded closely to the visually identified inflection point. The measured membrane threshold potential was subsequently corrected for liquid junction potential.

I analyzed evoked postsynaptic currents (PSCs) and potentials (PSPs) in the following way. Voltage-clamp records were baseline subtracted using the average amplitude of a 5 ms time window before the stimulus artifact. In some cases the stimulus artifact was subtracted by a double exponential fit to the mean

trace or a selected failure trace. Failures were separated from successes when the mean amplitude in a 1-2 ms window around the peak of the mean PSC (or PSP) was smaller than 3x SD of the mean background current of a 1 ms time window before the stimulus (inflected baseline; DiGregorio *et al.*, 2002). Successes occasionally contained slowly rising and low amplitude currents, which originated from the spillover of neurotransmitter onto postsynaptic receptors of neighboring release sites (DiGregorio *et al.*, 2002). To distinguish spillover currents I separated PSCs with a rise time 5x SD above the mean rise time (20-80%) of successes and a maximal derivative (dV/dt) smaller than -200 pA/ms. These events were grouped with failures. **Figure 2-1** illustrates the analysis for currents recorded in a granule cell in response to mossy fibre stimulation. EPSC and EPSP kinetics were characterized using the 20-80% rise time and a two-exponential fit to the decay, the 63% decay time or the weighted decay (peak normalized integral) over a 20 ms time window. EPSCs were also fitted with the following equation (Nielsen *et al.*, 2004) which captures EPSC rise and decay in a continuous function:

$$EPSC(t) = A_1\left(1-\exp\left(-\frac{t-t_0}{\tau_{rise}}\right)\right)^n\left(A_2\exp\left(-\frac{t-t_0}{\tau_{decay1}}\right)+(1-A_2)\exp\left(-\frac{t-t_0}{\tau_{decay2}}\right)\right) \quad \text{(Equation 2)}$$

Response latencies were measured between the artifact and the 20% rise time point of the EPSC or EPSP. Since monosynaptic EPSCs in granule cells have a mean latency of 0.8 ms (Sargent *et al.*, 2005) monosynaptic EPSCs in Golgi cells were expected to occur with a latency < 1.2 ms (mean + 5x SD). Action potentials latencies in current-clamp recordings were measured as the time to threshold crossing or to peak of the voltage transient.

Materials and Methods

The time course of synaptic reversal potential was calculated by summing the product excitatory and inhibitory conductances with their respective reversal potential and relating it to the total synaptic conductance (Johnston & Wu, 1995).

$$E_{Syn} = \frac{G_{exc}E_{exc} + G_{inh}E_{inh}}{G_{exc} + G_{inh}} \qquad \text{(Equation 3)},$$

E_{Syn} = synaptic reversal potential, G_{exc} = excitatory conductance, E_{exc} = reversal potential of excitatory conductance (estimated to be 0mV), G_{inh} = inhibitory conductance, E_{inh} = reversal potential of inhibitory conductance (estimated to be -75mV). When E_{Syn} is below the voltage threshold for spike initiation the total synaptic conductance acts inhibitory.

Deconvolution analysis was performed with a custom-made analysis routine in IGOR PRO similarly to Sargent et al. (2005) but without spillover correction. Putative uniquantal events were measured under low release probability conditions, aligned on their 20% rise time (determined from fits of equation 2 to individual currents) and averaged. The mean current was fit with equation 2 and deconvolved with a fit of the average stimulus evoked EPSC under control conditions. Occasionally, the "foot" (first two rising points) of the averaged aligned uniquantal current was removed to prevent oscillatory components in the deconvolution result. To obtain the vesicular release rate as a function of time across release sites at the connection the deconvolution result was divided by the sampling rate. The integral of the release time course amounted to cumulative release function. Deconvolution analysis only gives a true estimate of the release time course if quantal events sum linearly. Therefore the analysis was validated by comparing the cumulative release function obtained by deconvolution with

the cumulative first latency distribution of quantal events under low release probability conditions. At high failure rates (> 80%) the correction for the occurrence of later quantal events during a trial (Barrett & Stevens, 1972) was negligible.

The quantal size at the time of the peak of the evoked EPSC (Q_p) was determined in two ways. For one, I averaged stimulus aligned quantal events under low release probability conditions. Above a failure probability of 80% measured EPSCs are mostly uniquantal irrespective of the number of release sites (Silver, 2003), when quantal release is independent. However, we corrected the measured amplitude for the inclusion of multiquantal event by assuming the worst case scenario of a large number of release sites (10% overestimate; Silver, 2003). Secondly, I calculated Q_p from variance-over-mean analysis (Silver, 2003). For a binomial model of synaptic release the variance at the peak of the current is given by the following equation:

$$\sigma^2 = NQ^2P(1-P) \qquad \text{(Equation 4)}$$

where N = number of release sites, Q = Quantal size, P = Release probability. Hence, for low release probability conditions (low P) the variance divided by the mean amplitude approximates the quantal size.

$$P \to 0; \frac{\sigma^2}{NPQ} \cong Q \qquad \text{(Equation 5)}$$

But variance does not only arise from the stochastic amplitude variability of quantal release, but also from intra- and intersite trial-to trial variability in the latency of quantal release and quantal size. Assuming uniform release probability across sites the variance at the peak of the EPSC is given by:

$$\sigma^2 = \left[Q_p \bar{I} - \frac{\overline{I^2}}{N} \right] \left(1 + CV_{QII}{}^2 \right) + Q_p \bar{I} CV_{QI}{}^2 \qquad \text{(Equation 6)}$$

where I = mean current, CV_{QI} = coefficient of variation of intrasite variability consisting of latency and quantal size variability and CV_{QII} = coefficient of variation of intersite variability. For uniform release probability conditions this can be rearranged and simplified to:

$$Q_p = \frac{\sigma^2}{\bar{I}} \cdot \frac{1}{\left(1 + CV_T{}^2 \right)} \qquad \text{(Equation 7)}$$

where CV_T = coefficient of variation of the quantal variability at the peak of stimulus aligned successes including intra- and intersite variability and a small contribution of possible multiquantal successes (Silver, 2003).

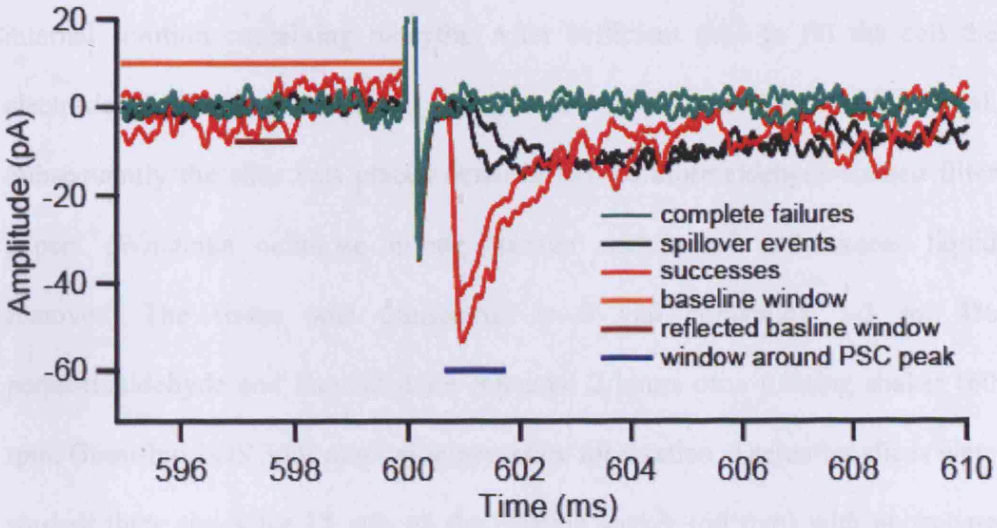

Figure 2-1 EPSC analysis. Whole-cell voltage-clamp recording of a granule cell at -70 mV. Excitatory postsynaptic currents (EPSCs) were recorded in response to mossy fibre stimulation. Three types of responses can be distinguished: (1) Complete failures (in green) where the average amplitude in the blue time window is smaller than the threshold value indicated by the brown line, which represents the value of three standard deviation above the average amplitude in that time window. Complete failures are uncommon for mossy fibre – granule cell synaptic transmission (DiGregorio *et al.*, 2002) and may reflect failures of fibre stimulation (2) Spillover currents (in black) which are currents with a rise time above five standard deviations above the average rise time of direct successes. (3) Direct successes (in red) have large average amplitude and a fast rise time. The orange line indicates the time window, over which individual currents were baselined.

2.6 Immunostaining

To stain cells and fibres in brain slices, I whole-cell patched Golgi cells with an internal solution containing biocytin. After sufficient time to fill the cell the electrode was slowly retracted so that the cell membrane could reseal. Subsequently the slice was placed between two paraformaldehyde-soaked filter papers (Whatman cellulose nitrate transfer membrane) and excess liquid removed. The tissue was transferred to a vial containing 2-3 ml 4% paraformaldehyde and incubated for maximal 2 hours on a rotating shaker (60 rpm, Grant-bio POS 300) at room temperature for fixation. Thereafter slices were washed three times for 15 min on the rotating shaker (60 rpm) with phosphate buffer (PB). During the washing process the filter papers were carefully removed. At this stage fixated tissue could be stored for longer time periods at 4°C in 0.05% sodium azide-containing PB. In the next step PB was washed out by repetitive treatment with TBS (3 times for 15min) and the tissue incubated for an hour in blocking solution. Subsequently slices were treated with a 1:1000 dilution of vGlut-1 antibody in 2% NGS and 0.05% Triton in TBS for 4-6 hours at room temperature (on rotating shaker) or at 4°C over night. The primary antibody was washed out by repetitive treatment with TBS and the tissue incubated for 2 hours at room temperature (on rotating shaker) with the secondary antibodies in a 1:1000 dilution of streptavidin-Alexa594 and a 1:500 dilution of the anti-rabbit-Alexa488 antibody. Finally, the secondary antibodies were washed out with repetitive treatment with TBS, excess liquid removed, embedded with Vectorshield (Vector Technologies, CA, USA) and covered with a glass cover slip on an objective slide. The preparation was sealed with clear nail polish to avoid dehydration of the sample.

Figure 2-2 Fluorescence excitation and emission. Excitation spectra (broken lines) of Alexa488 (green) and Alexa594 (blue) with the corresponding emission spectra represented in normalized relative units (r.u.). The thick grey lines indicate the excitation wavelength used for the two dyes. The green and orange bands show the detection bandwidth of the green and red channel, respectively (adapted from http://probes.invitrogen.com/servlets/spectraviewer).

2.7 Imaging Acquisition and Analysis

Bright-field fluorescence imaging

Golgi cell somata were identified in acute slices under DIC. The identity was confirmed by visualising their anatomy using fluorescence microscopy with the fluorescent dyes Alexa488 or Alexa594 (Molecular Probes, Invitrogen, UK) included in the patch pipette. Imaging was carried out using whole-field excitation (Olympus BX FLA lamphouse with USHIO 102 Mercury lamp) and imaging (excitation filters in nm: 480/40 and 580/20; dichroic 505lp and 595lp; emission filters 535/50 and 630/60 for Alexa488 and Alexa594 respectively, with a cooled ORCA100 (Hamamatsu) digital camera. Several images of cell body and dendritic arbourisation were taken to identify the cell type patched.

Ca^{2+} imaging

For Ca^{2+} measurements I substituted Alexa dye with the calcium-indicator dye OregonGreen BAPTA1 (200 μM OGB1, Molecular Probes). After spatial equilibration of the dye (>10 min) a series of 3-4 images was taken of various parts of the cell before and during a 100 Hz (100pulses) stimulation of the white matter. I used a custom-made image analysis routine in Matlab (Mathworks) to calculate the ΔF/F for each pixel in the image by averaging the images before and during stimulation and relating the intensity difference before and during stimulation to the average pixel intensity before stimulation. The distribution of ΔF/F values was fitted with a Gaussian function. Only contiguous groups of pixels with values 5xSD above the mean were assumed to represent a significant

increase in local calcium concentration. This allowed reliable detection of Ca^{2+} signals ($\Delta F/F > 0.1$) in response to fibre activation. During these Ca^{2+} imaging experiments series resistance compensation was disabled to induce poor voltage-clamp since this increased the probability of detecting a Ca^{2+} transient upon synaptic stimulation. The large depth of focus for CCD imaging allowed the simultaneous observation of fluorescence changes in large parts of the cell. This made it possible to map the cell with many fewer trials compared to confocal imaging.

Fluorescence Confocal Imaging

Fluorescence Confocal 3D image stacks were made with a Zeiss LM501. Objective slides with immuno-stained brain slices were examined with an oil-immersion Plan-NeoFluar 40x with a numerical aperture (NA) of 1.3 ($NA = n\sin\alpha$; n = refractive index of medium, α = collecting angle of the lens) which amounted to a theoretical lateral optical resolution of 250-300 nm ($R=1.22\lambda_{em}/2NA$; λ = emission wavelength) and 63x objective (NA 1.4) with a lateral resolution of 230-270 nm[15]. Excitation with a 488 nm Argon Laser in combination with bandpass filtered 505-530 nm fluorescence detection (with photomultiplier) visualized binding of Alexa488 coupled antibodies, whereas excitation with an 543 nm diode laser and fluorescence detection in the 585-615 nm bandwidth (or 560 nm long-pass) visualized binding of Alexa594 coupled streptavidin to biocytin. The excitation and emission spectra of Alexa488 and Alexa594 with excitation and detection wavelength are shown in **Figure 2-2** and illustrate that little crosstalk between detection channels was expected. The

[15] This does not take limitations due to insufficient fluorescence signal detection into account.

confocal pinhole size was varied between 60 and 90 μm which resulted in a vertical resolution of 0.6-1 μm. The optical sectioning was matched accordingly, between 0.7-1 μm.

3D stacks of green (showing vGlut-1 staining) and red channel (indicating Golgi cell staining) images were analysed with ImageJ (NIH, http://rsb.info.nih.gov/ij/index.html). Golgi cell morphology was characterised by first identifying the axon, as thin highly bifurcated (often forming T-junctions) structure and tracing it back to the initial segment contacting the cell body. This was sometimes problematic, because especially the proximal axon had a similar thickness to Golgi cell dendrites, which meant, when axon and dendrite crossed within a focal section they could not be traced unambiguously. Having identified the initial segment the dendritic arbourisation was characterized. Dendrites were typically 0.7-1 μm thick. Ascending dendrites were originating from the upper part of the soma to ascend into to molecular layer, whereas basolateral dendrites typically originated from basal and lateral parts of the soma. The dendritic length was manually measured from the centre of the soma along a dendritic branch. The expansion of morphological structures was measured as the largest extension in the respective dimension (see **Figure 2-3**). The expansion in z-dimension has to be considered a lower limit, since the fixation and embedding procedure will lead to shrinkage and compression of the slice.

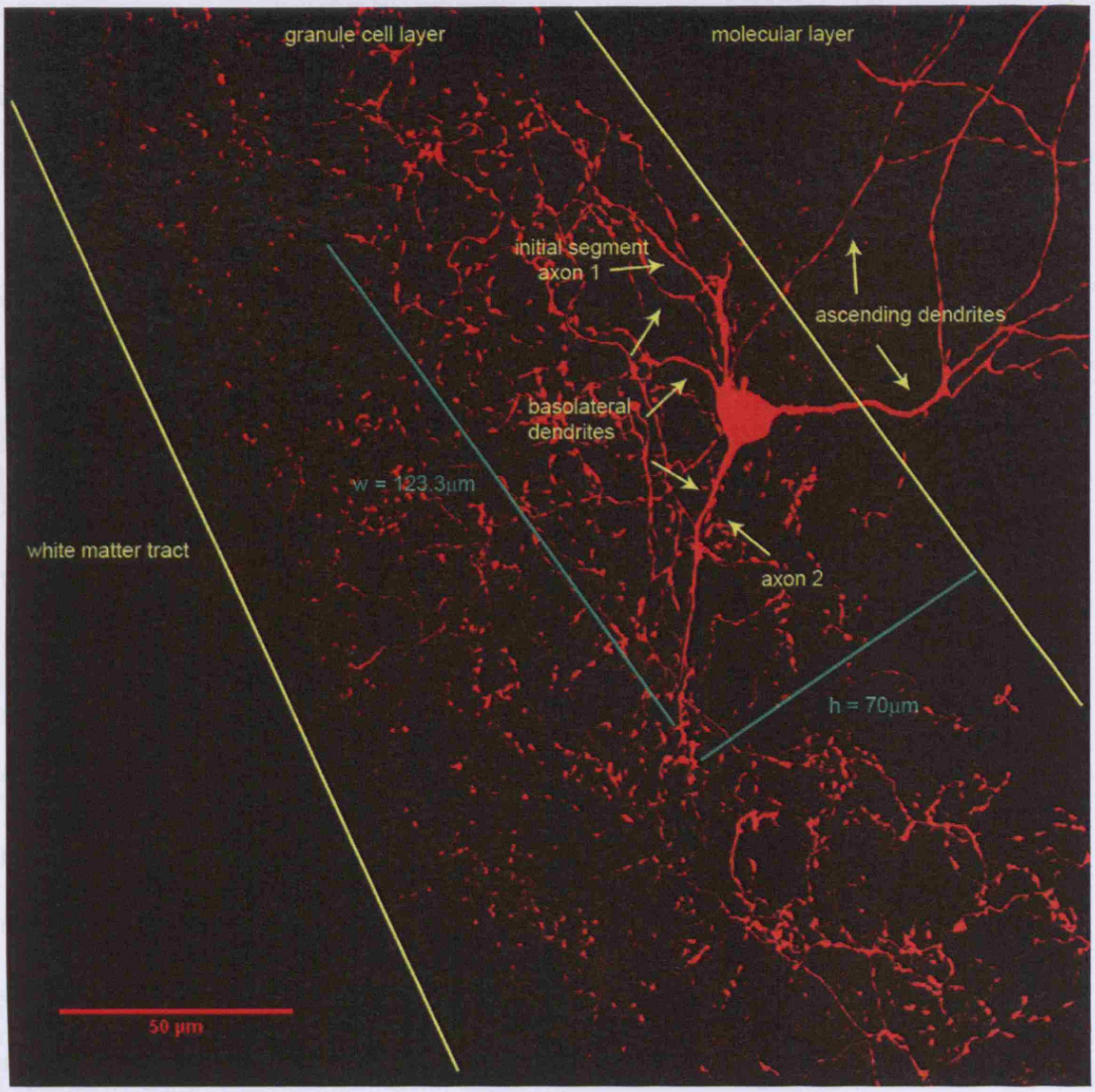

Figure 2-3 Golgi cell morphometry. Maximal intensity projection of biocytin filled Golgi cell. Biocytin was visualised with streptavidin-Alexa594. Yellow lines indicate approximate borders between granule cell layer with white matter tract and molecular layer. Dendritic and axonal arbourisation is pointed out with arrows. Green lines indicate the width (w) and height (h) of the basolateral dendritic arbourisation. Similar measurements were carried out for the dimensions of soma, ascending dendritres and axonal arbourisation.

Materials and Methods

To measure the number of mossy fibre terminals and their size distribution mossy fibre terminals defined as v-Glut1 stained 3D objects were counted within the granule cell layer. For this I utilised an ImageJ 3D-object counter Plug-In (http://rsb.info.nih.gov/ij/plugins/track/objects.html) programmed by Fabrice Cordelières and Jonathan Jackson. In a "thresholding" procedure the plug-in redraws contiguous structures in an image and connects them across image slices in a stack to construct 3D objects. The number, volume and size of objects could be analyzed. The threshold for binarising images was set to be three times above the average pixel intensity of the entire image, which ensured that only mossy fibre terminals (with high vGlut-1 staining) and not axonal structures (with less vGlut-1 staining) were included in the analysis (see **Figure 2-4**). The "thresholding" was performed for each image individually since the signal to noise ratio decreased for images taken at larger depths. Binary images were subsequently concatenated to a stack and the 3D object counter procedure executed. Objects smaller than 0.5 μm^3 typically represented small structures in the molecular layer, parts of mossy fibre or granule cell axons and were therefore excluded from further analysis.

To identify putative contacts between mossy fibres and Golgi cell we used ImageJ (NIH, http://rsb.info.nih.gov/ij/index.html) with the Plug-In "Colocalization" programmed by Pierre Bourdoncle (http://rsb.info.nih.gov/ij/plugins/colocalization.html) to identify areas of co-localized fluorescence. If the fluorescence at an image location in the green and the red channel image was above a certain threshold value that point was considered to represent colocalised fluorescence. The thresholds used for the

analysis routine were determined as five standard deviations above the average pixel intensity of an image. Contiguous points of colocalised fluorescence were considered mossy fibre terminal – Golgi cell contacts representing either Golgi cell axon innervations of mossy fibre terminals or mossy fibres synapsing onto Golgi cell dendrites. Using the previous characterisation of Golgi cell morphology putative mossy fibre to Golgi cell synapses were identified as colocalised points of mossy fibre terminals and Golgi cell dendrites or soma. Putative mossy fibre – Golgi cell synapses were additionally inspected at higher magnification. All other areas of colocalised fluorescence were assumed to be Golgi cell innervations of mossy fibre terminals. The proportion of terminals contacted by an axon was quantified by counting the number of objects formed by colocalised points and relating it to the total number of mossy fibre terminals (see measurement of 3D objects above) within the axonal arbour. Surface and texture rendered 3D representations of the confocal stacks were generated with the software package Volocity (Improvision, Coventry, UK) with the help of David Cianter (UCL, Anatomy).

2.8 Statistics

Data are presented as mean ± standard deviation (SD) and groups compared with paired or unpaired two-tailed Student's t-test. For pair-wise comparison of groups I employed a one- or two-way ANOVA and distributions were compared using a Kolmogorov-Smirnov (KS) test. Groups were considered significantly different at $p < 0.05$. Linear, exponential and gaussian functions were fit to data points using the least mean square method. Statistical analysis was performed either using Microsoft Excel or Wavemetrics Igor Pro.

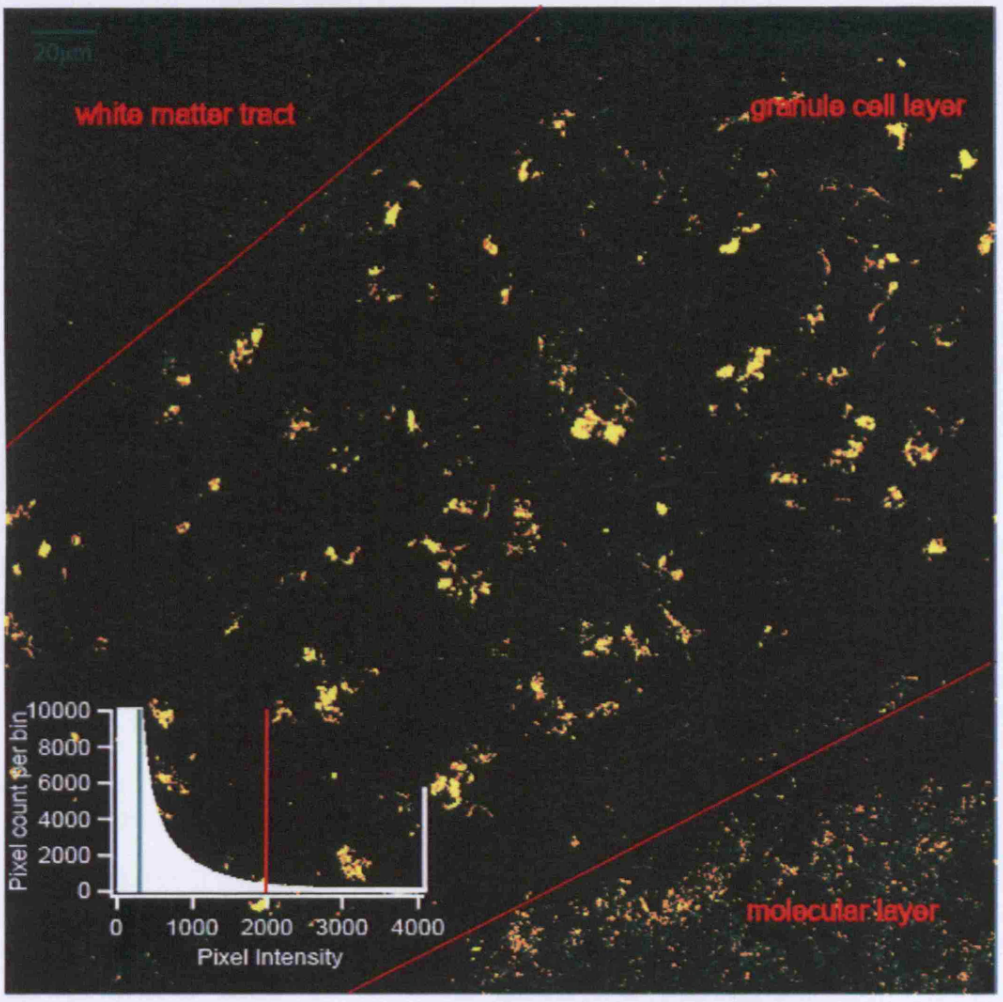

Figure 2-4 Mossy fibre morphometry. Confocal image of vGlut-1 immuno-staining in sagittal cerebellar slice in single focal plane. Mossy fibre terminals in the granule cell layer and parallel fibre terminals in the molecular layer are stained (in green). Red lines indicate borders between granule cell layer, molecular layer and white matter tract. Overlaid in yellow is a same image binarised with a threshold three-times the standard deviation above average pixel intensity. In the lower left corner of the image's pixel intensity distribution is shown (y-axis is cut at 100000). The average pixel intensity was 295 (green line)

and the standard deviation was 562 with amounted to a threshold value of 1981 (red line).

Chapter Three

3 Anatomy of the mossy fibre to Golgi cell synapse

3.1 Introduction

To understand how the granule cell layer, as the input layer of the cerebellar cortex, processes sensory information it is of crucial importance to characterize the connectivity of the circuitry. Although the cerebellar circuitry has been studied for a long time and is qualitatively well understood, certain aspects, most prominently the feed-forward connection between mossy fibres and Golgi cells are poorly characterized. It is generally accepted that mossy fibres synapse onto Golgi cells but controversy remains about the number of contacts and as to where they synapse (see Chapter 1). Maex and DeSchutter (1998) suggested that the number of mossy fibres contacting Golgi cells is small (around 4) whereas Pellionisz and Szentagothai (1974) estimated over 200 mossy fibres synapsing onto a Golgi cell. Hamori and Szentagothai (1966) proposed that mossy fibres contact the descending dendrites of Golgi cells, whereas Palay and Chan-Palay (1974) claimed mossy fibres preferentially synapse onto cell body and proximal descending dendrites in a specialized synaptic structure named "synapse en-marron". I attempted to resolve this controversy and visualized and quantitatively characterized the mossy fibre - Golgi cell innervation pattern using double immunostaining of mossy fibres and Golgi cells. This also provided quantitative information about the granule cell layer circuitry in general e.g. mossy fibre

density, extent of Golgi cell axons and number of mossy fibre terminals contacted. Although further experiments are required to confirm the estimates and their validity, e.g. verifying synaptic mossy fibre – Golgi cell contacts with electron microscopy, these findings together with known anatomical data on the cerebellar cortex allow some predictions on the way information is processed in the granule cell layer.

3.2 Results

To visualise the mossy fibre - Golgi cell innervation pattern I patched putative Golgi cells with an electrode containing internal solution supplemented with biocytin (see Materials and Methods) in sagittal slices of P25 rats. In the cell-attached configuration I observed the spontaneous firing pattern of cells (Mitchell & Silver, 2000b; Forti *et al.*, 2006) and subsequently broke the seal to dialyse the cell with biocytin. The slice was thereafter fixed in paraformaldehyde and processed with a steptavidin antibody conjugated to Alexa594 to visualise biocytin-filled cells. Because most mossy fibres express vesicular glutamate transporter-1 (vGlut-1) (Hisano *et al.*, 2002; Miyazaki *et al.*, 2003), I additionally incubated slices with an (primary) antibody against vGlut-1 (anti-vGlut-1 raised in rabbit) and visualised anti-vGlut-1 binding with a (secondary) anti-rabbit antibody conjugated to Alexa488. Antibody binding was visualised with a confocal fluorescence microscope using 488 nm excitation and 505-530 nm emission detection for Alexa488 (green channel) and 543 nm excitation and 585-615 nm (or 560 nm long-pass) emission detection for Alexa594.

Specificity of Immunostaining

The specificity of primary and secondary antibodies was tested to avoid potential artifacts and misinterpretation of the data. I incubated fixed cerebellar brain slices with each secondary antibody at 4°C overnight and measured the fluorescence in comparison to slices pre-incubated with the respective antigen. Images in **Figure 3-1a** show the immunoreaction of anti-rabbit-Alexa488 in the absence (left) and presence (right) of vGlut-1 primary antibody. A comparison of the images indicates that there is little non-specific binding of anti-rabbit-Alexa488 to the rat cerebellar slice. The specificity of the primary antibody was tested previously (Zhang *et al.*, 2004; Salazar *et al.*, 2005) and the immunoreaction shown on the right image is characteristic for vGlut-1 expression in the cerebellar cortex. Mossy fibre terminals in the granule cell layer and parallel fibre terminals in the molecular layer express vGlut-1 and are therefore stained (Hisano *et al.*, 2002)[16]. Occasionally additional staining of axonal structures was observed (see arrows **Figure 3-1a**). For streptavidin-Alexa594 binding the situation is similar (**Figure 3-1b**). The blank control (left image) shows little staining, whereas soma, dendrites and axon are clearly stained in the biocytin dialyzed cell (right image). Since nonspecific binding depends on type of tissue, fixation and incubation conditions, it varied among experiments. However, in all experiments secondary antibodies reacted highly selective with their intended antigens.

Because potential cross-reactivity of the secondary antibodies, that is the binding of the anti-rabbit antibody to biocytin and the streptavidin antibody to anti-vGlut-

[16] Climbing fibres express vGlut-2 (Miyazaki *et al.*, 2003)

1, and potential crosstalk of fluorescence from one channel into another it was necessary to assess how well Golgi cell and mossy fibre staining were discernable. **Figure 3-2** shows a maximal intensity projection of a biocytin-filled Golgi cell in the red channel (left) compared to the green channel (right). I related the average fluorescence intensity at the soma in the red channel to the green channel. At this location no fluorescence signal from vGlut-1 staining is expected. Accordingly the red channel fluorescence was approximately 5 times higher. In an analogous fashion, when measuring the average pixel intensity at selected mossy fibre terminals in the green channel and relating it to corresponding positions in the red channel the ratio was approximately 10-fold. **Figure 3-2b** shows the pixel intensity distribution for the respective images with average pixel intensity across selected points in the background (yellow line) and for the object of interest, i.e. mossy fibre terminal or Golgi cell (blue line). Values for average background fluorescence and its standard deviation across selected points (yellow dots in image) were similar to the average pixel intensity of all pixels and its standard deviation (705 ± 269 vs 695 ± 333 for green channel and 278 ± 76 vs 266 ± 210 for red channel). Therefore a fluorescence intensity that was three standard deviations above the mean overall pixel intensity reliably labeled v-Glut1 expressing mossy fibre terminals or biocytin-filled Golgi cells in the respective detection channel.

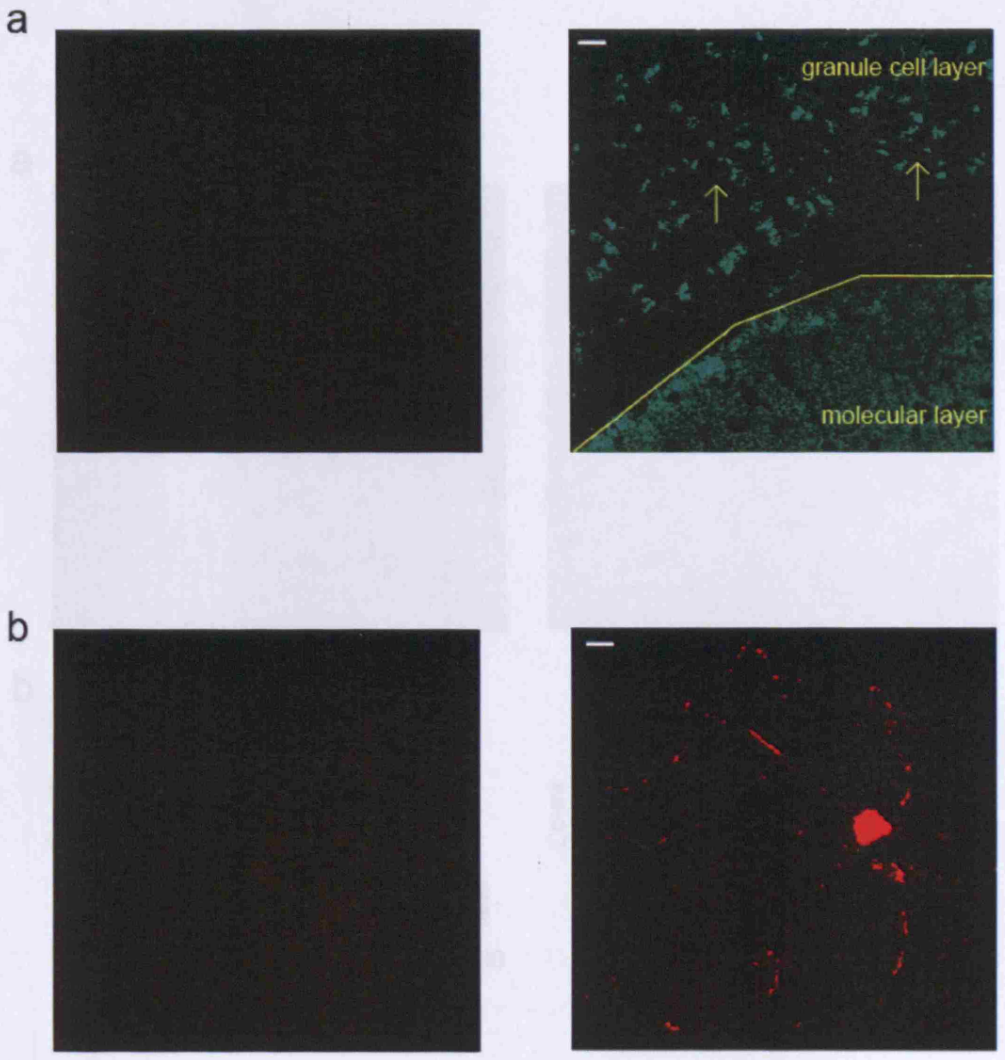

Figure 3-1 Antibody specificity *a)* Confocal pictures taken of anti-rabbit-Alexa488 and *b)* streptavidin-Alexa594 binding to tissue, that was not incubated (left) and pre-treated (right) with the respective antigen anti-vGlut-1/biocytin. Scale bars (white) in left image corner is 20 μm. Images are scaled to the same dynamic range.

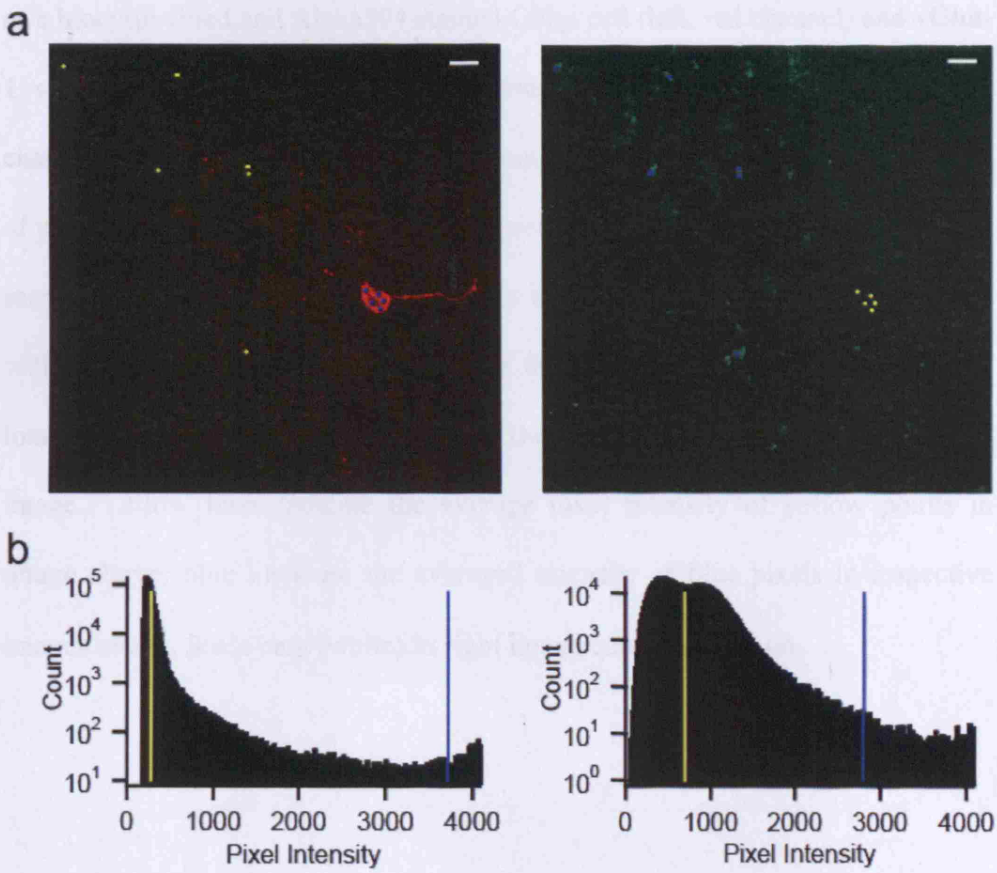
a
b
Count
Pixel Intensity
0
1000
2000
3000
4000

Figure 3-2 Discrimination of vGlut-1 and biocytin staining *a)* Confocal images of a biocytin-filled and Alexa594 stained Golgi cell (left, red channel) and vGlut-1 stained mossy and parallel fibres visualized with Alexa488 (right, green channel). Images show the respective staining of the same tissue. Pixel intensity of points that were clearly located at the cell soma (blue dots on left image) and mossy fibre terminals (blue dots on right image) were measured and compared with pixel values of identical locations in the other channel (yellow dots in both images). *b)* Pixel intensity histogram of the red (left) and green (right) channel image. Yellow lines indicate the average pixel intensity of yellow points in image above; blue lines are the averaged intensity of blue pixels in respective images above. Scale bars (white) in right image corner are 20 μm.

a

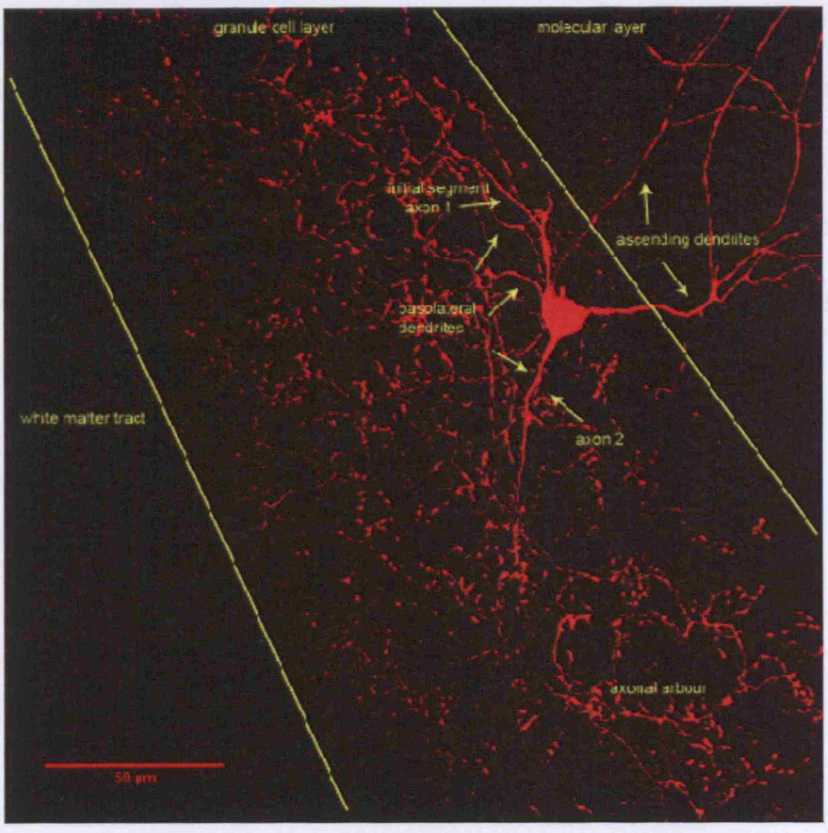
granule cell layer
molecular ayer
initial segment
axon 1
ascending dendrites
basolateral
dendrites
white matter tract
axon 2
axonal arbour
50 µm

b

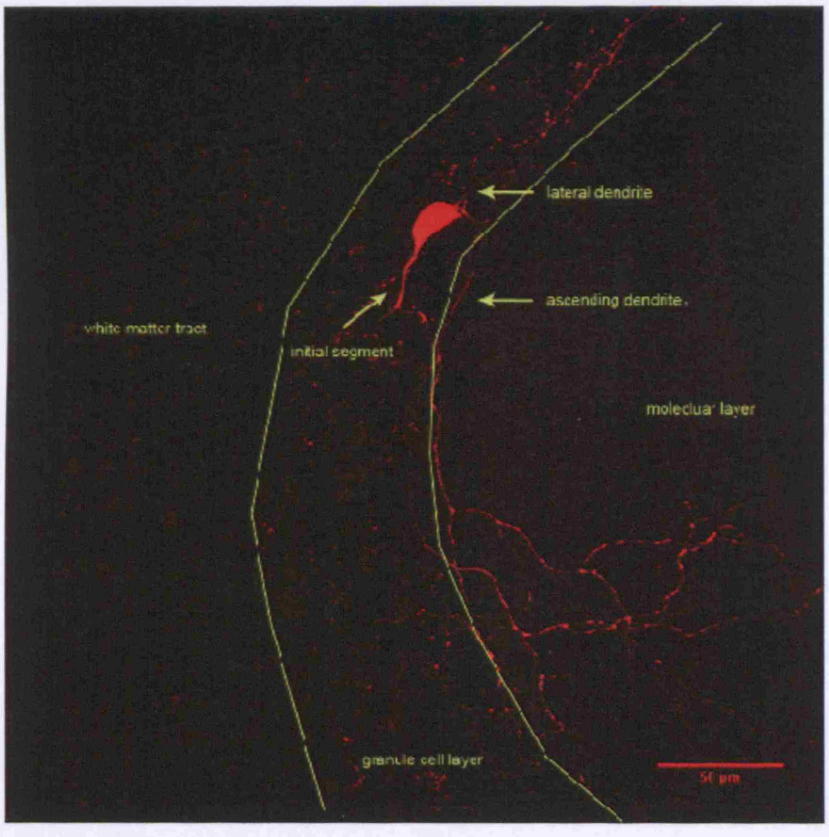
lateral dendrite
ascending dendrite
white matter tract
initial segment
molecular layer
granule cell layer
50 µm

Figure 3-3 Golgi cell morphology *a)* Maximal intensity projection of biocytin-filled Golgi cell (previously shown in **Figure 2-3**). Note the large axonal arbour in the granule cell layer, which is constituted by at least two primary axons, and the ascending dendrite reaching into the molecular layer. *b)* Maximal intensity projection of biocytin-filled Golgi cell with basolateral dendrite emerging from the proximal part of the ascending dendrite.

Golgi cell morphology

The axonal and dendritic arbourization within the slice could be recovered for 5 of 12 biocytin filled cells. Cell morphology showed some variability in terms of number and extent of dendrites, but all cells possessed at least one ascending dendrite transversing into the molecular layer and a large axonal arbourisation restricted to the granule cell layer (**Figure 3-3**). Additionally, all cells exhibited spontaneous rhythmic firing in cell-attached recordings (8 ± 2 Hz, n = 5). These features were previously described by Eccles et al. (1967), Palay and Chan-Palay (1974), Dieudonne (1998) and Simat et al. (2007) and have been ascribed to Golgi cells[17]. Therefore all 5 cells were classified as Golgi cells. On average Golgi cells had an ellipsoid soma with the average dimensions of 14 ± 5 μm height (h), 18 ± 6 μm width (w) and 15 ± 5 μm depth (d), measured as the largest extension of the cell body in each dimension, amounting to a volume of 3600 ± 2100 μm^3. The axon was identified based on its thin highly bifurcated (often forming T-junctions) structure. It inhabited a volume of 0.0029 ± 0.0005 mm^3 (h = 196 ± 79 μm, w = 215 ± 79 μm, d = 81 ± 20 μm) and could be traced back to 1-2 (average = 1.4 ± 0.5) initial segment(s) originating from the soma. Remaining structures originating from the soma were usually 0.7-1 μm thick processes which were classified as dendrites. 1-2 (average = 1.6 ± 0.5) primary ascending dendrites originated from the upper or lateral part of the cell body to transverse into the molecular layer and give rise to a extensive net of branchlets that covered a volume of approximately 0.0011 ± 0.0015 mm^3 (h = 170 ± 60 μm, w = 100 ± 55 μm and d = 52 ± 24 μm). In one case an ascending dendrite

[17] Internal solution with high potassium concentration was puffed onto the cell when approaching it. This can increase the excitability of the cell and make it spontaneously active.

gave rise to a lateral branch that terminated within the granule cell layer (**Figure 3-3b**). The ascending dendritic tree in the molecular layer had a three dimensional structure; in contrast to dendritic branching of Purkinje cells and molecular layer interneurons which have a quasi two-dimensional structure perpendicular to the parallel fibre axis. The number of basolateral dendrites varied from 1-4 (average: 2.2 ± 1.1) and they covered an average volume of 0.00010 ± 0.00006 mm^3 (h = 79 ± 39 μm, w = 71 ± 62 μm, d = 22 ± 17 μm). Notably, basolateral dendrites branched rarely and did not show any protrusions like branchlets or spines. The average basolateral dendritic length was 61 ± 15 μm. The morphological data is in good agreement with earlier quantitative morphological analysis of Golgi cells (Dieudonne, 1998). The numbers given here are rough volume estimates, which could be improved in accuracy by reconstructing and analyzing cells with Neurolucida. But this was not deemed necessary for the purpose of the study.

Mossy fibre density

Typically elongated globular structures, thought to be mossy fibre terminals, showed the most intense vGlut-1 staining. However, some non-terminal vGlut-1 positive structures, likely to be mossy fibre axons, were visible (**Figure 3-1a**). Therefore appropriate "thresholding" of images was necessary to investigate properties of mossy fibre terminals in isolation. For this, I thresholded images within a stack using a threshold three times above the average pixel intensity of the image and measured the number and volume of 3D objects in the granule cell layer (see Material and Methods). **Figure 3-4** shows a maximal intensity projection of the image stack containing 3D objects embodying mossy fibre

terminals (each colored differently, right image) and a projection of the original image stack (left image). The volume investigated here had the approximate dimensions h = 160 μm, w = 324 μm, d = 20 μm and contained 521 objects. There was a good correlation between identified objects and mossy fibre terminals. I calculated the density of mossy fibre terminals in the investigated volume which amounted to 500000 terminals per mm^3. Across experiments the density varied from 220000 to 540000 and averaged to 400000 ± 100000 terminals per mm^3. The volume of 3D objects varied from 12-385 μm^3 and averaged to 47.7 μm^3 in this experiment. Across the population terminal volumes varied between 10 and 750 μm^3 and averaged to 46.1 ± 21.2 μm^3 (n = 5). The volume of mossy fibre terminals is likely to be underestimated, since the threshold procedure used to construct 3D objects excludes weak fluorescence signals like the edges of mossy fibre rosettes and weakly stained terminals. Furthermore the analysis did not consider structures that were only partly in the volume of investigation. In fact, more detailed studies of glomerular anatomy suggest an average volume of 100-1000 μm^3 (Eccles *et al.*, 1967; Jakab & Hámori, 1988).

Mossy fibre – Golgi cell contacts

With Golgi cell and mossy fibre terminal morphology defined, I could investigate possible interaction points. Interactions can occur in two different forms: the Golgi cell axon can impinge on a mossy fibre terminal to make a symmetric inhibitory (Gray Type II) synapse onto granule cell dendrites and/or a Golgi cell dendrite can be contacted by a mossy fibre terminal to form an asymmetric (Gray Type I) excitatory synapse. Possible mossy fibre – Golgi cell

contacts were identified as areas of colocalisation, defined as image pixels with fluorescence intensity in both channels above certain threshold values (see Material and Methods). **Figure 3-5a** shows a maximal intensity projection of a biocytin-filled Golgi cell (red) and vGlut-1 stained terminals (green) obtained from a confocal image stack. Overlaid in white are points of fluorescence colocalisation. To distinguish between the two forms of interaction it was necessary to carefully trace back the axon to the initial segment as not to misclassify it as a dendrite. Areas where a dendrite or the cell body colocalised with a mossy fibre terminal were classified as potential mossy fibre – Golgi cell synapses. This cell had an extensive axonal arbour in the granule cell layer originating from the basal part of the cell body and an ascending dendrite transversing into the molecular layer as is typical for Golgi cells. Furthermore the cell had two lateral dendrites remaining in the granule cell layer, of which one was cut at the top of the slice. Mossy fibre terminals colocalised with Golgi cell soma, ascending (within the granule cell layer) and lateral dendrites in six places (indicated by arrows in **Figure 3-5a**). Three of these were on lateral dendrites, one on the ascending dendrite within the granule cell layer and two on the soma. For closer inspection I imaged locations of putative mossy fibre - Golgi cell contact at high magnification (63x objective with 2-3x zoom). **Figure 3-5b-d** portray confocal and volume rendered images of putative synapses on the lateral dendrite (b), the soma (c) and the ascending dendrite (d). The confocal images, which depict a single focal plane, demonstrate a close apposition to the point of intermingling of mossy fibre terminals and respective Golgi cell structure. Thus colocalisation suggested putative sites of synaptic contact. Golgi cell dendrites did not appear to have anatomical specializations like spines to contact mossy

fibre terminals rather the terminal seemed to (partially) wrap around the dendrite so that the neurite passed by or through the mossy fibre rosette – a synaptic connection called "en passage". I examined mossy fibre – Golgi cell contacts in 5 cells and found 3 - 9 putative synaptic contacts located on basolateral dendrites, soma and ascending dendrite within the granule cell layer. The average number of putative mossy fibre – Golgi cell synapses was 6.0 ± 2.5 across 5 cells of which the majority (60%) were located on the basolateral dendrite, 20% on the soma and 20% on the proximal part of the ascending dendrite within the granule cell layer. The average distance of mossy fibre – Golgi cell synapses from the soma was 32 ± 16 μm (range: 20-65 μm) for basolateral dendrites and 59 ± 41 μm (range: 20-143 μm) for ascending dendrites.

But areas of colocalisation representing mossy fibre – Golgi cell synapses accounted only for a small proportion of all contacts. All other contacts were considered to be contacts made by the Golgi cell axon within the mossy fibre rosette. **Figure 3-5e** shows a single plane confocal image and 3D volume representation of a Golgi cell axon ending impinging a mossy fibre terminal. They form a convoluted structure, which appears to have multiple possible interaction points.

To assess what proportion of mossy fibre terminals were contacted by the extensive Golgi cell axon, I counted the number of 3D objects formed by colocalised points and related it to the total number of mossy fibre terminals in this volume (see above). **Figure 3-6** shows a maximal intensity projection of vGlut-1 stained terminals a projection 3D object analysis formed by colocalised

points (in white). Volumes of colocalisation lay within mossy fibre terminals and 93% of mossy fibre terminals comprised volumes of colocalisation. In contrast, the molecular layer which showed vGlut-1 staining of parallel fibres was devoid of such interaction points. Across experiments 93 ± 6% (n = 4) of mossy fibre terminals showed areas of colocalisation with the Golgi cell axon. This means that the axonal arbour of a single Golgi cell contacts almost all mossy fibre rosettes within its extent. The potential error made by falsely including putative mossy fibre – Golgi cell synaptic contacts in this calculation is small (< 3%). Furthermore it is likely that colocalised volumes representing putative mossy fibre – Golgi cell synapses also contain Golgi cell axon endings.

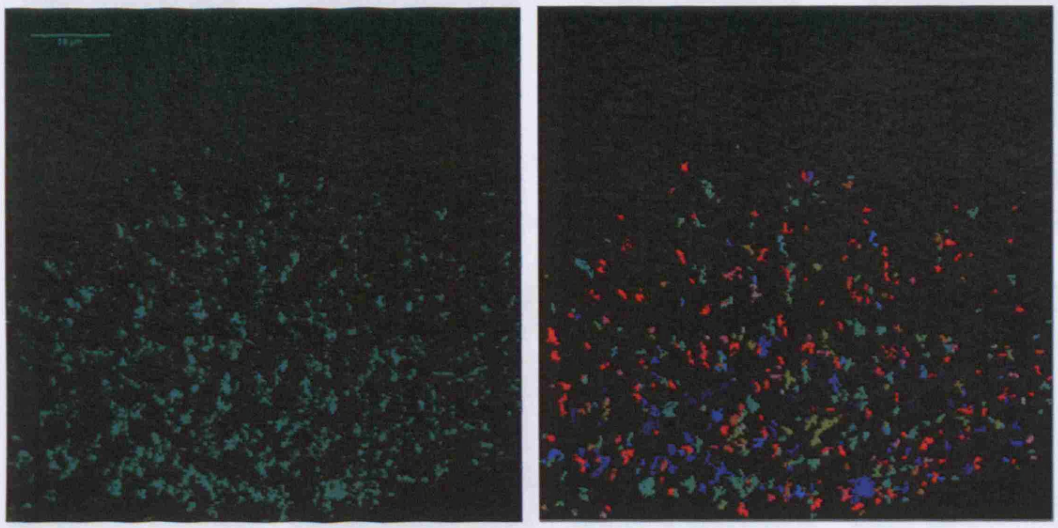

Figure 3-4 Mossy fibre density. Maximal intensity projection of 3D image stack of immunostained vGlut-1 (left) and a z-projection of 3D objects (each object coloured differently, right) detected through a 3D object analysis procedure (see Materials and Methods). There is a good agreement between mossy fibre terminals in the granule cell layer and detected 3D objects representing mossy fibre terminals.

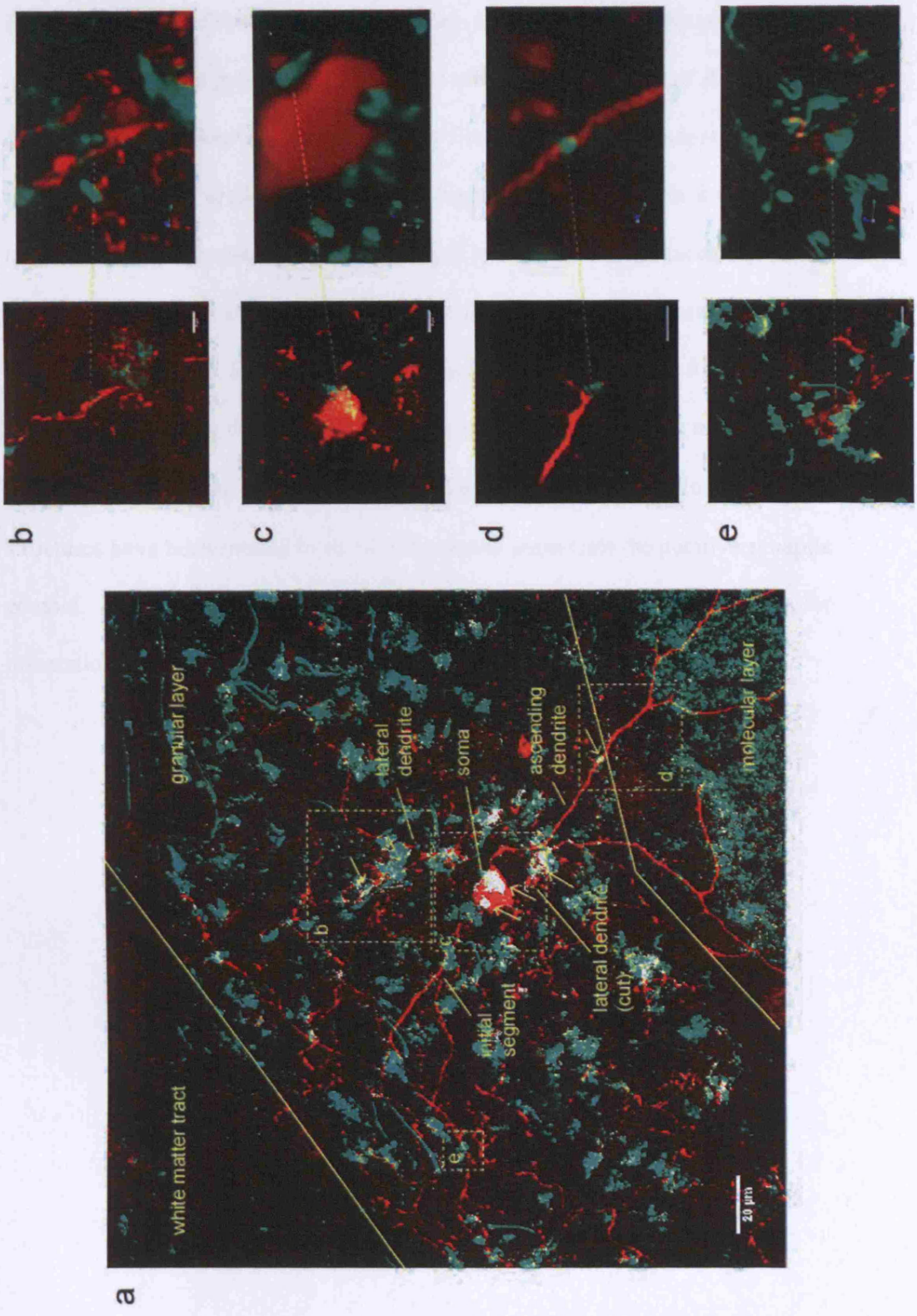
a
white matter tract
granular layer
lateral dendrite
soma
ascending dendrite
molecular layer
b
c
d
e
initial segment
lateral dendrite (cut)
20 µm
b
c
d
e

Figure 3-5 Mossy fibre – Golgi cell contacts *a)* Maximal intensity projection of red (Golgi cell) and green channel (vGlut-1 staining) with points of fluorescence colocalisation in white and putative mossy fibre to Golgi cell synapses indicated by arrows. Boxed areas are depicted at higher magnification in *b-e. b)* High magnification single plane confocal image of lateral dendrite contacted by mossy fibre terminal (left) and 3D volume rendered representation of same location (right). *c)* same as *b* for somatic mossy fibre contact *d)* same as *b* for terminal contacting ascending dendrite. *e)* Golgi cell axon terminal entering a mossy fibre rosette. Scale bars on *b-e* (for images on the left) are 5 μm. Volume rendered structures have been rotated to various degrees to appreciate the putative synaptic contact. Broken yellow lines indicate reference point in both images for orientation.

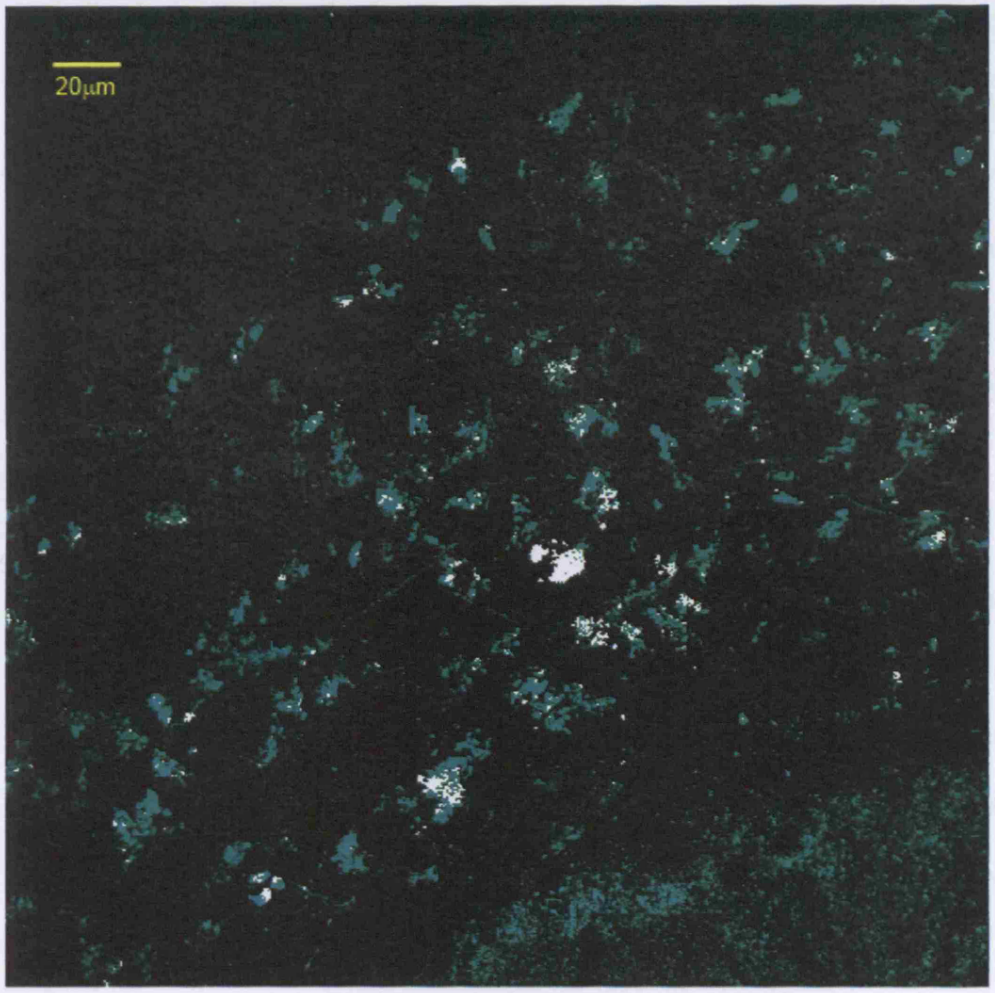

Figure 3-6 Golgi cell axon innervations. Maximal intensity projection of vGlut-1 stained mossy and parallel fibre terminals with points of fluorescence colocalisation with red channel (not shown here) in white. A large proportion of mossy fibre terminals appeared to be colocalised with Golgi cell derived red channel fluorescence. In contrast, for parallel fibres no colocalisation as reported.

3.3 Conclusions

Previous anatomical and computational studies on the granule cell layer have disagreed on the number and location of mossy fibre to Golgi cell synapses. I quantitatively assessed the number of mossy fibre to Golgi cell synapses in the cerebellar granular layer by filling individual Golgi cells with biocytin in rat cerebellar slices and double labeling slices with streptavidin, to visualize Golgi cells, and v-Glut1 antibody to recognize mossy fibre terminals.

Although most mossy fibres express vGlut-1 some terminals also, or exclusively express vGlut-2 and are vGlut-1 negative (Hisano *et al.*, 2002). I estimated, based on images of vGlut-1 and vGlut-2 staining in the granular layer (taken from Hisano *et al.*, 2002) that approximately 20-30% of mossy fibre terminals will not be recognized by the vGlut-1 antibody. The mossy fibre terminal density in the granule cell layer based on vGlut-1 staining was 400000 terminals/mm^3. Corrected for the vGlut-1 negative terminals this amounts to a mossy fibre terminal density of approximately 500000 terminals/mm^3. This estimate agrees with other estimates of glomerular density (660000 terminals/mm^3 not corrected for tissue shrinkage; personal communication with Andrea Lorincz and Zoltan Nusser), but does not account for tissue shrinkage induced by the fixation procedure[18]. The estimated mossy fibre density puts constraints on the maximal number of mossy fibres that can be contacted by a Golgi cell. An estimate of over 200 mossy fibre to Golgi cell synapses proposed by Pellionisz and Szentagathai would require Golgi cell dendrites to inhabit a volume of 0.0002 mm^3. This appears unreasonable considering basolateral dendrites within the

[18] Tissue shrinkage was not assessed quantitavely in this study. A plausible correction factor for shrinkage is 0.5 (personal communication with Andrea Lorincz and Zoltan Nusser).

granule cell layer encompass a volume only half that size and show little branching and no protrusion like branchlets or spines. I estimated the number of putative mossy fibre to Golgi cell synapses via colocalisation analysis to be 6.0 ± 2.5. This number has to be considered as a lower estimate due to the following reasons: (1) Contacts made by vGlut-1 negative mossy fibres were not detected. (2) The signal to noise ratio in the green channel showing vGlut-1 staining typically deteriorated with increasing image depth. This was likely due to insufficient penetration of the anti-vGlut-1 antibody caused by strong fixation of the tissue and absorption of the excitation wavelength by the tissue above. A signal to noise sufficient for colocalization analysis was typically only reached within the top 30 μm of a slice. If the Golgi cell dendritic structure extended deeper into the slice the colocalization analysis missed possible synaptic contacts. (3) The slicing procedure is likely to sever dendrites from the cell body (as seen in **Figure 3-5**). In fact, previous studies of Golgi cell morphology found on average 4 (Dieudonne, 1998) compared to 2.2 basolateral dendrites in this study. Synaptic connections on severed dendrites were missed. Taking these confounding factors into account the total number of mossy fibre – Golgi cell contacts is likely to be around 10. The majority of putative synaptic contacts (60%) were made on basolateral dendrites of Golgi cells. But putative synapses were also made at the cell body and ascending dendrite within the granule cell layer (20% each).

These data complement results made on light and electron microscopic level by Hamori and Szentagothai (1966) as well as Palay and Chan-Palay (1974). Szentagothai (in Eccles et al. 1967) expressed the opinion that mossy fibres

synapse onto Golgi cell basolateral dendrites in large numbers. I found evidence for preferential innervation of basolateral dendrites, but the number of putative contacts appeared to be less than previously proposed. Palay and Chan-Palay show mossy fibre – Golgi cell contacts located at the cell body and proximal dendrites (Palay & Chan-Palay, 1974). Indeed, I found evidence for such a connection, but only a small percentage (20%) of synapses were made at the cell body and for synapses at basolateral neurites no clustering of connections to the proximal dendrite was observed (the average distance between putative synaptic connection and cell body was 32 ± 16 μm with an average dendritic length of 61 ± 15 μm). Whether connections onto somata are specialized synapse *en-marron* (Palay & Chan-Palay, 1974) cannot be decided based on the current data. I also found that a small proportion (20%) of mossy fibres make putative synaptic connections on the proximal ascending dendrites; a finding not described in earlier publications.

Given a glomerular density of 500000 per mm^3 (D_{glom}), a granule cell density of $2.6x10^6$ per mm^3 (D_{GrC}; Eccles *et al.*, 1967) and each granule cell extending 4 dendrites (N_{dend}) the average number of granule cells contacting a single glomerulus can be calculated to ~20 granule cell dendrites with Equation 8.

$$\left(N_{dend/glom} = \frac{D_{GrC} \cdot N_{dend}}{D_{glom}} \right) \qquad \text{(Equation 8)}$$

This agrees with estimates on light microscopic level (Fox, 1967) but is significantly less than the number of 50 granule cell dendrites counted in electromicroscopic reconstructions of simple glomeruli of rat (Jakab & Hámori, 1988). This could be due to a large heterogeneity in glomerular anatomy or an overestimate of the glomerular density due to tissue shrinkage. Mossy fibres

could also make synaptic contacts with Lugaro cells, unipolar brush cells and Golgi cells ("synapse en-marron") without the involvement of granule cells, although this is unlikely to occur in great numbers.

Golgi cells provide synaptic inhibition to surrounding granule cells with their large axonal arbour. Due to the extent of the axon it is thought that a large proportion of surrounding granule cells are inhibited by a single Golgi cell, but this has not been quantified yet. The inhibition takes place in the glomerulus, the structure formed by a mossy fibre terminal making excitatory synapses onto dendrites of tens of different granule cells and Golgi cells. Within this structure Golgi cell axons makes inhibitory synapses onto granule cell dendrites. I related the total number of terminals within an axonal arbour to the number of terminals contacted by the axon of a single Golgi cell and found that 93% of all glomeruli were contacted by the axon. These contacts presumably represented Golgi cell – granule cell synapses within the glomerulus, which mediate synaptic inhibition. This suggested that a single Golgi cell can potentially inhibit all granule cells in its surrounding. But paired Golgi cell – granule cell recordings (Dugue *et al.*, 2005) have shown that the interneuron has an approximately 20% connection probability with surrounding granule cells. This discrepancy can be resolved if a Golgi cell axon contacts only a few granule cell dendrites within a glomerulus. But axonal arbours of Golgi cells overlap (Golgi, 1886; Eccles *et al.*, 1967) and therefore a single glomerulus is likely to be innervated by several interneurons, which potentially ensures direct synaptic inhibition onto many granule cell dendrites within a glomerulus.

Implication of anatomical findings for feed-forward inhibition of granule cells

These anatomical findings have important implications for the role of feed-forward inhibition in granule cell layer processing. A single granule cell receives excitatory input from on average 4 mossy fibres and is inhibited by one or more Golgi cells in its neighborhood. Since a single Golgi cell receives on the order of 10 mossy fibre inputs it is unlikely that granule cell and Golgi cell share the same input fibres. In fact, assuming the 10 inputs the Golgi cell receives are drawn randomly from a larger population of approximately 60 possible mossy fibre-Golgi cell contacts[19] which also provides the four inputs for a particular granule cell, the probability that a granule cell and a Golgi cell are contacted by the same mossy fibre is given by Bayes Law (see equation 9) and amounts to a less than 3%.

$$P(MF-GoC \mid MF-GrC) = \frac{P(MF-GoC)\cdot P(MF-GrC \mid MF-GoC)}{P(MF-GrC)} \quad \text{(Equation 9)}$$

where P(MF-GoC|MF-GrC) is the probability of a mossy fibre contacting a Golgi cell given it already is connected to a granule cell; P(MF-GoC) is the probability of a mossy fibre contacting a Golgi cell $\left(=\frac{10}{60}\right)$; P(MF-GrC|MF-GoC) = the probability that a mossy fibre contacts a granule cell given it is already connected to a Golgi cell $\left(=\frac{4}{60}\cdot\frac{10}{60}\right)$ and P(MF-GrC) the probability of a mossy fibre

[19] Volume spanned by basolateral dendrite, cell body and proximal ascending dendrite (0.0012 mm^3) multiplied by a terminal density of 500000 mm^3

contacting a granule cell $\left(=\frac{4}{60}\right)$. The calculation assumes random connectivity and that each terminal originates from a different mossy fibre.

Since Golgi and granule cell do not seem to share the same input, feed-forward inhibition of granule cells firing is driven by activity in surrounding mossy fibres, similar to lateral inhibition. Feed-forward inhibition in the classical sense (see Chapter 1) will only occur, if mossy fibre population activity is highly correlated. This is conceivable, because mossy fibres innervate the granule cell layer in a fractured somatotopic fashion, which means somatosensory inputs from a certain body area project to the same patch of granule cell layer.

With a granule cell density of 2.6×10^6 cells/mm^3 (Eccles *et al.*, 1967) and an average axonal arbour of 0.00029 mm^3 around 7500 granule cells are within the axonal arbour of a Golgi cell. Since only 20% of these granule cells are directly contacted by one Golgi cell (Dugue *et al.*, 2005), the interneuron will inhibit approximately 1500 granule cells in its surrounding. Therefore on a network level the circuitry offers the possibility for the amplification of the signal transmitted by a relatively small number of mossy fibres (~10) to the inhibition of over thousand granule cells simultaneously. To investigate whether this is realized, synaptic properties like the efficacy of the mossy fibre – Golgi cell synapse have been elucidated in the following chapters.

Chapter Four

4 Identification of mossy fibre – Golgi cell inputs

4.1 Introduction

Golgi cells receive excitatory input from mossy fibres, parallel fibres and potentially climbing fibres. Properties of parallel fibre – Golgi cell synapses have been studied in isolation by electrical stimulation of the molecular layer (Bureau *et al.*, 2000; Misra *et al.*, 2000; Beierlein *et al.*, 2007) and chemical stimulation of the granule cell layer (Dieudonne, 1998). Parallel fibre input has a low efficacy in driving Golgi cell firing (Dieudonne, 1998). In contrast, little is known about the properties of the mossy fibre – Golgi cell transmission, although this connection is thought to mediate Golgi cell feed-forward inhibition of granule cells. Progress in this field has been hampered, because mossy and climbing fibres intermingle in the white matter tract. This makes the unambiguous identification of an input in electrophysiological experiments difficult (Misra *et al.*, 2000). Therefore I investigated properties of synaptic currents elicted by electrical stimulation of the white matter tract to establish criteria that could help distinguish between these inputs. The following experiments were performed in sagittal cerebellar slices of postnatal day twenty-five (P25) rats at temperatures ranging from 34-36°C.

4.2 Results

Identification of Golgi cells

Interneurons of the granule cell layer are a biochemically and morphologically heterogeneous cell population. The majority of interneurons are Golgi cells with ascending dendrites reaching into the molecular layer and descending dendrites and the axon restricted to the granule cell layer (Golgi, 1886; Eccles *et al.*, 1967; Palay & Chan-Palay, 1974). The large majority of Golgi cells (90%) expresses metabotropic glutamate receptor 2 (mGluR2) as a characteristic molecular marker. Golgi cells also have been shown to exhibit spontaneous activity *in vivo* (Edgley & Lidierth, 1987; Van Kan *et al.*, 1993) and *in vitro* (Mitchell & Silver, 2000a; Forti *et al.*, 2006). Deep Lugaro cells have a similar dendritic arbourisation to Golgi cells, but project their axons to the molecular layer or white matter tract and express calretinin as a molecular marker. Nothing is known about their firing properties, but if similar to Lugaro cells, they only become spontaneously active when exposed to serotonin. Other interneuron cell types the unipolar brush cell and Lugaro cells are easily discernable due to their characteristic dendritic brush and bipolar somata, respectively. Initially Golgi cells were distinguished based on their relatively large soma (>15 μm diameter) within the granule cell layer. Subsequent inspection of cell morphology verified the cell type. Cell morphology was visualised after dialysing with a fluorescent dye in the whole-cell patch-clamp configuration by imaging the dendritic arbourisation with bright field fluorescence microscopy (see Materials and Methods). Only cells with ascending dendrites reaching into the molecular layer and basolateral dendrites were classified as Golgi cells (64 of 68 cells, see Chapter 3, (Eccles *et al.*, 1967; Dieudonne, 1998). The axonal arbourisation was

sometimes difficult to discern using bright-field epi-fluorescence. I therefore may have erroneously included a small number of deep Lugaro cells into the experimental group. Spontaneous rhythmic firing – a hallmark of Golgi cells (Edgley & Lidierth, 1987; Mitchell & Silver, 2000a; Forti *et al.*, 2006) - was observed in 83% (53 of 64) of cells. The mean frequency was 9 ± 5 Hz (measured in the loose cell-attached configuration with ACSF in the recording pipette for 38 cells; (Forti *et al.*, 2006). Identified Golgi cells exhibited frequent spontaneous excitatory postsynaptic events, a larger effective cell capacitance (37 ± 14 pF; range 10-74 pF, n = 64) than the surrounding granule cells (< 5 pF) and a relatively low input resistance (R_M = 330 ± 70MΩ).

Comparison of Golgi cell synaptic inputs

Inputs synapsing onto Golgi cells were activated by electrically stimulating the white matter tract (see Material and Methods, Chapter 2). To distinguish between the various fibre types potentially activated, I compared the properties of white matter tract-evoked currents with parallel fibre currents. **Figure 4-1a** and **d** show that both white matter tract and parallel fibre stimulation induced inward currents at -60 mV indicating an excitatory input (chloride reversal potential = -70 mV). Excitatory postsynaptic currents (EPSCs) were blocked by 10-100 μM NBQX confirming they were glutamate receptor mediated. The time between stimulation and the 20% rise of the mean synaptic current was short for both white matter tract and parallel fibre input (1.0 ± 0.1 ms and 1.0 ± 0.4 ms, respectively), consistent with monosynaptic activation. White matter tract stimulation produced EPSCs in Golgi cells with both a fast rise (20-80% rise time = 0.23 ± 0.04 ms) and weighted decay times (τ_{WD} = 1.6 ± 0.5 ms, n = 42, **Figure 4-1a** and **b**). In

contrast, parallel fibre-evoked EPSCs had significantly slower rise (0.5 ± 0.2 ms, $p < 0.05$, $n = 6$) and decay kinetics ($\tau_{WD} = 3 \pm 2$ ms; $n = 6$, $p < 0.05$, **Figure 4-1d** and **e**). Moreover, EPSCs arising from white matter tract stimulation occurred over a narrower time window (80% of events within 190 ± 50 μs; versus 80% of events within 430 ± 270 μs, **Figure 4-1c** and **f**). The distinct kinetics of short latency EPSCs arising from white matter tract and parallel fibre stimulation indicate that they arise from different synaptic inputs.

I next examined whether the properties of white matter tract-evoked EPSC depended on the stimulation voltage. As the stimulus intensity was increased the mean EPSC amplitude increased and the fraction of failures decreased (**Figure 4-1g** and **h**). However, the shape of the EPSCs (**Figure 4-1g**, inset) remained the same, indicating that the increase in EPSC size was due to the recruitment of conductances with similar kinetics. The initial step-like relationship between EPSC amplitude and stimulus voltage suggests that at low voltages a single fibre is activated, as previously observed for mossy fibre to granule cell synaptic connections (Silver *et al.*, 1996b). Minimal stimulation which is likely to represent single fibre activation exhibited a 22 ± 20% failure probability and a mean EPSCs amplitude of -66 ± 26 pA ($n = 42$, **Figure 4-2a**). Slowly rising low amplitude currents reminiscent of spillover currents at the mossy fibre – granule cell synapse (DiGregorio *et al.*, 2002) were observed in 12% of cells (see Material and Methods, 5 of 42). **Figure 4-2b** shows a representative example. Spillover-like currents together with transmission failures contributed 14.4% to the total charge carried by the mean EPSC at -60 mV in this cell. Across the subset of cells that showed slowly rising and decaying currents, spillover

contributed 32% of the total EPSC charge. The weighted decay in these cells was 2.5 ± 0.4 ms, significantly different from cells showing no spillover currents (1.4 ± 0.5 ms, n = 35; $p < 0.05$, t-test). Furthermore in 22% (10 of 42) of recordings a second longer latency (>2 ms) EPSC component was observed during high voltage white matter tract stimulation (see **Figure 4-2b**, arrow). The kinetics of this late component were similar to parallel fibre-evoked events (20-80% rise time = 0.4 ± 0.1 and τ_{WD} = 2.3 ± 0.03 ms, $p > 0.3$, n = 3), consistent with the recruitment of a disynaptic parallel fibre input.

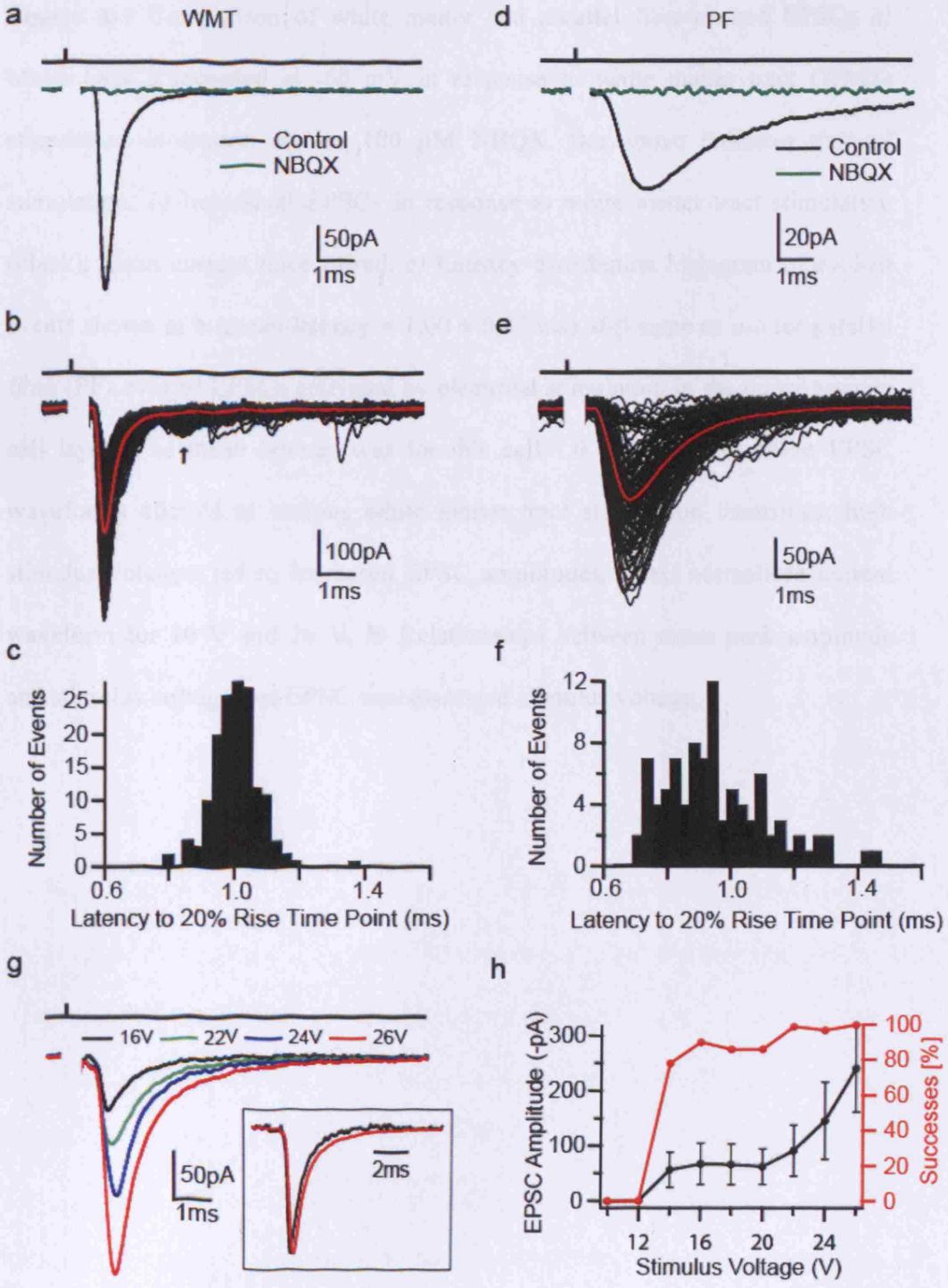
a
WMT
Control
NBQX
50pA
1ms
d
PF
Control
NBQX
20pA
1ms
b
100pA
1ms
e
50pA
1ms
c
Number of Events
Latency to 20% Rise Time Point (ms)
f
Number of Events
Latency to 20% Rise Time Point (ms)
g
16V
22V
24V
26V
50pA
1ms
2ms
h
EPSC Amplitude (-pA)
Successes [%]
Stimulus Voltage (V)

Figure 4-1 Comparison of white matter and parallel fibre-evoked EPSCs *a)* Mean EPSCs recorded at -60 mV in response to white matter tract (WMT) stimulation in control and in 100 µM NBQX. Bar above indicates time of stimulation. *b)* Individual EPSCs in response to white matter tract stimulation (black); mean current trace in red. *c)* Latency distribution histogram of evoked events shown in b (mean latency = 1.00 ± 0.07 ms). *d-f)* same as *a-c* for parallel fibre (PF) evoked EPSCs activated by electrical stimulation in the upper granule cell layer. The mean latency was for this cell 1.0 ± 0.2 ms. *g)* Mean EPSC waveforms elicited at various white matter tract stimulation intensities: high stimulus voltages led to increased EPSC amplitudes; inset: normalised current waveform for 16 V and 26 V. *h)* Relationships between mean peak amplitude and stimulus voltage and EPSC successes and stimulus voltage.

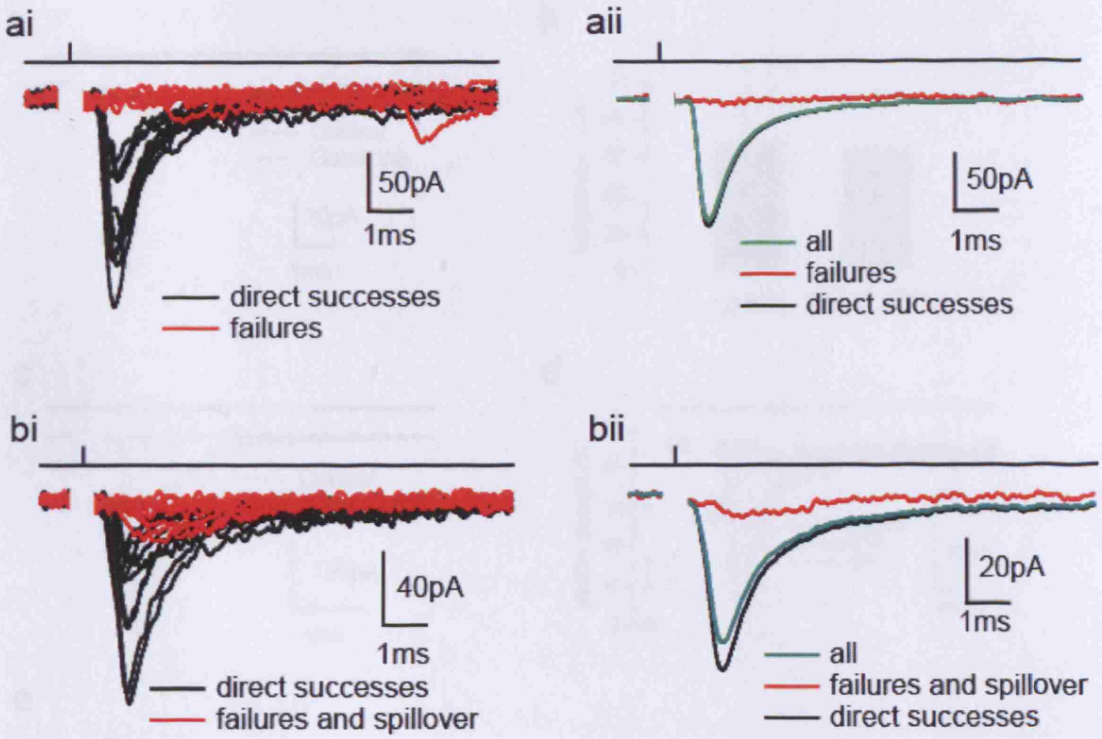

Figure 4-2 Spillover like currents in subset of cells. *ai)* shows individual failures (red) and successes (black) in response to putative single fibre stimulation for a cell representing the majority of Golgi cell responses *aii)* Average failures, success and overall current. bi) In subset of cells (5 out of 42) slowly rising low amplitude currents reminiscent of mossy fibre – granule cell spillover currents were observed. Slow rising current and failures (red) and direct successes (black). *bii)* Average spillover-like current (grouped with failures in red) shows that this component contributes to the overall EPSC charge. Also represented is the average overall current (green) and average of successes (black).

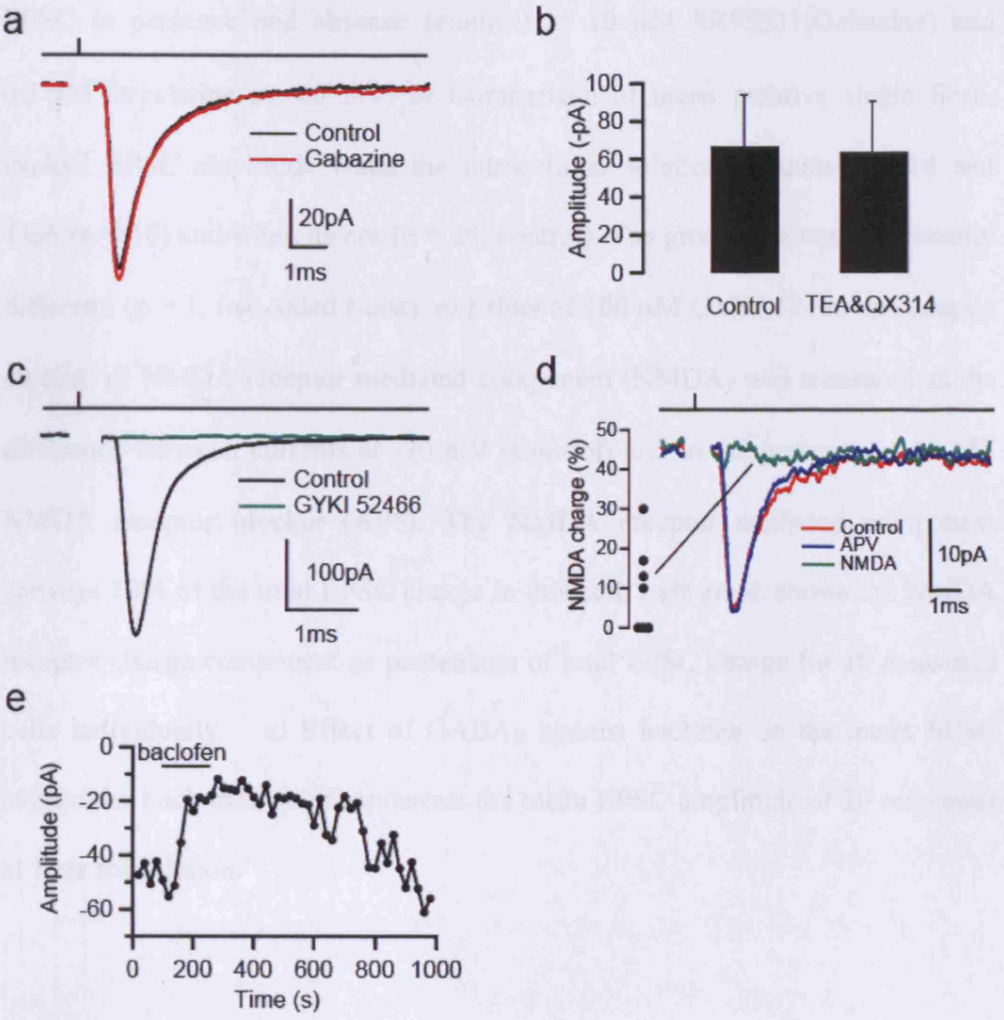
a
Control
Gabazine
20pA
1ms
b
Amplitude (-pA)
100
80
60
40
20
0
Control
TEA&QX314
c
Control
GYKI 52466
100pA
1ms
d
NMDA charge (%)
50
40
30
20
10
0
Control
APV
NMDA
10pA
1ms
e
baclofen
Amplitude (pA)
0
-20
-40
-60
0
200
400
600
800
1000
Time (s)

Figure 4-3 Pharmacological profile of white matter-evoked EPSCs *a)* Mean EPSC in presence and absence (control) of 10 μM SR95531(Gabazine) and 0.3 μM strychnine at -60 mV. *b)* Comparison of mean putative single fibre-evoked EPSC amplitude when the intracellular solution contains QX314 and TEA (n = 10) and when its not (n = 29, control). The groups are not significantly different. (p = 1, two-sided t-test). *c)* Effect of 100 μM GYKI 52466 on synaptic current. *d)* NMDA receptor mediated component (NMDA) was measured as the difference between currents at -30 mV (Control) and in the presence of 10 μM NMDA receptor blocker (AP5). The NMDA receptor mediated component conveys 13% of the total EPSC charge in this cell. Left graph shows the NMDA receptor charge component as percentage of total EPSC charge for all measured cells individually. *e)* Effect of $GABA_B$ agonist baclofen on the mean EPSC amplitude. Each data point represents the mean EPSC amplitude of 20 responses at 1 Hz stimulation.

Pharmacological signature

Bath application of GABA and glycine receptor blockers had no effect on the mean white matter-evoked EPSC during putative single fibre stimulation (n = 7, **Figure 4-3a**), nor did the incorporation of the potassium and sodium channel blockers, QX314 and TEA, in the patch-pipette (n = 10, **Figure 4-3b**) supporting the notion that the synaptic response was solely mediated by glutamate receptors and excluding the direct activation of Golgi cell axons. I wanted to investigate whether EPSCs had a pharmacological profile that could help distinguish between mossy, climbing and parallel fibre stimulation. Parallel fibre EPSCs in Golgi cells exhibit a kainate- and prominent NMDA receptor-mediated component (Bureau *et al.*, 2000; Misra *et al.*, 2000). But white matter-evoked EPSCs were fully blocked by the selective AMPA receptor blocker GYKI52466, suggesting little to no activation of kainate receptors even at high stimulus intensities when multiple fibres were recruited (**Figure 4-3c**). The contribution of NMDA receptors to the EPSC was tested by bath applying 10 μM AP5, while voltage-clamping the Golgi cell at -30 mV. AP5 did not change the EPSC in 3 out of 7 cells; in the remaining cells the overall EPSC charge was reduced by 18 ± 11%. This indicates that NMDA receptors contribute little to the EPSC waveform and currents remain fast at depolarised potentials (τ_{WD} = 1.9 ± 0.7 ms at -30 mV, n = 7, $p > 0.2$, paired t-test, **Figure 4-3d**). Since I did not observe a kainate nor prominent NMDA receptor mediated component it appeared unlikely that white matter-evoked EPSCs originated from parallel fibre activation.

I also tested the effect of $GABA_B$ receptor agonist baclofen. Baclofen acted on metabotropic GABA receptors on mossy fibres to reduce their apparent release

probability. This leads to a reduction in average EPSC amplitude in granule cells (Mitchell & Silver, 2000a) in response to mossy fibre stimulation. $GABA_B$ receptors have also been reported presynaptically on parallel fibres (Batchelor & Garthwaite, 1992), but climbing fibre synaptic transmission was not unaffected by baclofen application (Hashimoto & Kano, 1998). Bath application of 100 μM baclofen reversibly induced a ~40% reduction in EPSC peak response which correlated with an increase in response failures (n = 3, **Figure 4-3e**). This suggested that white matter stimulation led to mossy fibre rather than climbing fibre activation.

In conclusion, the pharmacological signature of the EPSCs suggests that the monosynaptic excitatory response in the Golgi cell induced by white matter stimulation originates from mossy fibres rather than parallel or climbing fibres.

Comparison of short-term plasticity behaviours

Synaptic connections made by parallel fibres (to Golgi cells and Purkinje cells), climbing fibres (to Purkinje cells) and mossy fibres (to granule cells) exhibit distinct short-term plasticity (STP) characteristics. White matter tract-evoked EPSCs onto Golgi cells exhibited little STP during 5 pulse 25 Hz stimulus trains (amplitude ratio EPSC5/EPSC1 = 0.95 ± 0.27, n = 14, **Figure 4-4ai**). Even when the stimulation frequency was increased to 100 Hz the EPSC only depressed by 22 ± 17% during 10 stimuli ($p < 0.05$; n = 10, Figure 4-4**aii**). STP behaviour was unchanged when increasing the stimulus strength from putative single fibre to multile fibre stimulation suggesting that the population of fibres recruited have the same STP characteristics (Figure 4-4**b**). This STP behaviour contrasted with

the 50% facilitation observed for 5 pulse 25 Hz parallel fibre stimulation ($n = 6$, $p < 0.05$, two-factor ANOVA on 25 Hz white matter tract versus parallel fibre, Figure 4-4**c**), consistent with previous studies of the parallel fibre input (Bureau *et al.*, 2000). The STP characteristics of white matter EPSCs are also distinct from climbing fibres to Purkinje cell transmission which depresses profoundly (Llano *et al.*, 1991; Silver *et al.*, 1998) but is reminiscent of the presynaptic component of mossy fibre to granule cell transmission which depresses little during high frequency stimulation (Saviane & Silver, 2006). The functional properties of white matter tract-evoked EPSCs are therefore consistent with mossy fibre rather than parallel fibre or climbing fibre input.

Mapping of synaptic activity onto Golgi cell morphology

Because of the segregation of fibre inputs onto the Golgi cell morphology (parallel fibres onto ascending dendrites in the molecular layer, mossy fibres predominantly onto basolateral dendrites but also soma and ascending dendrites of Golgi cells in the granule cell layer and climbing fibres potentially onto the cell's soma) I sought to map the synaptic input evoked by white matter stimulation onto the Golgi cell morphology, thereby identifying the fibre type stimulated. To achieve this, I patched Golgi cells with a pipette solution containing the high affinity calcium indicator OGB-1 to sense calcium influx upon synaptic activation. In voltage-clamp recordings I ensured that white matter stimulation led to the recruitment of 1-2 fibres. I then imaged various parts of the fluorescent cell with a CCD camera while stimulating the white matter tract. A comparison of the obtained images before and during stimulation revealed sites of calcium entry upon stimulation. When series resistance compensation was

active localized increases in calcium were only occasionally observed on the descending dendrite typically distal to the cell body, but in the current-clamp configuration I observed wide spread increase in Ca^{2+} indicator fluorescence reliably. Since NMDA receptor contribution to the synaptic current was small, I hypothesized that the source of calcium influx was via voltage-gated calcium channels (VGCCs), which were activated by EPSCs only if they escaped voltage-clamp at the soma. Therefore all following Ca^{2+} imaging experiments were performed with series resistance compensation disabled to induce poor voltage-clamp conditions which allows localized activation of voltage-activated calcium channels.

Figure 4-5a shows a 2D projection of a Golgi cell manually reconstructed from a montage of fluorescence images taken with a cooled CCD camera at different focal planes (e.g. **Figure 4-5b**). The three fluorescent images in **Figure 4-5b** show part of the ascending dendrite (top), soma and basal dendritic arbour (below). **Figure 4-5c** shows the fluorescent change during white matter tract stimulation for the same regions. In this cell, the fluorescence ($\Delta F/F$) and therefore calcium concentration, increased in one of the basal dendrites. In cells where calcium changes were detectable (7 out of 11), white matter tract stimulation induced local calcium changes ($\Delta F/F = 0.31 \pm 0.29$) in descending or lateral dendrites of Golgi cells within the granular layer but never in the ascending dendrites or soma. Perfusion of 100μM NBQX and 10μM AP5 fully and reversibly blocked both the white matter tract-evoked EPSCs and the calcium signal confirming their synaptic origin ($n = 7$). The lack of any calcium signals from the ascending dendrites was not due to an inability of the ascending

dendrites to respond, because robust calcium signals were observed in the ascending dendrite during molecular layer stimulation (**Figure 4-6**; n = 3).

To investigate the source of calcium entry I perfused 100 μM $NiCl_2$, a non-specific blocker of T-Type voltage-gated calcium channels (VGCCs). $NiCl_2$ blocked the calcium signal fully. Therefore a role of VGCCs in mediating the calcium signal was likely. It is worth noting that the large volume of the cell body may dilute somatic calcium influx and hence reduce the amplitude of somatic calcium transients. This could preclude detection of synaptic events at the soma. Nevertheless, the spatial resolution of this technique allowed the localisation of synaptically induced calcium transient to basolateral dendrites in most cases and thus demonstrated that white matter stimulation led to activation of synaptic connections on Golgi cell basolateral dendrites, where mossy fibres make synaptic connections.

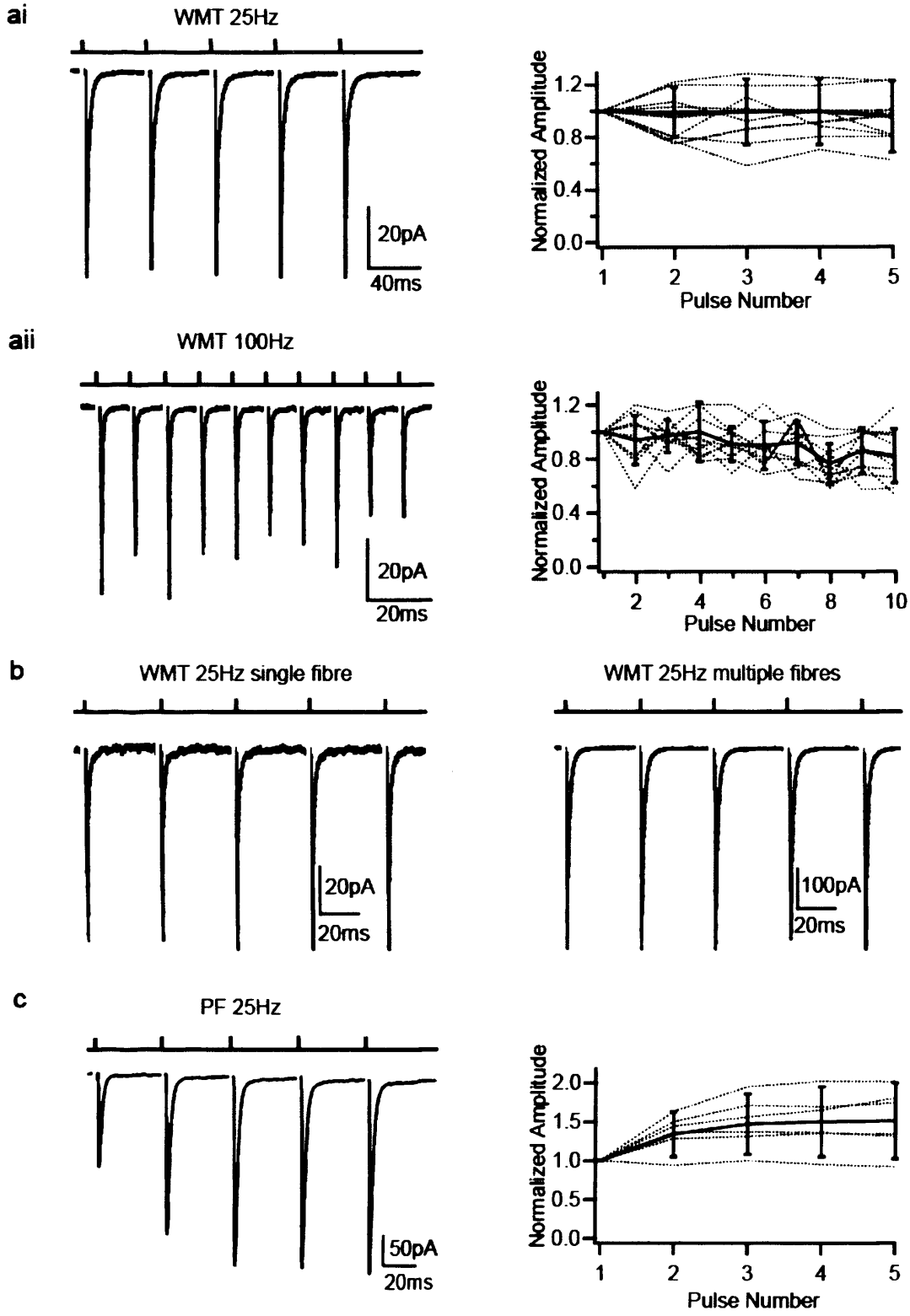
ai
WMT 25Hz
20pA
40ms
Normalized Amplitude
1.2
0.8
0.4
0.0
1
2
3
4
5
Pulse Number
aii
WMT 100Hz
20pA
20ms
Normalized Amplitude
1.2
0.8
0.4
0.0
2
4
6
8
10
Pulse Number
b
WMT 25Hz single fibre
20pA
20ms
WMT 25Hz multiple fibres
100pA
20ms
c
PF 25Hz
50pA
20ms
Normalized Amplitude
2.0
1.5
1.0
0.5
0.0
1
2
3
4
5
Pulse Number

Figure 4-4 Short-term plasticity of white matter tract and parallel fibre-evoked EPSCs *ai*) Left panel shows averaged evoked EPSCs in response to 5 white matter tract (WMT) stimulus pulses with 40 ms interval (25 Hz). Right panel shows normalized EPSC amplitudes for individual cells (dotted), and population mean (n = 14, solid line). The peak amplitudes of evoked events were normalized for the first peak. *aii*) same as *ai* for 10 stimuli at 100 Hz. *b)* STP behaviour of white matter tract-evoked EPSC in the same cell for low (left) and high (right) stimulus intensity at 25 Hz. *c*) Parallel fibre (PF) EPSCs evoked by granular layer stimulation. 5 pulses at 25 Hz as for panel *ai*. Right panel shows normalized parallel fibre EPSC amplitude for individual cells (dotted), and population mean (n = 6, solid line). Vertical error bars denote SD.

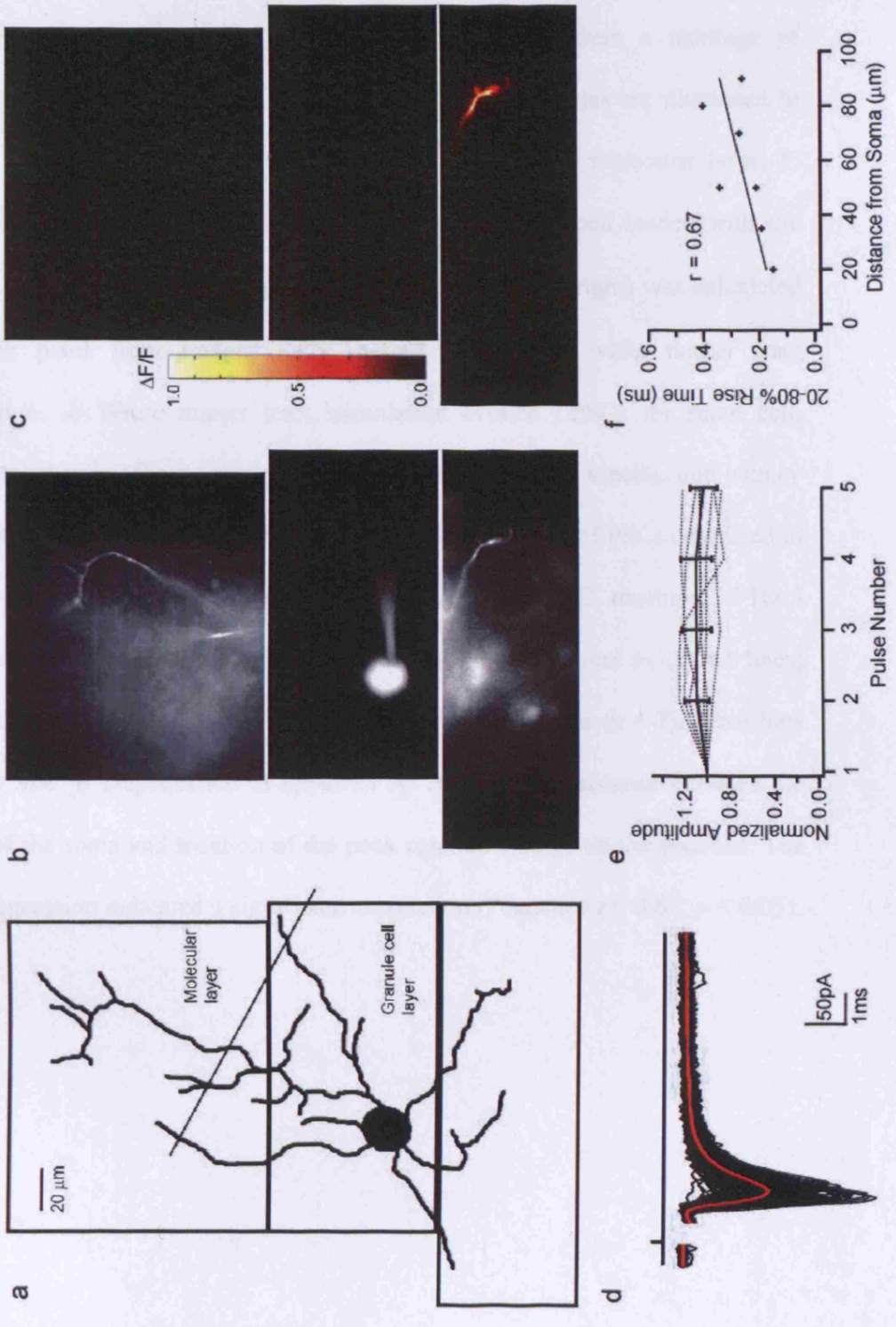
a
Molecular layer
Granule cell layer
20 µm
b
c
ΔF/F
1.0
0.5
0.0
d
50pA
1ms
e
Normalized Amplitude
Pulse Number
f
20-80% Rise Time (ms)
r = 0.67
Distance from Soma (µm)

Figure 4-5 Calcium imaging of Golgi cell morphology during white matter stimulation *a)* Drawing of a Golgi cell reconstructed from a montage of fluorescent images acquired in various focal planes (examples are illustrated in *b*). The line indicates the border between the granular and molecular layer. *b)* Fluorescent images (one focal plane) of the same Golgi cell loaded with the calcium indicator OGB-1. *c)* $\Delta F/F$ (pseudocolour scale on right) was calculated for each pixel from images taken before and during white matter tract stimulation. *d)* White matter tract stimulation evoked EPSCs for same cell. Individual currents shown in black and mean in red. Current kinetics and latency distribution were indistinguishable from putative mossy fibre EPSCs described in **Figure 4-1**. *e)* EPSC amplitude, normalized to the 1st EPSC, during a 25 Hz 5 pulse white matter tract stimulation (individual cells indicated as dotted lines) from cells that exhibited Ca^{2+} signal on descending dendrites (n = 7). Error bars indicate SD. *f)* Dependence of mean EPSC rise time on distance between the centre of the soma and location of the peak calcium change on the dendrite. The linear regression indicated a significant correlation (Pearson's $r = 0.67$, $p < 0.05$).

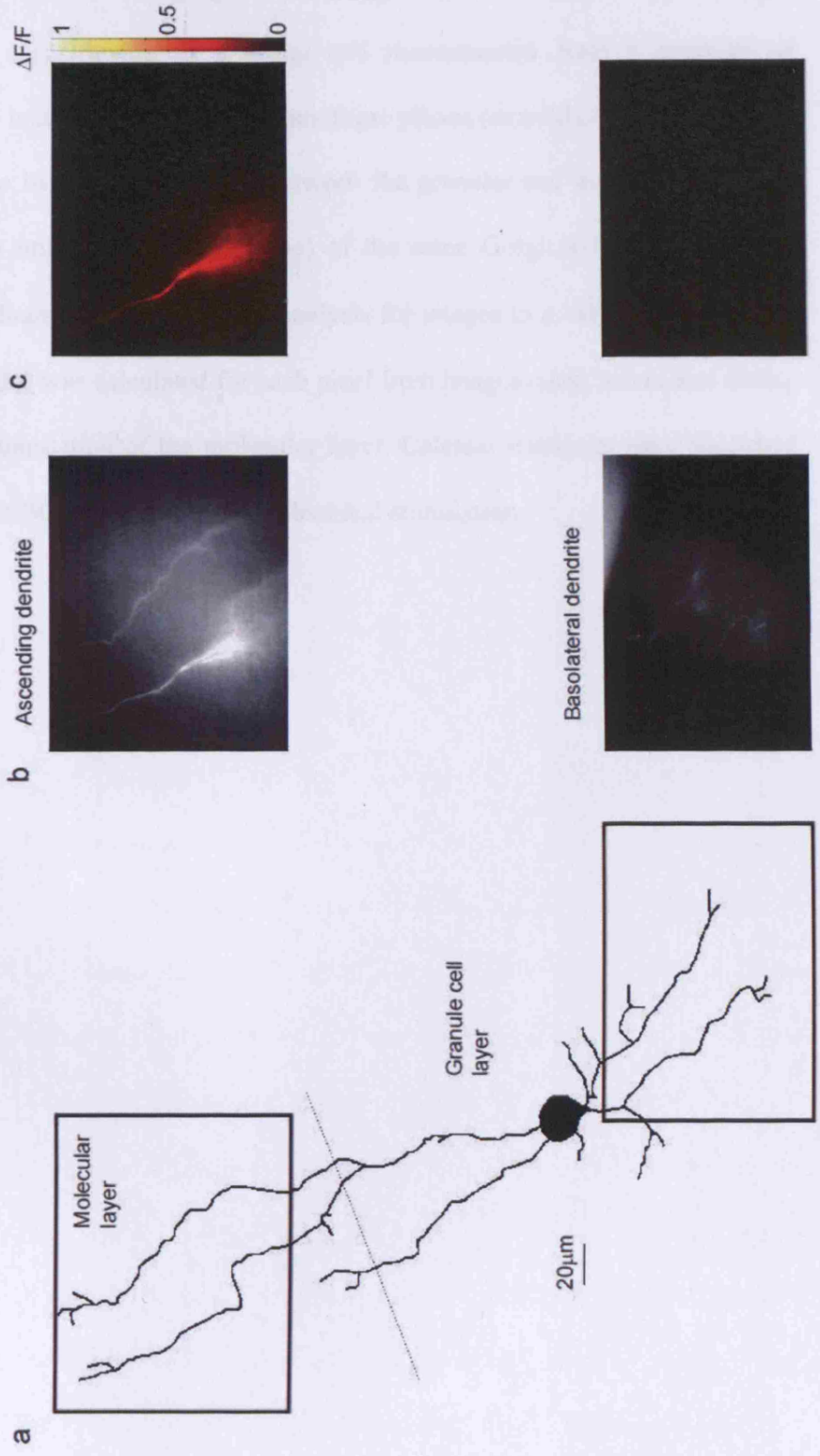
ΔF/F
1
0.5
0
c
b
Ascending dendrite
Basolateral dendrite
a
Molecular layer
Granule cell layer
20µm

Figure 4-6 Calcium imaging in ascending dendrites during molecular layer stimulation *a*) Drawing of a Golgi cell reconstructed from a montage of fluorescent images acquired in various focal planes (examples are illustrated in *b*). The line indicates the border between the granular and molecular layer. *b*) Fluorescent images (one focal plane) of the same Golgi cell loaded with the calcium indicator OGB-1. *c*) ΔF/F analysis for images in *c*. ΔF/F (pseudocolour scale on right) was calculated for each pixel from images taken before and during electrical stimulation of the molecular layer. Calcium transients were abolished in 100 μM NBQX ruling out direct electrical stimulation.

4.3 Conclusions

Although there is anatomical evidence for the existence of mossy fibre synapses onto Golgi cells this connection has not been studied functionally, despite its potential relevance for granule cell layer processing. Golgi cells receive excitatory input from mossy, parallel and potentially climbing fibres. But the anatomy of the cerebellar preparation makes unambiguous fibre stimulation difficult and a functional connection has only been demonstrated for the parallel fibre input (Dieudonne, 1998). I conducted a series of experiments to establish criteria which enable identification of the mossy fibre input onto Golgi cells. For this, white matter-evoked events were compared with parallel fibre-evoked EPSCs. The outcome shows significant differences between the two inputs in terms of current kinetics, pharmacology, short-term plasticity and synaptic localization. Therefore granule cell axons (parallel fibres) could be excluded as the source of white matter-evoked EPSCs. Because the evidence for climbing fibre input onto Golgi cells is scarce and it is not clear whether a functional connection exists at all (Ekerot & Jorntell, 2001) I could not conduct a direct comparison with white matter-evoked events, but pharmacology and short-term plasticity of white matter-evoked EPSCs are very different from features of climbing fibre to Purkinje cell transmission. Additionally, multiple fibres eliciting similar current kinetics and STP were recruited by white matter stimulation at a single location. This is unlikely to be due to the activation of multiple climbing fibres synapsing onto Golgi cells because climbing fibre innervation is scarce in the granule cell layer (Crepel *et al.*, 1980). In conclusion, the most likely source for white matter-evoked EPSCs is the activation of mossy fibres, although climbing fibre activation cannot be completely ruled out. The

results suggest that selective activation of mossy fibre to Golgi cell synapses is possible and allows the examination of mossy fibre inputs in isolation. Immunohistochemical experiments (Chapter 3) and Ca^{2+}-imaging indicates that these synapses are preferentially located on the basolateral dendrites of Golgi cells. The evoked synaptic currents occur within a narrow latency window, have remarkably fast kinetics and show little short-term plasticity in response to trains of stimuli. Surprisingly, the overall time course of most evoked EPSCs at the mossy fibre – Golgi cells connection is significantly faster than mossy fibre-evoked EPSCs in cerebellar granule cells (τ_{WD} = 1.4 ms vs 2.9 ms; DiGregorio *et al.*, 2002). The prominent slow current component of the mossy fibre – granule cell EPSC decay, which is mediated by glutamate spillover (DiGregorio *et al.*, 2002), was only observed at few connections and was smaller at mossy fibre – Golgi cell synapses even though these two connections are made within the same glomerular structure (Eccles *et al.*, 1967). The lack of EPSC depression during trains is likely to arise from the rapid reloading of release ready vesicles from a large releasable pool in the mossy fibre terminal (Saviane & Silver, 2006) and an apparent lack of receptor desensitization in comparison to granule cell AMPA receptors (DiGregorio *et al.*, 2007).

Chapter Five

5 Effect of mossy fibre input on Goigi cell firing

5.1 Introduction

Golgi cells in rats are spontaneously active *in vivo* and in the slice preparation. Many other cells involved in motor coordination, e.g. deep cerebellar nuclei neurons, Purkinje cells, interneurons in the spinal cord and the cerebellar molecular layer also process synaptic input on the background of autorhytmic firing. However, little is known about how spontaneous activity interacts with synaptic inputs and how this influences the neuron's spiking behaviour. Here I have investigated the effect of mossy fibre excitation on Golgi cell firing to understand the interaction between intrinsic activity and excitatory synaptic input in general, as well as to provide information on feed-forward excitation of Golgi cells and its role in granule cell layer processing.

5.2 Results

To investigate the effects of mossy fibre excitation on Golgi cell firing I used the non-invasive loose cell-attached (LCA) recordings in order to prevent disruption of the internal milieu. 83% of cells showed spontaneous rhythmic firing with a mean frequency of 9 ± 5 Hz (see Chapter 4).

Mossy fibre-evoked Golgi cell action potential resets spontaneous rhythmic firing

Figure 5-1a shows a LCA recording trace from a Golgi cell that exhibited spontaneous rhythmic firing at 12 Hz. Single-pulse stimulation of the mossy fibre input induced an action potential soon after the onset of the stimulus. Action potentials induced by white matter tract stimulation were blocked in the presence of 10-100 μM NBQX confirming their synaptic origin and ruling out direct activation of the Golgi cell axon. The peri-stimulus time histogram in **Figure 5-1b** shows that mossy fibre stimulation induced a Golgi cell action potential that was time locked to the stimulus. Mossy fibre-evoked action potentials occurred in a narrow time window, but entrainment of subsequent spikes was variable across cells. Records were ordered according to the spike time of the action potential preceding the stimulus in the raster plot in **Figure 5-1c**. The plot shows that the stimulus was ineffective in triggering an action potential when a spontaneous action potential occurred shortly before. To understand how the MF input affected Golgi cell rythmicity as a function of stimulus timing we calculated the phase-response curve for each cell (see Materials and Methods). **Figure 5-1d** shows the phase-response averaged over 21 cells for the 1st (solid line) and 2nd (broken line) action potential after the stimulus as a function of stimulus phase. A phase response of 0 indicates that the stimulus had no effect on the spike timing of subsequent spikes, as seen for the 2nd action potential after stimulation. A value greater 0 implies a phase advance, which is observed for the 1st action potential after stimulation when the stimulation phase was > 0.2. The two phase response curves are statistically significantly different ($p < 0.0001$;

single factor ANOVA). This implies that the phase of spontaneous firing can be reset for stimulation phases greater 0.2.

Thus the probability of mossy fibre input eliciting a spike appeared to depend on the time since the preceding spike. To quantify this further I used a paired-pulse protocol with variable latency to the second stimulus (**Figure 5-1e**). The second mossy fibre stimulus achieved a 50% probability in triggering an action potential only after an interval of 52 ± 29 ms (range 20-120 ms, n = 9) following the initial spike. This value was very similar to the time during which mossy fibre stimulation was ineffective in producing an action potential after a spontaneous spike ($p > 0.9$, paired t-test, n = 6). As the interval approached the spontaneous inter-spike interval the probability of evoking a spike increased (**Figure 5-1e, f**). Since the mossy fibre inputs exhibited little short-term depression, even at high stimulus frequencies, this relative refractory period is likely to be due to the intrinsic properties of the Golgi cell. These results show that the feed-forward excitatory mossy fibre input onto Golgi cells can reset the spike timing and thus the phase of the Golgi cell firing pattern, but that the transmission reliability depends on the timing of the input with respect to the phase of the spontaneous activity.

Action potential precision at low and high mossy fibre firing frequencies

Action potentials evoked by low frequency mossy fibre stimulation had a mean latency across cells of 1.1 ± 0.4 ms (n = 35) and exhibited remarkably little temporal jitter (**Figure 5-2a, b**). Their precision, defined as the standard

deviation (SD) of action potential times, was 200 ± 120μs (n = 35). This precision was not due to strong stimulation since there was no correlation between SD and action potential probability across cells (**Figure 5-2c**). But, when comparing the precision at different action potential probabilities in individual cells a weak (Pearson's r = -0.28) but significant correlation was evident ($p < 0.05$, n = 9, t-test on fractional change). On average action potentials were evoked in 52 ± 21% of trials across 35 cells. These results show that the mossy fibre - Golgi cell synapse can achieve a greater precision in EPSP-spike coupling than has been reported for other inhibitory interneurons (Fricker & Miles, 2000; Galarreta & Hestrin, 2001; Carter & Regehr, 2002).

To examine whether the precision in EPSP-spike coupling was maintained during trains of mossy fibre input, I examined the action potential precision in response to 10 -100 Hz stimulation trains. The spike raster plots in **Figure 5-2d** and **e** show action potential evoked by 10 and 100 Hz mossy fibre stimulation. Golgi cells fired in a brief time window following the stimulus. Analysis of the spike jitter in response to the 1st and consecutive stimuli showed that spike latency distributions did not change during the train (KS test $p > 0.9$ for 10 and 100 Hz, n = 6) indicating that spike precision was maintained. Above a 25 Hz stimulation frequency both the mean values of the SD and the absolute latency of evoked action potentials increased to 0.4 ± 0.2 ms (**Figure 5-2f**) and 2.0 ± 0.2 ms, respectively (data not shown). This is likely to be due to a reduction in Golgi cell excitability after high frequency stimulation as a decline in spontaneous firing was observed (0.4 ± 0.4 Hz after 100 Hz mossy fibre stimulation; $p < 0.05$; n = 5; paired t-test). The probability of an action potential occurring on a

particular trial depended on both the initial probability and on the time since the last spike occurred as expected from the relative refractory period. Thus, at stimulation frequencies of 1 Hz and 10 Hz the action potential probability did not change during a train. However, when the frequency was increased to 100 Hz the reliability dropped from 51 ± 31% on the first spike to approximately 20% during the rest of the train (single-factor ANOVA $p < 0.01$, **Figure 5-2g**). Accordingly, during low frequency mossy fibre stimulation (1-10 Hz) there was little change in the Golgi cell firing rate from the baseline firing rate of 6 ± 3 Hz ($n = 5$). Above 10 Hz mossy fibre stimulation frequency the Golgi cell firing increased sub-linearly to a saturated level of 17 ± 12 Hz ($n = 5$) at 100 Hz (**Figure 5-2h**). These results show that mossy fibre input can reset Golgi cell firing with high precision over a wide range of input frequencies, but mossy fibre stimulation only weakly modulated the mean Golgi cell firing rate due to the presence of a relative refractory period during which excitability is reduced.

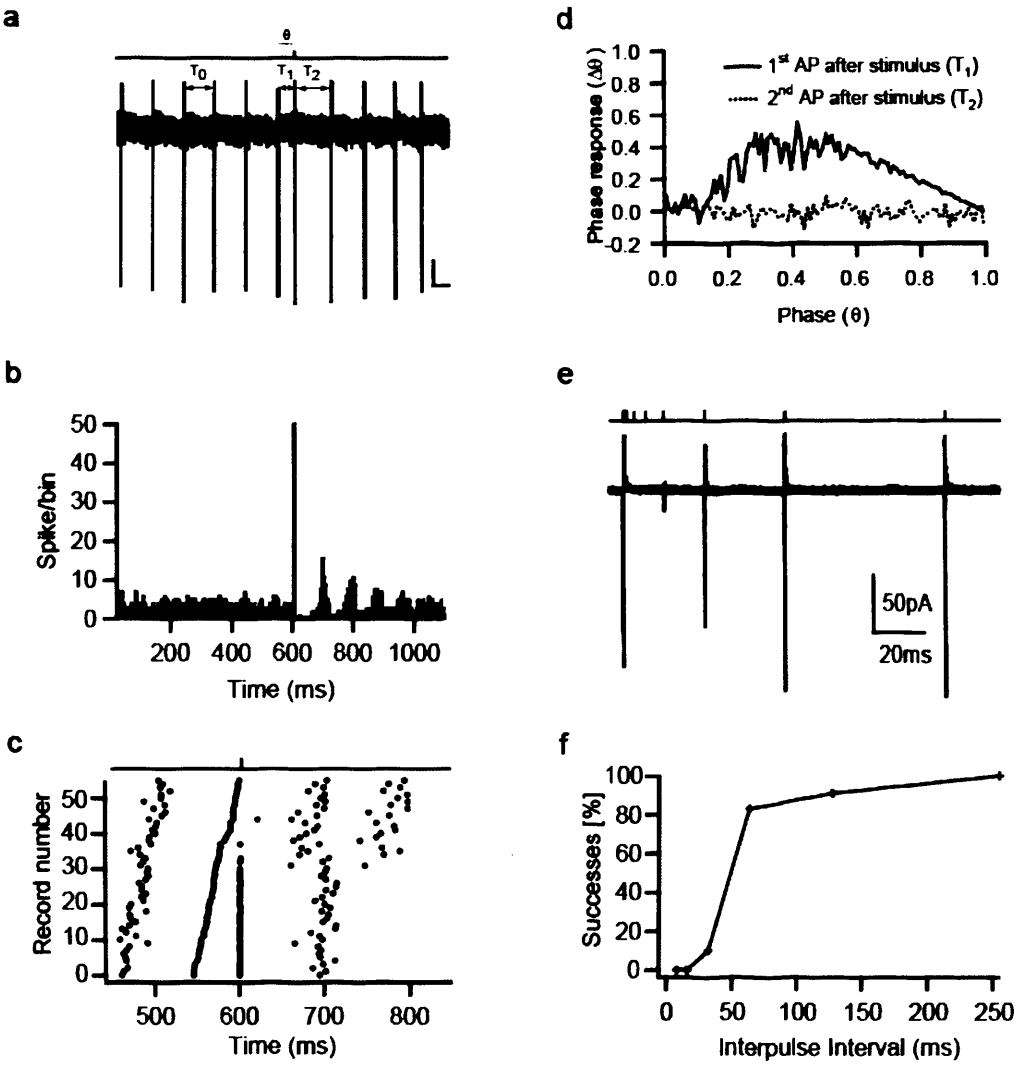
a
θ
T0
T1
T2
L
b
Spike/bin
50
40
30
20
10
0
200
400
600
800
1000
Time (ms)
c
Record number
50
40
30
20
10
0
500
600
700
800
Time (ms)
d
Phase response (Δθ)
1.0
0.8
0.6
0.4
0.2
0.0
-0.2
1st AP after stimulus (T1)
2nd AP after stimulus (T2)
0.0
0.2
0.4
0.6
0.8
1.0
Phase (θ)
e
50pA
20ms
f
Successes [%]
100
80
60
40
20
0
0
50
100
150
200
250
Interpulse Interval (ms)

Effect of mossy fibre input in Golgi cell firing

Figure 5-1 Effect of mossy fibre input on spontaneous Golgi cell firing *a*) Loose cell-attached voltage-clamp recording from a Golgi cell during single-shock mossy fibre stimulation. The bar above indicates time of mossy fibre stimulation. T_0 indicates representative interspike interval (ISI) before stimulation, T_1 the ISI between spikes before and after stimulation and T_2 the ISI between the 1st and 2nd spike after stimulation. θ denotes the phase of stimulation in oscillatory cycle of the rhythmic firing. Scale bars: vertical 20 pA; horizontal 50 ms. *b*) Peri-stimulus spike time histogram for same recording. The frequency of action potential occurrences in a 1 bin after the stimulation was significantly increased above the pre-stimulus baseline ($p < 0.0001$, single-factor ANOVA). *c*) Spike raster plot from same cell as *b*. Dots represent spike times measured at the 50% time point of the action potential inward deflection. Records are ordered according to the timing of the action potential preceding the stimulus. *d*) Phase reset curve averaged across 21 cells. Black solid curve shows phase of 1st action potential following stimulation and black broken graph shows behaviour of the 2nd action potential depending on the phase of stimulation. The datasets were significantly different ($p < 0.0001$, single-factor ANOVA) indicating a phase reset was induced by stimulation. *e*) Averaged cell-attached recordings during a paired-pulse mossy fibre stimulation protocol. A conditioning mossy fibre stimulation pulse that triggered an action potential was followed by a second test pulse at various time intervals. The reduction in current amplitude indicates increased failures in triggering an action potential. *f*) Relationship between percentage of trials that resulted in an action potential on the second pulse as a function of the inter-pulse interval for the cell in *e*.

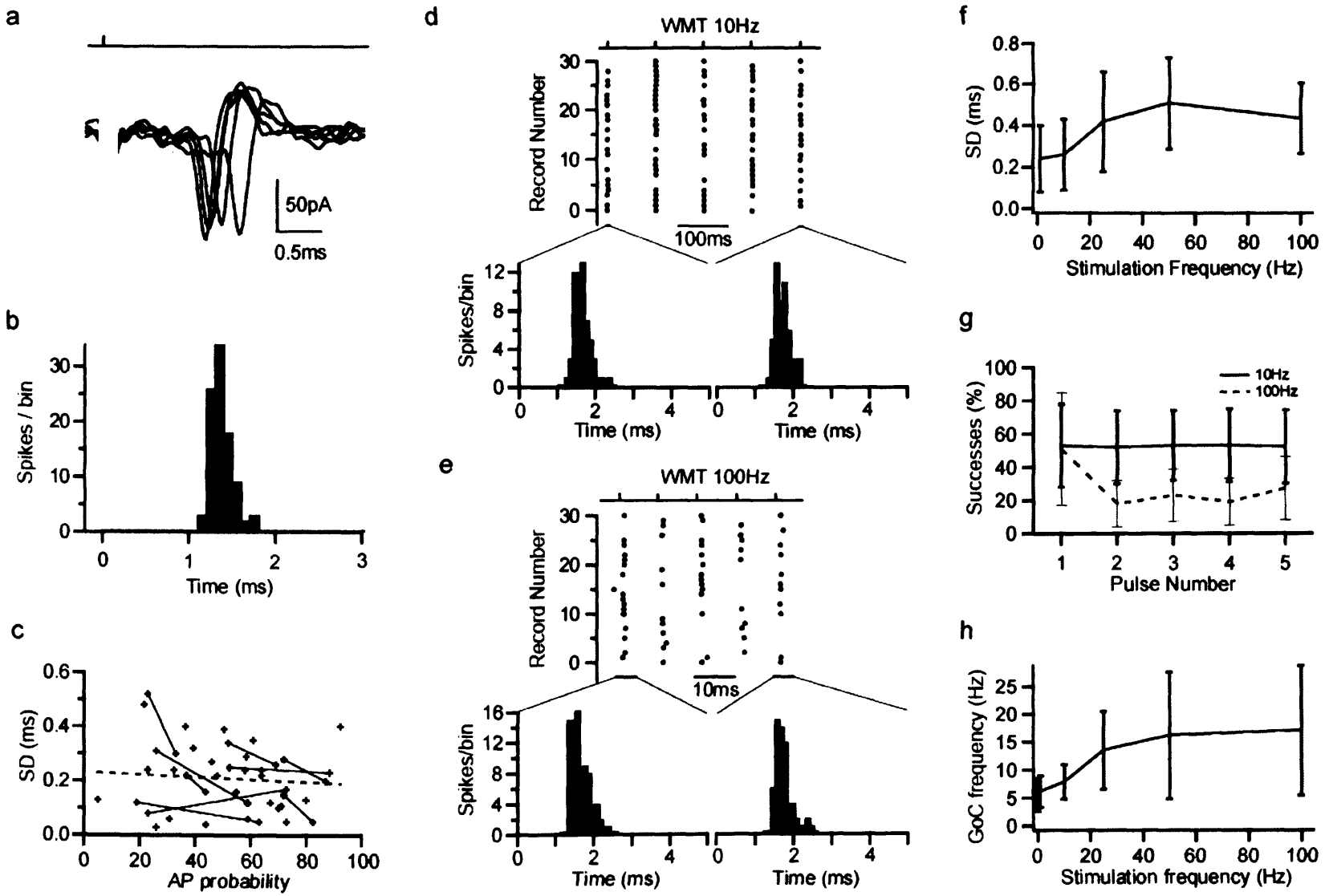
a
50pA
0.5ms
b
Spikes / bin
Time (ms)
c
SD (ms)
AP probability
d
WMT 10Hz
Record Number
100ms
Spikes/bin
Time (ms)
e
WMT 100Hz
Record Number
10ms
Spikes/bin
Time (ms)
f
SD (ms)
Stimulation Frequency (Hz)
g
Successes (%)
10Hz
100Hz
Pulse Number
h
GoC frequency (Hz)
Stimulation frequency (Hz)

Figure 5-2 Precision of mossy fibre-evoked Golgi cell firing *a*) Mossy fibre-evoked action potentials recorded in LCA configuration at high temporal resolution. *b*) Spike latency histogram of action potentials evoked during 1 Hz stimulation. *c*) Dependence of standard deviation of action potential times (precision) on action potential probability for LCA recordings. Data points connected with lines show the action potential precision at two different action potential probabilities (stimulus intensities) for the same cell. Broken line indicates linear regression to all data points (Pearson's $r = -0.14$, $p > 0.2$). *d*) Spike raster plot showing Golgi cell firing in response to 10 Hz white matter tract stimulation. The distributions shown below illustrate the spike jitter for action potentials in response to the 1^{st} and 5^{th} stimulus. *e*) same as 5d for 100 Hz stimulation. *f*) Dependence of spike time precision on stimulation frequency across cells. Spike time precision deteriorates slightly but significantly with increasing input frequency ($n = 5$). *g*) Probability of generating amossy fibre-evoked spike in Golgi cells during trains of 5 stimuli at 10 Hz (solid line) and 100 Hz (dashed line, $n = 5$). *h*) Effect of mossy fibre stimulation frequency on Golgi cell mean firing rate. The moderate increase in firing rate was significant for stimulation frequencies greater than 10 Hz ($p < 0.05$, paired t-test).

Properties of EPSP-spike coupling

To examine how mossy fibre synapses induce Golgi cell spiking with such high temporal precision and yet have little effect on Golgi cell firing rate, I examined the membrane potential directly. To do this I established a stimulus intensity necessary to evoke an action potential with approximately 50% reliability in the LCA configuration (49 ± 18%, n = 5) and then re-patched with an electrode containing internal solution in the whole-cell current-clamp configuration. **Figure 5-3a** shows two voltage trajectories of a spontaneously firing Golgi cell during mossy fibre stimulation. The action potential threshold was -55 mV and action potentials produced a pronounced afterhyperpolarization to -80 mV, followed by a slower depolarising phase leading to the next spike. These values were similar to the averages across cells (-55 ± 6 mV and -80 ± 5 mV, n = 5, respectively) and to previous findings (Forti *et al.*, 2006). When mossy fibre input was stimulated soon after the spike, during the hyperpolarised phase, no action potential was induced (**Figure 5-3a**, black trace), but when it occurred later, during the depolarising phase, an action potential was triggered (**Figure 5-3a**, red trace). This is also illustrated in **Figure 5-3b** which plots the preceding membrane potential before a mossy fibre induced event (action potential = red; EPSP = black). On average, the minimum interval between an evoked action potential and the preceding spontaneous action potential was 58 ± 17 ms (n = 5), similar to the relative refractory period determined in LCA recordings (**Figure 5-1f**). These results suggest that the after-hyperpolarisation prevents EPSPs reaching threshold, and underlies the relative refractory period observed in LCA and current-clamp recordings (**Figure 5-1f**).

Effect of mossy fibre input in Golgi cell firing

The upper panel in **Figure 5-3c** shows examples of successes and failures on an expanded timescale. On average mossy fibre-evoked EPSPs had a rise time of 0.42 ± 0.07 ms (20-80%), a mean amplitude of 8.5 ± 2.2 mV, a coefficient of variation of 0.2 ± 0.1 and a rapid initial decay time constant (τ_{decay1} = 2 ± 1 ms, n = 5). The latency jitter of mossy fibre - Golgi cell EPSPs was only 80 ± 40 μs (20% rise point, n = 5). Mossy fibre-evoked action potentials tended to be triggered off the rising phase of the EPSP and had a narrow latency distribution (SD = 0.25 ± 0.04 ms, n = 5), consistent with LCA recordings (**Figure 5-2c**). The lower panel in **Figure 5-3c** compares the time courses of a typical spike latency histogram (measured as time to threshold crossing), corresponding mean sub-threshold EPSP for that cell and aligned population mean EPSC time course (see Methods). The average interval between the EPSP (20% rise time) and time of threshold crossing was 400 ± 200μs (n = 5), confirming that many of the action potentials were triggered during the rise of the EPSP. Comparison of EPSP and the population mean EPSC time course shows that the EPSC rise (0.23 ms, 20-80%RT) and initial decay (τ_{decay1} = 0.7 ms, A_{decay1} = 76%) occur during the rising phase of the EPSP. Interestingly, the shape of the spike latency distribution shared more similarity with the mean EPSC than EPSP waveform (Fetz & Gustafsson, 1983; Galarreta & Hestrin, 2001). Previous work in other cells has found that voltage-gated conductances in dendrites can contribute to rapid EPSP-spike coupling (Fricker & Miles, 2000). However, the lack of dependence of EPSP amplitude on preceding membrane potential (**Figure 5-3d**; n = 5) suggests that they do not play a major role in boosting the mossy fibre-Golgi cell EPSP. These results show that EPSP-spike precision is achieved by triggering spikes

predominantly during the rising phase of the EPSP, which is determined by the rapid initial components of the EPSC time course.

To investigate how many mossy fibre inputs were necessary to trigger an action potential I examined the mean EPSC amplitude under whole-cell voltage-clamp at the same stimulus settings that gave a spike probability of 51 ± 14% (n = 9) in the LCA configuration. The EPSCs had a mean amplitude of -260 ± 172 pA (n = 9). Comparison with EPSCs arising from putative single mossy fibre recorded in the same cells (-66 ± 29 pA, n = 9) revealed that on average 4 mossy fibre inputs were sufficient to trigger a Golgi cell action potential with 50% probability (**Figure 5-3e**). These results show that the synchronous activation of a small number of mossy fibres can trigger action potentials in Golgi cells with remarkable precision.

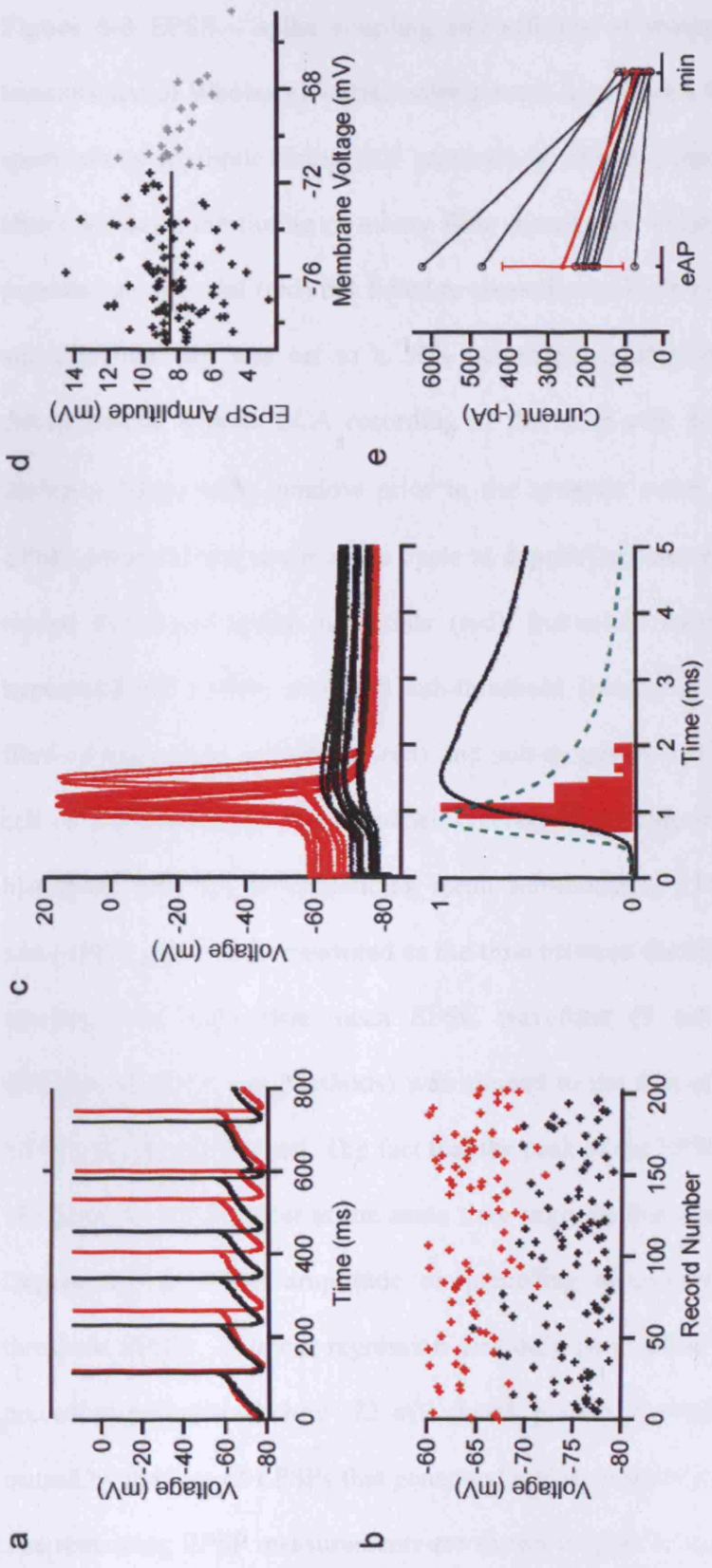
a
Voltage (mV)
0
-20
-40
-60
-80
0
200
400
600
800
Time (ms)
b
Voltage (mV)
-60
-65
-70
-75
-80
0
50
100
150
200
Record Number
c
Voltage (mV)
20
0
-20
-40
-60
-80
1
0
0
1
2
3
4
5
Time (ms)
d
EPSP Amplitude (mV)
14
12
10
8
6
4
-76
-72
-68
Membrane Voltage (mV)
e
Current (-pA)
600
500
400
300
200
100
0
eAP
min

Figure 5-3 EPSP – spike coupling and efficacy of mossy fibre - Golgi cell transmission *a)* Whole-cell current-clamp recordings from a Golgi cell exhibiting spontaneous rhythmic firing and pronounced after-hyperpolarization. The bar above indicates the timing of mossy fibre stimulation which triggered an action potential on one trial (red) but failed to cross threshold on the other (black). The stimulus intensity was set to a 50% action potential probability, which was determined in a prior LCA recording of the same cell. *b)* Membrane voltage during a 500μs time window prior to the synaptic event. When mossy fibre EPSPs occurred late in the spike cycle at depolarized membrane potentials they tended to trigger action potentials (red), but when membrane voltage was hyperpolarized EPSPs remained sub-threshold (black). *c)* Upper panel:mossy fibre-evoked action potentials (red) and sub-threshold EPSPs (black) for same cell on expanded scale. Lower panel: Overlay of peak normalized spike latency histogram (red) and corresponding mean sub-threshold EPSP (black) from the same cell. Latency was measured as the time between the stimulus and threshold crossing. The population mean EPSC waveform (9 cells, recorded with a different amplifier, see Methods) was aligned to the foot of the uncompensated EPSC recorded in this cell. The fact that the peak of the EPSC and maximum rate of rise of the EPSP occur at the same time suggests this alignment is correct. *d)* Dependence of EPSP amplitude on preceding membrane potential for sub-threshold EPSPs. A linear regression was only fit to EPSP measurements with preceding potentials below -72 mV (black points) to avoid the sampling bias caused by the loss of EPSPs that generated action potentials from the population. The remaining EPSP measurements are shown in grey. *e)* Average amplitudes of mossy fibre EPSCs recorded at stimulus voltages that induced action potentials

with on average 50% probability (eAP) and EPSC amplitudes evoked with minimal stimulation (min) in the same cells.

5.3 Conclusions

The effect of mossy fibre activation on Golgi cell firing has been investigated using LCA recordings in sagittal cerebellar slices. In agreement with previous *in vitro* and *in vivo* recordings in rat (Forti *et al.*, 2006), cat (Edgley & Lidierth, 1987) and monkey (Van Kan *et al.*, 1993), Golgi cells were spontaneously active[20]. They responded to white matter stimulation with a temporally precise action potential followed by a period of reduced excitability. Subsequent whole-cell patch clamp recordings confirmed that the evoked action potential was generated due to simultaneous activation of on average 4 mossy fibres. Therefore mossy fibres have a high efficacy in driving Golgi cell firing in comparison to parallel fibres, which require the synchronous activation of approximately 30 fibres to trigger a spike (Dieudonne, 1998). However, because approximately 10 mossy fibres synapse onto a Golgi cell the simultaneous activation of about 40% of mossy fibre – Golgi cell inputs is required to elicit a spike. Since mossy fibre – Golgi cell EPSPs decay rapidly, consecutive synaptic events have little time to summate, implying that synchronous activation of input is important to generate the Golgi cell response. Hence the mossy fibre – Golgi cell connection can be viewed as a detector for coincident mossy fibre activity.

How does mossy fibre input interact with ongoing intrinsic activity of Golgi cells? At a low mossy fibre stimulation frequency (1 Hz) the elicited action potential shifted or reset the phase of the spontaneous rhythmic firing. The action potential was followed by a relative refractory period due to a pronounced after-

[20] Curiously, *in vitro* recordings in mice suggested that Golgi cells show little spontaneous activity at rest (Dugue et al., 2005) which may represent a true species difference or a differences in the experimental preparation e.g. anesthesia used in this study.

hyperpolarisation. Previous studies showed that the after-hyperpolarisation is mediated by M and SK channels and is overcome by an intrinsic depolarization, that is due to the activation of HCN channels underlying I_h and sub-threshold Na^+ conductances (Forti *et al.*, 2006). Therefore, only after ~50 ms mossy fibre input was again effective in triggering a spike. Hence the efficacy - the ability of the input to elicit an action potential - was dependent of the timing of the input in respect to the intrinsic Golgi cell activity. As a result Golgi cell firing rate was only weakly modulated by mossy fibre input even at high frequencies, although the charge injected by mossy fibre synapses is an approximately linear function of frequency, because the EPSC amplitude exhibited little frequency-dependent depression.

A remarkable feature of Golgi cell response to mossy fibre activation is the temporal precision with which it occurred. Its temporal precision (SD = 200 μs) lies between that observed at specialized giant synapses in the auditory pathway, which are able to signal reliably with a precision of tens of microseconds (Zhang & Trussell, 1994; Trussell, 1999) and other interneurons in the cerebellum, hippocampus and cortex, which signal with 0.3-1 ms precision (Miles, 1990; Fricker & Miles, 2000; Galarreta & Hestrin, 2001; Carter & Regehr, 2002; Glickfeld & Scanziani, 2006) and is maintained even at high mossy fibre input frequencies.

How does the Golgi cell achieve this precise EPSP-spike coupling? Most action potentials are triggered from the EPSP rising phase (Fricker & Miles, 2000; Galarreta & Hestrin, 2001). The EPSC time course sets rise time of the EPSP and

is therefore particularly important in determining action potential precision (Fetz & Gustafsson, 1983; Galarreta & Hestrin, 2001; Mittmann *et al.*, 2005) - especially, since there was no evidence for boosting of sub-threshold EPSPs. Therefore the rapid kinetics and lack of synaptic depression of mossy fibre – Golgi cell EPSCs is likely to contribute to the maintenance of spike time precision. Additionally, intrinsic Golgi cell properties contribute. The pronounced after-hyperpolarisation to -80 mV in Golgi cells is likely to reduce jitter accumulation during trains of action potentials as has been shown in a number of different cell types (Schaefer *et al.*, 2006). However, it also makes action potential transmission less reliable particularly at higher input frequencies.

The synaptic mechanisms underlying the precision of EPSP-spike coupling in Golgi cells will be investigated and discussed in more detail in the following chapter.

Chapter Six

6 Synaptic mechanisms underlying spike timing precision

Introduction

In electronically compact cells, in which synaptic currents are not attenuated, EPSC kinetics are a major determinant of spike time precision (Jack *et al.*, 1975; Galarreta & Hestrin, 2001). Since kinetics of mossy fibre – Golgi cells EPSCs showed little dependence on synaptic location (e.g. dendritic filtering, see Chapter 4) and I did not observe any dendritic "boosting" (see Chapter 5), it is likely that rapid kinetics of mossy fibre-evoked synaptic currents are the major determinant of spike time precision in Golgi cells. Therefore I studied the synaptic mechanisms underlying rapid mossy fibre – Golgi cell transmission. To examine the components underlying the rapid mean EPSC I recorded quantal currents under low release probability conditions (Sargent *et al.*, 2005). I also recorded EPSCs under high release probability conditions to observe the possible effects of increased neurotransmitter spillover (DiGregorio *et al.*, 2002) on the EPSC time course.

Results

To investigate the synaptic features underlying rapid signaling at the mossy fibre Golgi cell synapse I determined the quantal size, quantal content and release time course at this connection. Under low release probability conditions (> 80%

failures) evoked EPSCs are predominantly uniquantal irrespective of the number of release sites present (Silver, 2003). I therefore reduced the release probability by changing the external Ca^{2+} and Mg^{2+} concentration from 2/1 to 1/5 (mM). This increased the failure probability from ~0.2 to >0.8 at a putative single fibre connection.

Quantal content

Figure 6-1a shows a group of evoked uniquantal EPSCs and failures. Averaging successes and correcting for multiquantal contamination gave a mean quantal size across cells of -37 ± 11 pA (n = 9, **Figure 6-1a**; see Experimental Procedures). However this is likely to be an overestimate of the quantal size since small uniquantal events may not have been resolved above the recording noise. To account for this, the quantal size was estimated by variance-over-mean analysis (Clements & Silver, 2000; Silver, 2003), which takes successes and apparent failures into account. For a binomial model of synaptic release the variance at the peak of the current is given by:

$$\sigma^2 = NQ^2P(1-P) \qquad \text{(Equation 4, p.64)}$$

where N = number of release sites, Q = Quantal size, P = Release probability. Hence, for low release probability conditions (low P) the variance divided by the mean amplitude approximates the quantal size:

$$P \to 0; \frac{\sigma^2}{NPQ} \cong Q \qquad \text{(Equation 5, p.64)}$$

But variance does not only arise from the stochastic amplitude variability of quantal release, but also from trial-to trial intra- and intersite variability in the latency of quantal release and quantal size. These variances add to produce the

total variance at the peak of stimulus aligned successes and Q_p, the quantal size at the time of the peak of the evoked EPSC, can be calculated by:

$$Q_p = \frac{\sigma^2}{\bar{I}} \cdot \frac{1}{\left(1 + CV_T^{\,2}\right)}$$ (Equation 7, p.65)

(see also Chapter 2 –Materials and Methods). CV_T varied between 0.23 and 0.56 and was 0.36 ± 0.10 on average, n = 9 (for comparison CV_T at the mossy fibre – granule cell synapse is 0.49; Sargent *et al.*, 2005). The mean quantal size determined with variance-over-mean analysis was thus Q_p = -34 ± 10 pA, n = 9. Surprisingly, the mean putative single fibre EPSC amplitude under control conditions was often comparable to the quantal size (**Figure 6-1b**). Dividing the mean EPSC amplitude under control conditions (-52 ± 14 pA, not significantly different from the average putative single fibre EPSC across all cells; $p > 0.2$) by the uniquantal size for these cells yielded a quantal content of 1.5 ± 0.4 (n = 9). This suggests that few quanta are released from a mossy fibre onto a Golgi cell under control conditions. Since the synchronous activation of 4 mossy fibres triggered a Golgi cell spike, the findings indicate that the release of only 6 quanta can generate spike output with high temporal precision.

Vesicular release time course

The rise time distribution of mean quantal waveforms overlapped with the fastest mean stimulus-aligned evoked currents (**Figure 6-1c**) in control conditions as did the weighted decay distribution of the quantal and control currents (**Figure 6-1d**). Currents in control conditions with slowest decay kinetics typically exhibited a noticeable slow spillover-mediated current component (see Chapter 4). On average mossy fibre-evoked EPSCs in control conditions had a decay that

could be fit by a two-exponential function (τ_1 = 0.6 ± 0.4 ms, A_1 = 79 ± 16% and τ_2 = 4.4 ± 3.0 ms, A_2 = 21 ± 16%, n = 38). The mean time course of rise-aligned quantal EPSCs, recorded in low calcium solution, was only marginally faster (20-80% rise time = 0.16 ± 0.04 ms and a two-exponential decay of τ_1 = 0.4 ± 0.1 ms; A_1 = 85 ± 11% and τ_2 = 4.2 ± 2.2 ms; A_2 =15 ± 11%, giving a τ_w = 1.1 ± 0.3 ms, n = 9; **Figure 6-1e**). The similarity of the waveforms suggests that the time course of quantal release is brief producing little temporal 'smearing'. I quantified the release time course under normal release conditions by deconvolving the evoked EPSC waveform with the quantal waveforms measured from the same cells (see Experimental Procedures; Sargent *et al.*, 2005). The time course of quantal release under normal conditions increased and decayed rapidly (**Figure 6-1f**). Across cells the peak release rate was 4.3 ± 1.2 ms^{-1} and the release function decayed with a time constant of 133 ± 99μs (n = 9). This is comparable to release at giant auditory synapses (Isaacson & Walmsley, 1995; Taschenberger *et al.*, 2005), but slower than reported at the mossy fibre-granule cell connection (τ = 75 μs; Sargent *et al.*, 2005). While the 58μs difference between mossy fibre-granule cell and mossy fibre-Golgi cell synapses could reflect differences in the vesicular release process, it could also be due to the lower temperature of the recordings (35°C vs 37°C) and subtle differences in deconvolution methods used (see Materials and Methods). To verify the results obtained by deconvolution analysis I directly measured the time course of quantal release in four cells that had sufficient numbers of events, by examining the latency of uniquantal EPSCs under low probability conditions (**Figure 6-1g**). Cumulative release functions for the direct measurement and deconvolution had similar shapes ($p > 0.5$, KS test, **Figure 6-1h**, n = 4) and their 10-90% rise time

were 253 ± 145μs (n = 4) and 255 ± 113μs (n = 9), respectively. Vesicular release was therefore largely over by the time of the peak of the EPSC (black section on **Figure 6-1f**). These results show that highly synchronous vesicular release and a rapid time course of quantal currents allow mossy fibre inputs to reset Golgi cell firing, precisely, with only few quanta.

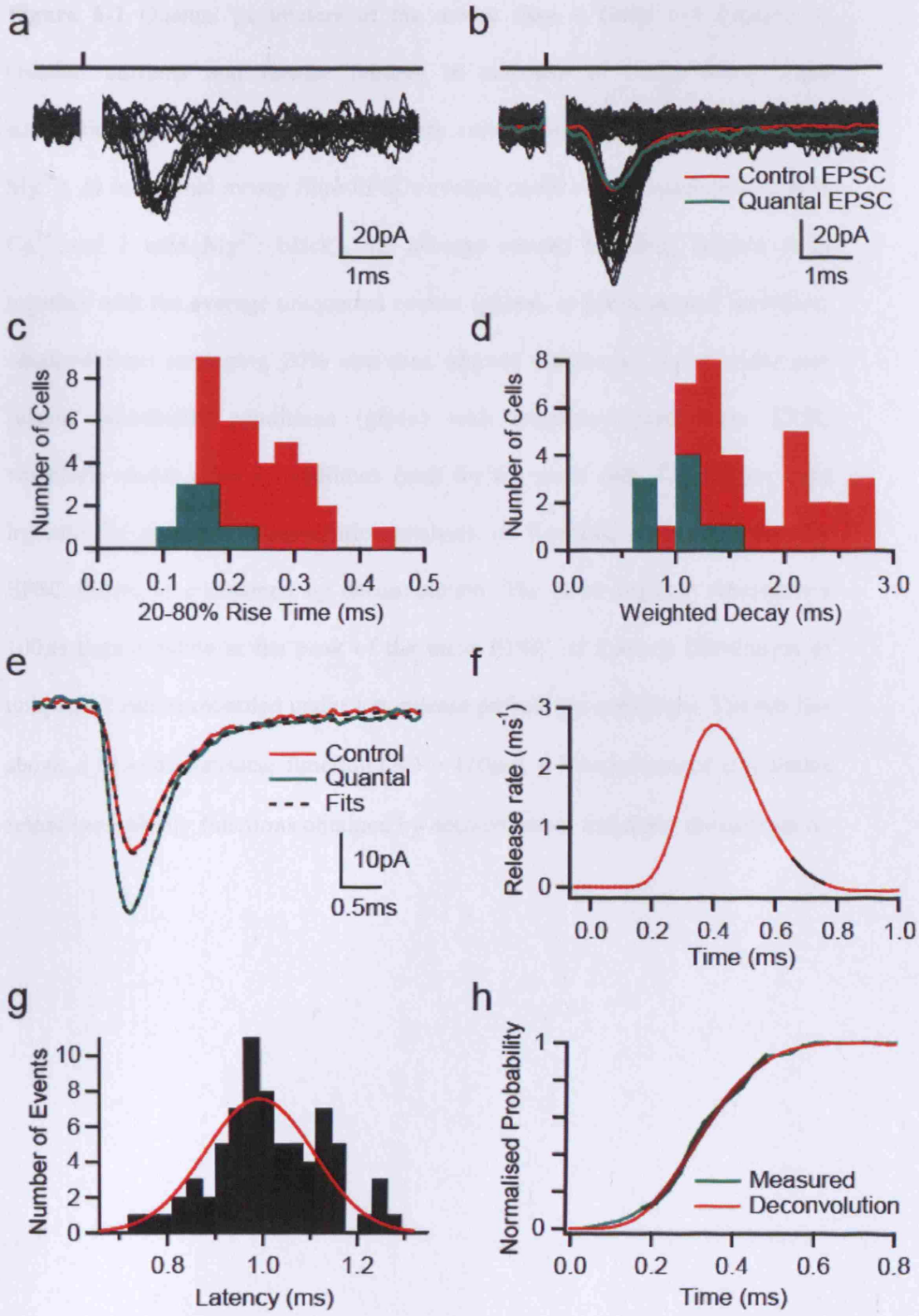
a
20pA
1ms
b
Control EPSC
Quantal EPSC
20pA
1ms
c
Number of Cells
20-80% Rise Time (ms)
d
Number of Cells
Weighted Decay (ms)
e
Control
Quantal
Fits
10pA
0.5ms
f
Release rate (ms-1)
Time (ms)
g
Number of Events
Latency (ms)
h
Normalised Probability
Measured
Deconvolution
Time (ms)

Figure 6-1 Quantal parameters of the mossy fibre – Golgi cell synapse *a)* Quantal currents and release failures in response to single mossy fibre stimulation under low release probability conditions (1 mM Ca^{2+} and 5 mM Mg^{2+}). *b)* Individual mossy fibre EPSCs evoked under control conditions (2 mM Ca^{2+} and 1 mM Mg^{2+}; black), the average current including failures (red) together with the average uniquantal current (green). *c)* Mean quantal waveform obtained from averaging 20% rise time aligned uniquantal events under low release probability conditions (green) with stimulus-aligned mean EPSC waveform under control conditions (red) for the same cell. The broken lines indicate fits used for deconvolution analysis. *d)* Vesicular release function for EPSC shown in *c* obtained by deconvolution. The black segment represents a 100μs time window at the peak of the mean EPSC. *e)* Latency distribution of uniquantal events recorded under low release probability conditions. The red line shows a fit with Gaussian function (SD = 110μs). *f)* Comparison of cumulative release probability functions obtained by deconvolution and direct measurement.

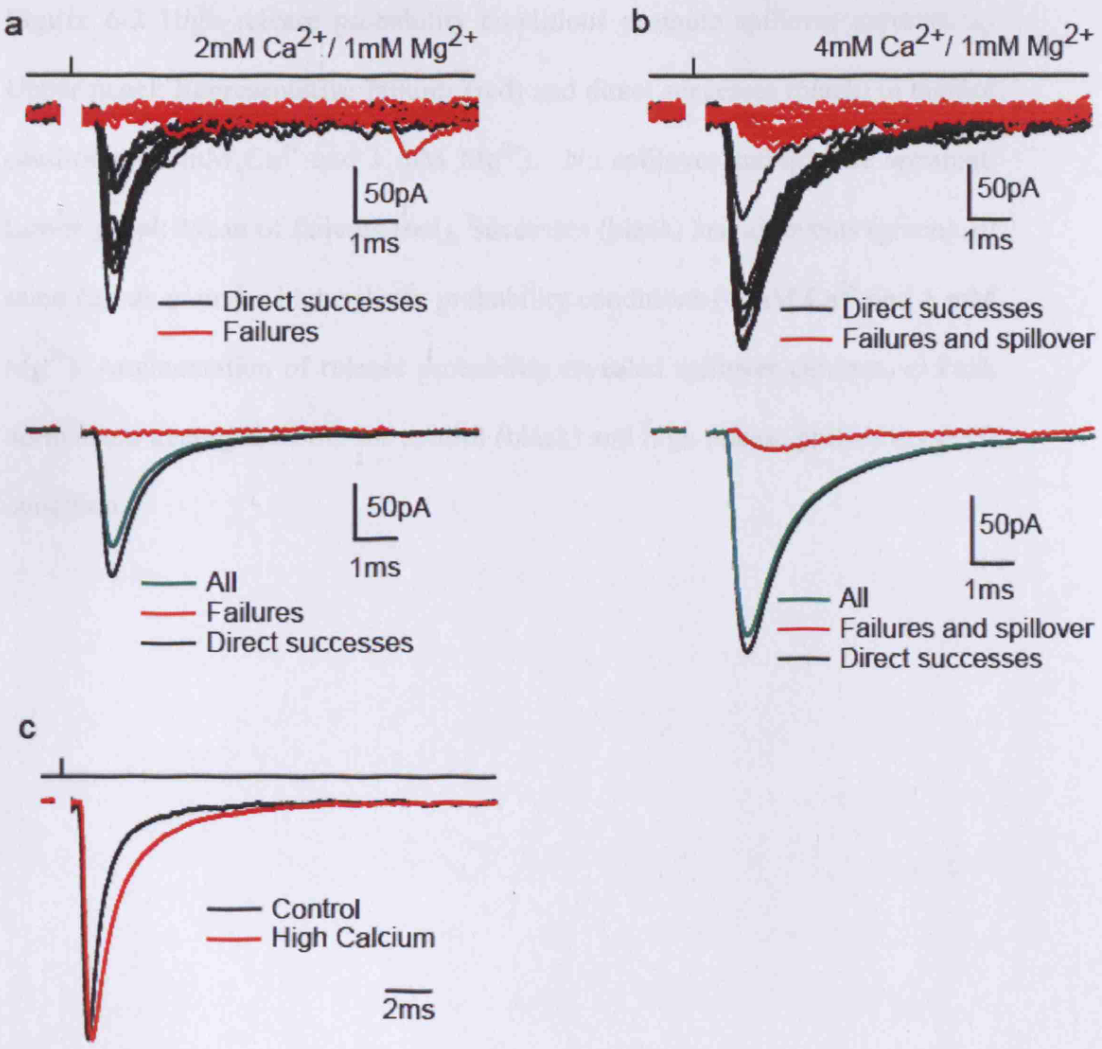
a
2mM Ca^{2+}/ 1mM Mg^{2+}
50pA
1ms
Direct successes
Failures
50pA
1ms
All
Failures
Direct successes
b
4mM Ca^{2+}/ 1mM Mg^{2+}
50pA
1ms
Direct successes
Failures and spillover
50pA
1ms
All
Failures and spillover
Direct successes
c
Control
High Calcium
2ms

Figure 6-2 High release probability conditions promote spillover currents. *a)* Upper panel: Representative failures (red) and direct successes (black) in control conditions (2 mM Ca^{2+} and 1 mM Mg^{2+}). No spillover currents are apparent. Lower panel: Mean of failures (red), Successes (black) and all events (green). *b)* same cell as *a.* under high release probability conditions (4 mM Ca^{2+} and 1 mM Mg^{2+}). Augmentation of release probability revealed spillover currents. *c)* Peak normalized averaged EPSC for control (black) and high release probability (red) condition.

Spillover shapes EPSC decay at high release probabilities

The rapid release time course is likely to be responsible for the rapid rise of the mossy fibre – Golgi cell EPSC similar to findings at the mossy fibre – granule cell synapse (Sargent *et al.*, 2005). However, in contrast to the mossy fibre – granule cell transmission, the mossy fibre – Golgi cell EPSC is rarely prolonged by spillover currents, characteristic for the decay of mossy fibre - granule cell EPSCs, although the connections are made within the same glomerular structure (Chapter 1, **Figure 1-4**). Instead, the apparent lack of spillover makes mossy fibre – Golgi cell EPSCs decay considerably faster than EPSCs in granule cells (τ_{WD} = 1.6 ms vs 2.9 ms, respectively; (DiGregorio *et al.*, 2002). Neurotransmitter spillover from neighbouring presynaptic release sites onto postsynaptic receptors is a common phenomenom in the cerebellar glomerulus (Mitchell & Silver, 2000a, 2000b; DiGregorio *et al.*, 2002). It is therefore surprising that spillover currents were rarely detected at the mossy fibre - Golgi cell synapse (in 5 of 42 cells, see Chapter 3). At high release probabilities neurotransmitter released from neighbouring release sites can pool more efficiently and increase the local transmitter concentration at postsynaptic receptor sites. Therefore I augmented the release probability to investigate whether this increased the probability of observing spillover currents. I changed the external Ca^{2+} and Mg^{2+} concentration from 2/1 to 4/1 or 6/1 (mM) and recorded putative single fibre EPSCs in 8 Golgi cells. Spillover currents were observed in 3 out of 8 cells, the remaining cells either showed no spillover currents (n = 1) or direct successes on every trial, so that spillover currents could not be discerned in isolation (n = 4). The weighted decay changed from 1.8 ± 0.7 in control conditions to 2.2 ± 0.9 in high release probability conditions ($p < 0.05$,

n = 8, paired t-test). **Figure 6-2** shows the individual failures and direct successes for mossy fibre – Golgi cell transmission in control conditions opposed to those in high release probability conditions. In this cell the average spillover current (failures and spillover together) had an amplitude of -14.3 pA, a 20-80%RT of 0.4 ms and a weighted decay of 2.2 ms. Spillover contributed 9.4% to the EPSC charge. Across cells the average spillover current had an amplitude of -23 ± 8 pA, a 20-80%RT of 0.6 ± 0.2 ms, a weighted decay of 2.4 ± 0.7 ms and contributed 25 ± 14% of the total charge carried by the EPSC. A comparison of the normalised EPSC time course in control and high release probability conditions shows that spillover currents prolonged the EPSC decay (**Figure 6-2c**). This indicates that spillover transmission at mossy fibre – Golgi cell synapse occurs at high release probability conditions, but implies that the synapse has evolved to minimise the influence of spillover currents to maintain a rapid EPSC decay.

Conclusions

Connections tuned for temporal signaling are found in the hippocampus, cerebellum and neocortex, particularly onto interneurons. The hippocampal granule cell – basket cell synapse is characterized by a fast neurotransmitter release time course (Geiger *et al.*, 1997), (peri-)somatic localization of synapses, a depolarized postsynaptic membrane potential, fast-gating AMPA receptors and little NMDA receptor contribution to synaptic currents. These features allow fast feed-forward inhibition of hippocampal pyramidal cells and shape their spike timing (Pouille & Scanziani, 2001). Similar features are found at connections to neocortical layer IV interneurons (Gabernet *et al.*, 2005). In the cerebellum at the

parallel fibre – stellate cell synapse electronic compactness and a high input resistance ensures high quantal efficacy (Carter & Regehr, 2002) and spike time precision. In the auditory brain stem bushy cells synapse onto cells of the medial nucleus of trapezoid body (MNTB) to form a giant excitatory synapse, the Calyx of Held. A large number of release sites exhibiting a low release probability and a rapid release time course contribute to spike timing precision and maintenance of synaptic efficacy at this connection (Scheuss *et al.*, 2007).

Common to all these synaptic specializations is that currents injected at a synaptic site experience little attenuation when propagating to the action potential generation site. This is achieved either by anatomical proximity, electronic compactness of the dendritic tree or active conductances in dendrites. In contrast to the Calyx of Held, many feed-forward excitatory connections onto interneurons signal with only few quanta (Gulyas *et al.*, 1993; Carter & Regehr, 2002). When only few quanta are involved in synaptic transmission (and quantal efficacy is high) the asynchrony in quantal release might limit EPSP-spike coupling to a precision of around a millisecond.[21] Also synaptic efficacy can only be maintained at low stimulus frequencies due to limitations imposed by presynaptic depression (Schneggenburger *et al.*, 2002).

The mossy fibre – Golgi cell synapse bears many hallmarks of rapid synaptic signalling. The cell body and proximal dendrites appear to constitute an electronically compact compartment, ensuring that synaptic events undergo little

[21] Synapses with many release sites, like the Calyx of Held, overcome this limitation by releasing hunderds of vesicles over a short time window, thereby averaging out stochasticity and reducing EPSC variability. This makes the timing of threshold crossing reproducible.

dendritic filtering. Therefore the rapid EPSC time course (20-80% rise time = 0.21 ms) results in a fast EPSP rise time (20-80% rise time = 0.42 ms) and is a fundamental determinant of EPSP-spike coupling (Jack *et al.*, 1975; Galarreta & Hestrin, 2001). Rapid EPSC kinetics are achieved by little contribution or no NMDA receptor-mediated components and spillover currents. The reduced or absent spillover currents could be due to differences in the anatomical arrangement (Cathala *et al.*, 2005) of the mossy fibre to Golgi and granule cell synapses. Electronmicroscopic studies of the mossy fibre – Golgi cell synapse in the glomerulus show postsynaptic protrusions which seem to separate individual synaptic specialisations. This might hinder neurotransmitter diffusion and reduce spillover. But the difference could also be due to a lower release probability (DiGregorio *et al.*, 2002), an increased activity of glutamate transporters, or lower affinity AMPA receptors at the mossy fibre-Golgi cell synapse than the mossy fibre-granule cell synapse (DiGregorio *et al.*, 2007). To ascertain which explanation is responsible further experiments are required.

Presynaptically, a rapid vesicular release time course contributes to fast EPSC kinetics. The release time course was comparable to measurements at the Calyx of Held (Taschenberger *et al.*, 2005) but slower than at the mossy fibre – granule cell synapse (Sargent *et al.*, 2005). The quasi-synchronous release also reduces jitter in EPSP-spike coupling resulting from the non-synchronous release of few quanta allowing Golgi cells to transmit mossy fibre input with a precision of 200μs. This precision can be preserved over a range of frequencies, because a rapid reloading of mossy fibre release sites and an apparent lack of receptor desensitization allows the maintenance of synaptic efficacy although only few

release sites are involved. Thereby the mossy fibre – Golgi cell connection can signal with a precision intermediate between the Calyx of Held and other feed-forward excitatory synapses onto interneurons although employing only few quanta in synaptic transmission.

Chapter Seven

7 Feed-forward inhibition of granule cells

7.1 Introduction

Although commonly assumed, based on the cerebellar anatomy, it has not been shown that mossy fibre, Golgi and granule cell from a functional feed-forward inhibitory circuit. Thus it is also not clear what the implications of feed-forward inhibition for granule cell integration of mossy fibre input are. To address these questions I recorded from granule cells while stimulating the white matter tract. I made voltage-clamp recordings at approximately 0 mV, near the reversal potential for AMPA and NMDA receptors, and -70 mV, near the $GABA_A$ receptor reversal potential, to determine the timing and size of excitatory and inhibitory conductances in granule cells.

7.2 Results

Inhibitory postsynaptic currents (IPSCs) could be evoked in 16 of 19 granule cells clamped at approximately 0 mV (average holding potential = 3 ± 6 mV, n = 19) in response to white matter tract stimulation. IPSCs had two latency components in 9 of these cells (black traces in **Figure 7-1a**). The distinct IPSC components could be due to direct monosynaptic stimulation of the Golgi cell axons and a disynaptic activation of Golgi cells via mossy fibres. Application of 10 μM NBQX blocked the later (disynaptic) response leaving only the

monosynaptic IPSC evoked by direct Golgi cell axon stimulation (red traces in **Figure 7-1a**).

Monosynaptic ISPCs arising from direct Golgi axon stimulation

Figure 7-1b shows a group of monosynaptic IPSCs (red and black traces) recorded in 10 μM NBQX. Application of 10 μM Gabazine fully blocked the synaptic currents confirming that they were due to activation of $GABA_A$ receptors (blue trace in **Figure 7-1b**). The average IPSC for this cell (green trace in **Figure 7-1b**) had an amplitude of 63 pA with a coefficient of variation (CV) of 0.5, a 20-80% rise time of 0.35 ms and a weighted decay of 7.6 ms. Across cells IPSCs had a 81 ± 20% success probability, a mean amplitude of 30 ± 20 pA with rise time of 0.4 ± 0.2 ms and a weighted decay of 8 ± 1 ms (n = 7). All, but one cell, also showed low amplitude, slowly rising IPSCs. These apparent spillover currents could be separated based on their peak amplitude and rise time (see **Figure 7-1bii**), similar to excitatory spillover currents (see Chapter 2 – Materials and Methods, **Figure 7-1bi** red traces, see also Rossi & Hamann, 1998). Spillover currents (averaged together with failures) had an average amplitude of 14 ± 11 pA, a rise time of 1.3 ± 0.6 ms and a weighted decay of 10.4 ± 1.9 ms (n = 6). These data show that a large majority of granule cells (>80%) receive fast synaptic inhibition with little temporal jitter and high reliability due to spillover currents. **Figure 7-1c** represents the pooled latency distribution of NBQX insensitive monosynaptic (black) and NBQX sensitive disynaptic (grey) IPSCs. The distributions show little overlap. This allowed us to classify all events with a latency >1.6 ms (5xSD above the mean latency of monosynaptic, NBQX insensitive events) as IPSCs of disynaptic origin.

Feed-forward (disynaptic) IPSCs onto granule cells

Of the 16 granule cells 7 exhibited only disynaptic IPSCs (average latency 1.8 ± 0.2 ms; range: 1.6-2.1 ms). A group of these IPSCs is shown in **Figure 7-2a** (black traces). They were readily blocked by NBQX (n = 3, red trace in **Figure 7-2a**) and Gabazine (n = 2, data not shown) confirming that these IPSCs arose from disynaptic activation of Golgi cell synapses onto granule cells. Across cells disynaptic IPSCs occurred with a success probability of 52 ± 29% (range: 18-91%, n = 7) and had an average amplitude of 13.3 ± 10.2 pA (range: 4.8-31 pA, n = 7). The kinetics of averaged disynaptic IPSCs were very similar to monosynaptic IPSCs described earlier. They had an average 20-80% rise of 0.4 ± 0.1 ms and a weighted decay of 7 ± 1 ms ($p > 0.2$, t-test). IPSCs had a latency jitter (SD of latency distribution) of 0.3 ± 0.1 ms (n = 7), which is similar to the predicted SD based on mossy fibre-Golgi cell and Golgi cell-granule cell transmission jitter (predicted SD[22] = 260μs, $p > 0.2$, one sample t-test).

Effect of feed-forward inhibition on granule cell EPSCs

Cells that showed disynaptic inhibition were subsequently hyperpolarised to -70 mV to see if a mossy fibre-evoked excitatory current was also present as expected for an intact feed-forward inhibitory circuitry. EPSCs were observed in 6 out of 7 granule cells. The remaining cell did not show an excitatory response. Latency (0.8 ± 0.2 ms), kinetics (20-80% rise time of 0.20 ± 0.02 ms and weighted decay of 2.3 ± 1.1 ms) and average amplitude (-41 ± 37 pA, n = 6) of

[22] When two distributions are convolved their variances add. The expected jitter of disynaptic granule cell inhibition is $SD = \sqrt{\sigma^2_{MF-GoC} + \sigma^2_{GoC-GrC}}$.

Feed-forward inhibition of granule cells

EPSCs were comparable to single mossy fibre-evoked currents in granule cells described earlier (DiGregorio *et al.*, 2002; Sargent *et al.*, 2005). **Figure 7-2b** shows the timing and average time courses of both excitatory (EPSG) and inhibitory conductance (IPSG) for a representative cell. Although the EPSG peak amplitude was 1.5 ± 0.4 times larger than the IPSG (340 ± 230 pS vs 230 ± 130 pS) across cells (n = 6), by the time the peak of the inhibitory conductance occurred the EPSG had decayed by 30 ± 11%, so that the inhibitory conductance was comparable in size (n = 6; **Figure 7-2b**). The time course of the calculated synaptic reversal potential (see Materials and Methods) is plotted in red in **Figure 7-2b** (solid line). For this cell the synaptic reversal potential drops below spike threshold (red broken line; -35 mV; Cathala *et al.*, 2003) 1.8 ms after the onset of the EPSG due to the inhibitory action of the IPSG. This signifies a net inhibitory effect of the total synaptic conductance. Averaged across cells the IPSG restricts the excitatory action of the EPSG to a 1.4±0.3 ms time window (n = 6, see **Figure 7-2b** lower panel).

These results confirm that a functional feed-forward inhibitory network is present in the granule cell layer and shows that the disynaptic IPSG truncates slow mossy fibre – granule cell EPSG components, thereby narrowing the time window of synaptic integration.

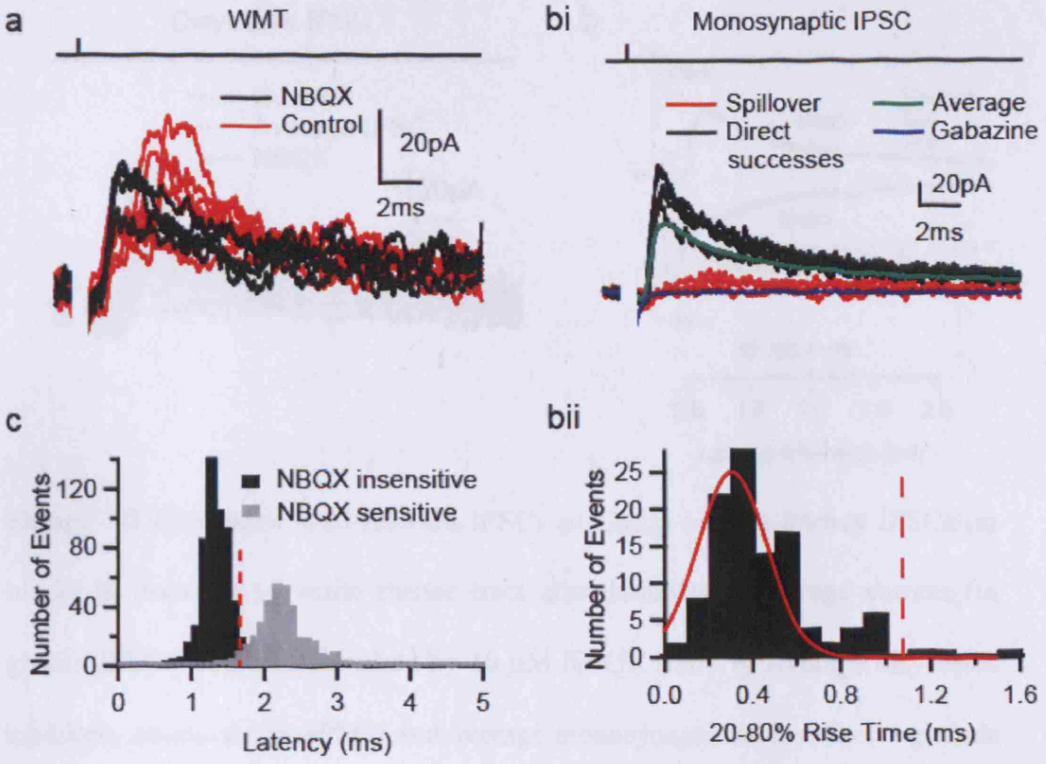

Figure 7-1 IPSCs in granule cells *a)* IPSCs recorded in a granule cell (GrC) at 0 mV during white matter tract (WMT) stimulation in control conditions and in presence of 10 μM NBQX. *bi)* Monosynaptic IPSCs in the presence of NBQX (direct successes in black and spillover currents in red), the average of all IPSCs (green) and IPSC block by 10 μM Gabazine (blue). *bii)* Distribution of rise times for all currents. Red curve shows Gaussian fit to data with a mean of 0.31 ms and a standard deviation (SD) of 0.15 ms. Broken line indicates threshold value (5xSD above mean) used to separate spillover currents (IPSCs with rise times larger than threshold value). *c)* Latency distribution of NBQX sensitive (grey) and insensitive IPSC (black bars) pooled across cells. Red broken line indicates latency criterion used to distinguish granule cells receiving disynaptic inhibition.

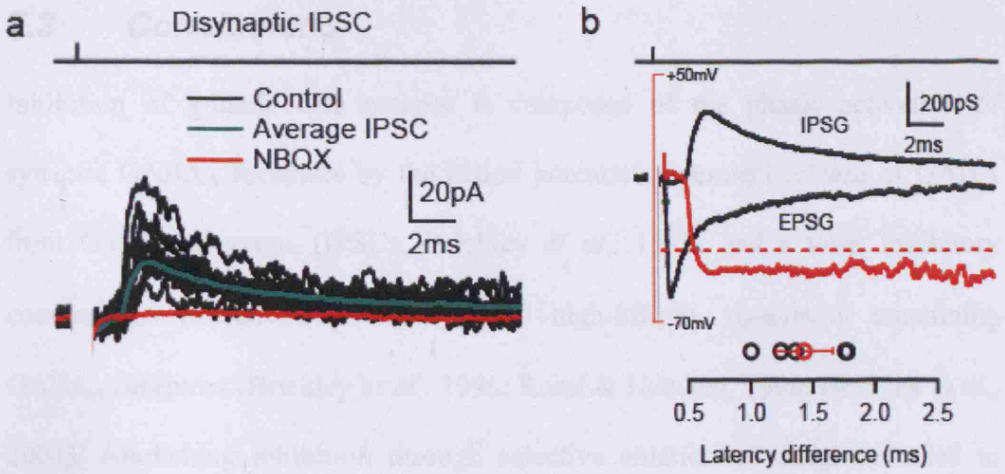

Figure 7-2 Disynaptic feed-forward IPSCs *a)* Group of long latency IPSCs (in black) in response to white matter tract stimulation with average current (in green). IPSCs were fully blocked by 10 μM NBQX (red). *b)* Average disynaptic inhibitory conductance (IPSG) and average monosynaptic mossy fibre – granule cell excitatory conductance (EPSG) in the same cell at same stimulus intensity. Red trace shows the time course of calculated synaptic reversal potential with the red broken line indicating the spike threshold (Cathala *et al.*, 2003). Green circles show the 20% rise time point of the EPSG and crossing of synaptic reversal potential with spike threshold (-35mV) indicating a net inhibitory effect of the total synaptic conductance from that time point onwards. Lower panel: Latency difference between 20% rise time point of the EPSG and starting point of the net inhibitory effect for 6 cells. Mean value with SD is shown in red.

7.3 Conclusions

Inhibition of granule cell synapse is composed of the phasic activation of synaptic $GABA_A$ receptors by the action potential-dependent release of GABA from Golgi cell axons (IPSCs, Brickley *et al.*, 1996) and a tonic inhibitory conductance mediated by extrasynaptic high-affinity α_6-subunit containing $GABA_A$ receptors (Brickley *et al.*, 1996; Rossi & Hamann, 1998; Brickley *et al.*, 2001). Abolishing inhibition through selective ablation of Golgi cells led to severe motor deficits (Watanabe *et al.*, 1998). Tonic inhibition has been suggested to play a role in multiplicative gain (input-output relationship) modulation of granule cells (Mitchell & Silver, 2003). But what role phasic inhibition plays in granule cell processing remains speculative. In early stages of development (postnatal day 1-7) the phasic GABA release is dominant and excitatory (Brickley *et al.*, 1996), but with developmental maturation spontaneous GABA release occurs less frequently and undergoes kinetic acceleration. In contrast, the tonic conductance increases in size, so that by postnatal day 45 it represents over 90% of the overall inhibitory charge (Brickley *et al.*, 1996; Wall & Usowicz, 1996). Action potential-dependent release of GABA contributes to tonic inhibition via GABA spillover (Rossi & Hamann, 1998).

My experiments show a large majority of granule cells received phasic inhibition at mature age. Inhibitory transmission between Golgi and granule cells occurred with high reliability, indicated by a low failure rate and CV. One mechanism contributing to reliability was the presence of spillover currents. Spillover suggests that phasic inhibition might affect the level of tonic inhibition as it does

in younger animals (Rossi & Hamann, 1998). It furthermore implies that GABA can spill over to presynaptic $GABA_B$ receptors to reduce the mossy fibre release probability (Mitchell & Silver, 2000a) in older animals[23]. Monosynaptic IPSCs exhibited little temporal jitter as seen for paired Golgi cell – granule cell recordings in cerebellar slices of mice (Dugue *et al.*, 2005).

Disynaptic feed-forward IPSCs could be distinguished pharmcologically and subsequently based on IPSC latency. They exhibited a jitter similar to the combined jitter of mossy fibre – Golgi cell and Golgi cell – granule cell transmission. Since both connections operate with high precision the overall jitter of feed-forward inhibition was narrow. The feed-forward IPSC had such timing and amplitude that the slow components of a monosynaptic mossy fibre input into granule cells were approximately canceled. My previous findings (Chapter 5) show that feed-forward inhibition required the recruitment of at least four mossy fibres exciting a Golgi cell. Provided white matter stimulation activates mossy fibres in a random fashion and approximately 10 mossy fibres synapse onto a Golgi cell (Chapter 3) a network activation of 40% is required to trigger a Golgi cell spike. This predicted mossy fibre population activity will activate 1-2 out of 4 mossy fibres contacting a granule cell. Indeed, the granule cell EPSC amplitude at stimulus intensities required to induce disynaptic feed-forward inhibition was comparable to EPSCs evoked with minimal stimulation (DiGregorio *et al.*, 2002; Sargent *et al.*, 2005), suggesting that on average 1 mossy fibre was activated. Hence anatomical (Chapter 3) and

[23] The presence of $GABA_B$ receptors at this age was confirmed (Chapter 4).

electrophysiological observations (Chapter 4-7) of the mossy fibre – Golgi cell – granule cell circuitry seem to agree.

My results establish that mossy fibre, Golgi cell and granule cell form a functional feed-forward inhibitory circuitry. The synaptic and cellular properties of this circuitry appeared to be tuned to transmit temporal signals with high accuracy. As a result feed-forward inhibition in granule cells resulted in a curtailment of the synaptic integration time window for mossy fibre inputs. Further physiological implication will be discussed in the General Discussion.

Chapter Eight

8 General Discussion

I have investigated the feed-forward circuitry in the input layer of the cerebellum. In this circuitry, mossy fibres (sensory afferents) excite granule and Golgi cells. Golgi cells are the main interneuron in the granule cell layer and provide the sole source of inhibition to granule cells. This network is thought to transform the sensory information conveyed by mossy fibres and relay it to Purkinje cells. The importance of granule cell inhibition has been demonstrated by pharmacological ablation of Golgi cells which led to severe motor deficits. Animals with motor deficits recovered only partially and deficits prevailed for sophisticated motor tasks (Watanabe *et al.*, 1998). Granule cells receive phasic inhibition in the form of action potential-dependent synaptic IPSCs and tonic inhibition mediated by the activation of extrasynaptic $GABA_A$ receptors by ambient GABA (Brickley *et al.*, 1996; Nusser *et al.*, 1998; Rossi & Hamann, 1998). The level of ambient GABA is dependent on synaptic GABA release due GABA spillover onto extrasynaptic receptors (Rossi & Hamann, 1998; Carta *et al.*, 2004). But the role of Golgi cell mediated inhibition in granule cell layer network computations remains elusive.

A first step towards answering this question is to characterize the anatomy of the circuitry and the functional properties of cells and their synaptic connections. I attempted to do this with a combination of anatomical, electrophysiological and imaging techniques. The results of these experiments provide some insight into

the properties of the microcircuitry conferred by the feed-forward excitation of Golgi cells and lead to some predictions about granule cell layer network dynamics.

Anatomical arrangement of the mossy fibre - Golgi cell - granule cell circuitry

Golgi cells were identified based on their large somata in the granule cell layer, ascending dendrites projecting into the molecular layer and basolateral dendrites restricted to the granular layer. Biocytin fills of Golgi cells showed that ascending dendrites covered a large three-dimensional volume in the molecular layer. The ascending dendritic tree is innervated by 1000-5000 parallel fibres (Pellionisz & Szentagothai, 1973), each of them making one or two synapses (Dieudonne, 1998). In contrast, interneurons of the molecular layer and Purkinje cells have a two-dimensional dendritic tree in the sagittal plane. Electrophysiological investigation of the parallel fibre input has shown the low efficacy of this input in driving Golgi cell firing (Dieudonne, 1998). Less is known about the mossy fibre input onto Golgi cells. Although already discovered by Ramon y Cajal (1911) there is considerable controversy about the location and number of mossy fibres synapsing onto Golgi cells (see Chapter 3). I addressed this issue by double-labeling mossy fibre terminals and Golgi cells and analyzing their colocalisation. The experimental results suggested that mossy fibres preferentially make synapses onto basolateral dendrites of Golgi cells, but also synapse onto the cell body and proximal part of the ascending dendrite. Functional synaptic contacts on basolateral dendrites were confirmed by Ca^{2+} imaging experiments (Chapter 4), but whether putative contacts on cell body and

proximal ascending dendrite were functional remains unclear. Interestingly, the basolateral dendritic tree had an approximately 3 times larger expansion in the sagittal plane and was therefore aligned with the preferred orientation of the somatotopic innervation of the granule cell layer (Shambes *et al.*, 1978; Bower & Kassel, 1990). My results indicate that the number of mossy fibre – Golgi cell synapses is approximately 10. This suggests that a Golgi cell samples approximately 1/6 of the mossy fibre activity within the expansion of its basolateral dendrites, given the extent of the dendritic tree and the mossy fibre terminal density (see Chapter 3). Since the average distance between glomeruli originating from the same mossy fibre is 50-70 μm it is possible that a small proportion of mossy fibres makes more than one glomerular contact with a single Golgi cell. But, the probability that a mossy fibre contacts both a granule cell and a Golgi cell, which inhibits that granule cell, is rather small (< 3%, Chapter 3). Therefore feed-forward excitation of Golgi cells is likely to result in lateral inhibition of granule cells driven by a subset of the surrounding mossy fibre activity. On the output side, the Golgi cell axon appears to contact almost all (93%, Chapter 3) glomeruli in the three-dimensional volume it inhabits (0.003 mm^3). Interestingly, the dimensions of the axonal arbour are comparable to the size of a receptive field in the fractured somatotopic map in the granule cell layer (Woolston *et al.*, 1982).

Based on the Golgi cell density (D_{GoC}) and the extent of the axonal arbour (V_{axon}) the number of Golgi cell axons innervating a glomerulus can be calculated with equation 10.

$$N_{axons/glom} = D_{GoC} \cdot V_{axon} = \quad 4600 \text{ per mm}^3 \cdot 0.003 \text{ mm}^3 \qquad \text{(Equation 10)}$$

(D_{GoC} = cellular density of Golgi cells based on mGluR2 immunohistochemistry; personal communication with Andrea Lörincz and Zoltan Nusser and V_{axon} = extent of axonal arbourisation; Chapter 3). This suggests that a glomerulus is innervated by approximately 13 different Golgi cell axons.

The number of granule cells contacted by a Golgi cell axon within a glomerulus can be calculated as follows:

$$N_{dend\_in\_glom/axon} = \frac{f_{glom\_contacted} \cdot N_{glom\_in\_Vaxon}}{N_{GrC\_in\_Vaxon} \cdot P_{GoC-GrC}} = \frac{0.93 \cdot 1450}{7500 \cdot 0.2} \qquad \text{(Equation 11)}$$

where $f_{glom\_contacted}$ = fraction of glomeruli contacted by a single Golgi cell axon (Chapter 3); $N_{glom\_in\_Vaxon}$ = number of glomeruli in extent of axonal arbour (Chapter 3); $N_{GrC\_in\_Vaxon}$ = number of granule cells in axonal arbour (Chapter 3); $P_{GoC-GrC}$ = connection probability of a Golgi cell with surrounding granule cells (Dugue *et al.*, 2005). The calculation suggests that on average only about 1 granule cell is directly contacted by a Golgi cell axon within a glomerulus.

Based on these numbers the total fraction of granule cells inhibited within a glomerulus can be determined with equation 12.

$$F_{GrC-GoC} = \frac{N_{dend\_in\_glom/axon} \cdot N_{axon/glom}}{N_{GrC/glom}} = \frac{1 \cdot 13}{20} \qquad \text{(Equation 12)}$$

where $N_{GrC/glom}$ = number of granule cells per glomerulus (Chapter 3, Fox, 1967). The fraction of granule cells receiving direct synaptic Golgi cell inhibition is thus 62%.

These estimates fit well with electron-microscopic studies of glomeruli which show that ~60% of granule cell dendrites receive direct inhibitory input from Golgi cell varicosities within a glomerulus (Hamori & Somogyi, 1983). This suggests that the anatomical measurements and calculations in this study, which assume random connectivity in the network, are consistent with previous methodologically independent analysis of the granule cell layer circuitry (Hamori & Somogyi, 1983). Rather surprisingly, these back-of-the-envelope calculations indicate that most granule cells receive direct synaptic inhibition from maximally one Golgi cell axon within a glomerulus. In consequence, a granule cell receives, on average, 3 inhibitory inputs across its four dendrites and if connectivity is probabilistic inputs are likely to originate from different Golgi cells. Since Golgi cell basolateral dendritic arbours do not overlap the interneurons contacting a given granule cell are likely to receive different mossy fibre input. For such an arrangement a particular mossy fibre contacting a granule cell therefore has a < 10% probability of exciting a Golgi cell, that inhibits the given granule cell (see equation 13).

$$N_{GoC} \cdot P_{MF-GoC\,/\,MF-GrC} = 3 \cdot 3\% \qquad \text{(Equation 13)}$$

N_{GoC} = number of Golgi cells inhibiting a granule cell; $P_{MF\text{-}GoC/MF\text{-}GrC}$ = probability of a mossy fibre contacting a Golgi cell inhibiting a granule cell.

Implications for granule cell inhibition

These calculations should be considered approximations due to the experimental limitations mentioned in Chapter 3. However, even a false estimate of e.g. mossy fibre terminal or Golgi cell density by a factor of 3 would still imply that a granule cell receives direct synaptic inhibition from few Golgi cells, which do

not receive the same excitatory input as the target cell. This anatomical arrangement suggests that granule cells receive lateral rather than classical feed-forward inhibition. However a glomerulus is innervated by multiple Golgi cells and GABA spillover can potentially regulate tonic inhibition based on surrounding feed-forward excitation. Additionally, the sensory input into the granule cell layer is organized in a fractured somatotopic map, which indicates that input is spatially highly correlated (Shambes *et al.*, 1978; Bower & Kassel, 1990; Garwicz *et al.*, 1998).

Comparison of mossy fibre-evoked EPSCs in Golgi and granule cells

A defining characteristic of mossy fibre-evoked EPSCs in Golgi cells was their fast kinetics. Golgi cell EPSCs had a rapid rise time which was due to highly synchronous release of quanta from mossy fibres, comparable to granule cell EPSCs (Chapter 6; Silver *et al.*, 1996; Sargent *et al.*, 2005). But NMDA and spillover currents contributed little to the EPSC waveform making the decay considerably faster compared to mossy fibre – granule cell EPSCs (Chapter 4 and 6; (Cathala *et al.*, 2000; DiGregorio *et al.*, 2002). Furthermore trains of mossy fibre – Golgi cell EPSCs showed little short-term depression (Chapter 4). This was most likely due to a large vesicle pool and rapid reloading of release sites in mossy fibre terminals as well as an apparent lack of receptor desensitization for Golgi cell AMPA receptors. Receptor desensitization contributes substantially to short-term depression at mossy fibre – granule cells synapses (Saviane & Silver, 2006); however receptors do not desensitize fully and thus are able to mediate a tonic current component due to spillover-related neurotransmitter build-up in the

synaptic cleft (DiGregorio *et al.*, 2007). The comparison suggests that the presynaptic mossy fibre exhibits similar properties for transmission onto Golgi and granule cells with the important exception of the quantal content (~2.5 for mossy fibre – granule cell; Sargent et al.; 2006 vs ~1.5 for mossy fibre – Golgi cell, Chapter 6). Also the apparent lack of spillover currents at the mossy fibre – Golgi cell synapse (Chapters 4 and 6) may be due to differences in the glutamate waveform experienced by postsynaptic receptors; either due to anatomical differences (Cathala *et al.*, 2005), differences in release probability or differential expression of glutamate transporters (DiGregorio *et al.*, 2002). Also differences in AMPA receptor expression between Golgi and granule cells (Nielsen *et al.*, 2004; DiGregorio *et al.*, 2007) may be responsible. Spillover and the associated tonic current component (DiGregorio *et al.*, 2002; Saviane & Silver, 2006; DiGregorio *et al.*, 2007), which carries most of the synaptic charge in granule cells during high frequency stimulation, allows the reliable transmission of rate-coded information with a broad bandwidth. In contrast, the fast kinetics of mossy fibre – Golgi cell currents appear to be tuned for precise temporal signaling. Fast EPSCs were also observed at other synapses thought to be specialized at the transmission of temporal information (Geiger *et al.*, 1997; Taschenberger & von Gersdorff, 2000; Galarreta & Hestrin, 2001). A comparison between the hippocampal granule cell – basket cell synapse, the Calyx of Held and the cerebellar mossy fibre to granule and Golgi cell synapse (**Table 2**) shows remarkable similarities between the hippocampal, cerebellar and auditory synapses.

EPSC parameter	GC – BC	Calyx	MF - GrC	MF - GoC
Temperature	34°C	35°C	37°C	35°C
Animal, Age	rat, P15-23	rat, P14	rat, P25	rat, P25
Mean evoked EPSC				
20-80% rise time (μs)	249	127	130	210
τ_1 decay (μs)	772	440	470	600
Rel. amplitude (%)	100	80	72	71
Weighted decay (ms)	0.77	1.2	2.4	1.5
Failures (%)	20	0	0	22
Uniquantal EPSC				
20-80% rise time (μs)	143	149	150	160
τ_1 decay (μs)	367	220	390	400
Rel. amplitude	100	77	83	84
τ_{decay} release time course (μs)	298	202	75	131

Table 2 Comparison of kinetic parameters at different central synapses: GC-BC = hippocampal granule cell to basket cell synapse (Geiger *et al.*, 1997); Calyx = Calyx of Held (Taschenberger & von Gersdorff, 2000; Taschenberger *et al.*, 2005; Scheuss *et al.*, 2007); MF-GrC = cerebellar mossy fibre to granule cell (Silver *et al.*, 1996a; DiGregorio *et al.*, 2002; Cathala *et al.*, 2003; Cathala *et al.*, 2005); MF – GoC = mossy fibre to Golgi cell .

Integration of mossy fibre inputs by Golgi cells

Little filtering of synaptic currents suggested that the soma and basolateral dendritic tree form an electronically compact compartment. In combination with a relatively low input resistance the fast EPSC kinetics resulted in rapidly rising and decaying EPSPs in the absence of sub-threshold boosting. The rapid initial EPSP decay (τ = ~2 ms) suggests that the integration time window for mossy fibre events is short and only coincident mossy fibre activity is effective in producing sufficient depolarization to elicit a spike. Experimentally the integration of on average 4 synchronously activated mossy fibre inputs was required to reach spike threshold. The quantal content of a mossy fibre – Golgi cell connection was ~1.5. This indicates that spatiotemporal integration of synaptic inputs distributed across the dendritic tree releasing a total of 6 quanta was sufficient to trigger a spike. Action potentials in Golgi cells were followed by a pronounced after-hyperpolarisation. Therefore the synaptic efficacy varied with the timing of the input in respect to the ongoing Golgi cell activity. The quantal efficacy is comparable to the cerebellar parallel fibre – stellate cell connection, where due to spontaneous activity, electronic compactness and high input resistance, single or few quanta can trigger action potentials (Carter & Regehr, 2002).

Mechanisms and implications of action potential precision

Several synaptic and cellular mechanisms contribute to remarkable spike time precision at the mossy fibre – Golgi cell connection. The interaction between a depolarising voltage change (e.g. EPSP) with voltage-gated sodium and potassium channels can produce an action potential at the site of spike initiation

(Hodgkin & Huxley, 1952). The precision of EPSP-spike coupling depends on the state and kinetics of voltage-gated channels mediating the action potential and the speed of voltage change - dV/dt (Jack *et al.*, 1975). In Golgi cells action potentials were predominantly triggered off the rising phase of the EPSP, where the rate of voltage change (dV/dt) is greatest (Jack *et al.*, 1975; Henze & Buzsaki, 2001), thereby facilitating the precision of spiking. The dV/dt (equivalent to EPSP kinetics at the site of action potential generation) is correlated with the input resistance and duration of current injection (Johnston & Wu, 1995) and inversely correlated with the axial resistance and membrane area (capacitance) between site of current injection and action potential generation (i.e electronic length (Jack *et al.*, 1975). As a consequence, EPSC kinetics are a major determinant of the precision of EPSP-spike coupling (Galarreta & Hestrin, 2001; Cathala *et al.*, 2003) as they determine the rising phase of the EPSP. The mossy fibre EPSPs in Golgi cells exhibited rapid kinetics due to low input resistance and electronic compactness in combination with rapid EPSC kinetics. Fast EPSC kinetics were achieved through synchronous neurotransmitter release, rapid AMPA receptor kinetics and little contribution of kainate-, NMDA receptor and spillover currents. Golgi cells can maintain spike timing precision because EPSC waveform and amplitude does not change much during trains of stimuli. Furthermore pacemaker currents underlying intrinsic Golgi cell activity produce a pronounced afterhyperpolarization that ensures rapid recovery of voltage-gated sodium channels from inactivation (Berry & Meister, 1998). Prolonged membrane hyperpolarisation has been shown to improve action potential precision by reducing jitter accumulation during trains (Schaefer *et al.*, 2006).

Together the synaptic and cellular properties at this connection allowed action potential signaling with a 200μs precision.

Other central synapses thought to be tuned for temporal signaling employ similar mechanisms to achieve spike time precision. The hippocampal granule cell – basket cell synapse has a fast neurotransmitter release time course, synapses located (peri-) somatically and little contribution of NMDA receptors to synaptic currents (Geiger *et al.*, 1997; Lawrence & McBain, 2003; Jonas *et al.*, 2004). At the cerebellar parallel fibre – stellate cell synapse a high quantal efficacy is also achieved through fast EPSC kinetics, electronic compactness and a high input resistance (Carter & Regehr, 2002). But the spike precision at these connections is limited to around a millisecond (Pouille & Scanziani, 2001; Carter & Regehr, 2002), possibly because when few quanta are involved in synaptic transmission the stochastic nature of vesicular release produces temporal jitter in the EPSC timing and shape from trial-to-trial. The mossy fibre – Golgi cell connection overcomes this limitation with a rapid vesicular release time course, comparable to release at the Calyx of Held, and thus achieves a considerably higher spike time precision than has been shown for other central synapses signaling with few quanta.

The higher precision of mossy fibre – Golgi cell transmission suggests a high information content of a spike initiated through this connection. The information content can be calculated as the entropy per spike (in bits) with equation 14 (Rieke *et al.*, 1997).

$$\frac{S}{T} = \bar{r} \cdot \log_2\left(\frac{e}{\bar{r} \cdot \Delta\tau}\right) \qquad \text{(Equation 14)}$$

S = Entropy, T = duration of spike train (defined as 100 ms), $\bar{r}$ = mean firing rate, $\Delta\tau$ = spike time precision (measured as SD of spike jitter). The entropy per spike for the mossy fibre-Golgi cell connection in a range of mean firing rates from 1 to 100 Hz is between 20% ($\bar{r}$ =1 Hz) and 50% ($\bar{r}$ =100 Hz) greater than that seen for synaptic connections with 1 ms precision (Miles, 1990; Fricker & Miles, 2000; Galarreta & Hestrin, 2001; Carter & Regehr, 2002; Gabernet *et al.*, 2005). However, the observed temporal precision *in vitro* represents an upper limit to the signalling accuracy of Golgi cells and its utilization *in vivo* remains uncertain.

Decoupling of mossy fibre input and Golgi cell output rate

Spike initiation was not reliable especially at high input frequencies although EPSC amplitude and waveform showed little frequency dependent change (Chapter 5). The unreliability was due to dominant pacemaker currents responsible for the relative refractory period after an action potential. In consequence the increase in Golgi cell firing rate with mossy fibre stimulation frequency was sub-linear and meant that Golgi cell firing rate was effectively decoupled from the mossy fibre input rate. Therefore mossy fibre rate-coded information is poorly transmitted via this connection. Instead, the synaptic and cellular properties appear to be tuned to selectively transmit temporal information, i.e. correlation in the mossy fibre train. These observations are consistent with *in vivo* experiments, where Golgi cell exhibited instantaneous firing rates up to 50 Hz in response to sensory stimulation, but showed little rate modulation over larger time windows (Edgley & Lidierth, 1987; Vos *et al.*,

1999b; De Schutter *et al.*, 2000). Differences in the maximal Golgi cell firing rate between *in vivo* and *in vitro* recordings are likely to reflect differences in the excitatory drive of the parallel fibre – Golgi cell input.

Feed-forward inhibition of granule cells

Granule cells receive phasic inhibition mediated by the action potential-dependent release of GABA onto synaptic $GABA_A$ receptors and tonic inhibition mediated by the activation of α_6 and δ-subunit containing extrasynaptic $GABA_A$ receptors (Brickley *et al.*, 1996; Nusser *et al.*, 1998; Rossi & Hamann, 1998; Stell *et al.*, 2003). The level of ambient GABA level is partially dependent on Golgi cell firing activity (Carta *et al.*, 2004). This dependence is likely to be mediated by a GABA spillover component of synaptic IPSCs (Rossi & Hamann, 1998). With development a shift from almost pure phasic GABA release at juvenile age (P7 rats, Wall & Usowicz, 1997) to predominant tonic inhibition at P21 occurs. At older age the tonic component carries 99% of the total inhibitory charge at rest (Brickley *et al.*, 1996) and contributes significantly to noisy membrane voltage fluctuations. Tonic inhibition in combination with membrane voltage fluctuations arising from excitatory synaptic input has been implicated in gain control of granule cells (Rossi & Hamann, 1998; Mitchell & Silver, 2003). But the role of phasic inhibition of granule cells remains elusive. My results show that a large majority of granule cells (>80%) receive phasic inhibition. Direct Golgi cell axon stimulation evoked IPSCs with fast rise time and little transmission jitter confirming earlier results obtained through paired Golgi – granule cell recordings (Dugue *et al.*, 2005). In combination with the temporally precise activation of Golgi cells by mossy fibre input, the feed-forward inhibition

of granule cells occurred with high temporal precision. These results establish the presence of a functional feed-forward inhibitory circuit in the granule cell layer. The disynaptic IPSC canceled slow excitatory mossy fibre EPSC components and is likely to curtail the granule cell integration time window. Previous studies of feed-forward inhibition of hippocampal pyramidal cells suggested that such an arrangement enhances the temporal precision of neuronal firing (Pouille & Scanziani, 2001).

However, as discussed above, the connection probability of mossy fibres onto Golgi and granule cells would suggest that interneuron and target cell do not share the same excitatory input. Therefore, unless mossy fibre input is spatiotemporally correlated, Golgi cells direct synaptic inhibition will be temporally uncorrelated with excitatory mossy fibre input. Since the disynaptic IPSC amplitude is small in comparison to mossy fibre EPSCs, it is unlikely to affect granule cell firing significantly. However, GABA spillover onto extrasynaptic receptors (Rossi & Hamann, 1998), which I confirmed also occurs in adult animals (Chapter 7), may contribute to regulation of tonic inhibition and thereby influence granule cell firing on larger timescales. In contrast, spatiotemporally correlated input, mimicked by electrical stimulation of the white matter tract *in vitro*, has the appropriate timing to potentially control granule cell spike timing. Thus the spatiotemporal properties of the mossy fibre input determine whether Golgi cells mediate feed-forward, controlling spike timing, and/or lateral inhibition, controlling firing rate of granule cells.

Mossy fibre firing patterns *in vivo*

Mossy fibres originate from various extracerebellar sources and carry information about different sensory modalities. They code for different stimulus features with varying sensitivity and can be multimodal. *In vivo* recordings of mossy fibres and granule cells give some insight into how mossy fibres encode information in various sensory stimulation paradigms. Tactile skin stimulation activates multiple mossy fibres converging onto a single granule cell (Jorntell & Ekerot, 2006) and produces a barrage of EPSPs that results in high frequency firing of granule cells *in vivo* (Jaeger & Bower, 1994; Jorntell & Ekerot, 2006). This suggests a high spatial correlation in mossy fibre population activity in response to certain stimuli. In contrast, whisker stimulation of mice typically results in a burst of high frequency firing (up to 700 Hz) in a single mossy fibre contacting a granule cell. Synaptic integration of this input can produce a burst of action potentials in granule cells (Chadderton *et al.*, 2004; Rancz *et al.*, 2007). On the contrary, vestibular and spinocerebellar mossy fibres coding for centrifugal acceleration (Lisberger & Fuchs, 1978) and joint angle (Van Kan *et al.*, 1993) show tonic firing behaviour between 0 and 150 Hz which is converted to tonic granule cell firing (Mitchell & Silver, 2003) modulated by the respective sensory stimulus parameter. The influence of different mossy fibre firing patterns on Golgi cell firing will be discussed in the following section.

Golgi cell response to sensory stimulation

Golgi cells *in vivo* react with a transient increase in instantaneous firing rate to tactile stimulation of face and forelimbs in anesthetized animals at the onset of sensory stimulation (Vos *et al.*, 1999b; Holtzman *et al.*, 2006). In rat (not in cats

and monkeys) this is followed by a period of firing inactivity (Vos *et al.*, 1999b). The silent period can also occur in the absence of the transient increase in firing rate and has a broader receptive field (Holtzman *et al.*, 2006). The transient increase in firing rate often displayed multiple peaks in the peristimulus spike histogram. A short latency (5-10 ms) very precise peak with a small receptive field, a broader large latency (~20 ms) peak with a larger receptive field and combination of these behaviours are observed in rats (Vos *et al.*, 1999b; Holtzman *et al.*, 2006). It has been speculated that the initial component is due to trigeminal mossy fibres and later inputs due to corticopontine and parallel fibre inputs. But the origin of distinctive peaks remains elusive since Golgi cells receive excitatory input from mossy, parallel and potentially climbing fibres. These inputs cannot be distinguished in extracellular unit recordings.

The *in vitro* experiments presented in this thesis show the activation of Golgi cells by mossy fibre input in isolation. The rapid initial decay time course of the mossy fibre - Golgi cell EPSP (τ ~2 ms) suggests that the integration time window for mossy fibre events is small. Only synchronous mossy fibre activity will therefore be effective in producing sufficient depolarization to elicit a spike. The connectivity together with synaptic and cellular properties of a Golgi cell confer the ability to selectively detect correlated activity in multiple mossy fibres or high frequency firing (>300 Hz) in a single fibre. Such activity has been observed in anesthetized and decerebrate animals in response to tactile stimulation of skin (Jorntell & Ekerot, 2006) and whisker deflection (Rancz *et al.*, 2007), respectively. The prediction from my *in vitro* data is that Golgi cells respond to such sensory input with a temporally precise action potential followed

by a relative refractory period. This behaviour mimics the initial response of Golgi cells to sensory stimulation *in vivo* and suggests that mossy fibre activation underlies the precisely timed, short latency response occurring at the onset of tactile stimulation of facial skin and forelimbs. But, low frequency and uncorrelated tonic mossy fibre input, observed during vestibular stimulation (Barmack & Yakhnitsa, 2008) and joint displacement (Van Kan *et al.*, 1993) is likely to only weakly activate the mossy fibre – Golgi cell pathway. In tune with this idea, those sensory stimuli have been shown to produce slow modulations of tonic Golgi cell firing of in anesthetized and awake animals (Edgley & Lidierth, 1987; Barmack & Yakhnitsa, 2008). Thus the mossy fibre – Golgi cell connection may be tuned to selectively signal the onset-timing of certain sensory stimuli.

This illustrates that the variability of Golgi cell responses observed *in vivo* is likely to reflect differences in spatiotemporal mossy fibre input associated with different stimuli, together with influences of Golgi cell intrinsic activity and differential inhibition of Golgi cells by Lugaro, basket and stellate cells (Dumoulin *et al.*, 2001).

Physiological implications for granule cell processing

My experimental results suggest that mossy fibre input on the basal dendrites of Golgi cells is likely to extract coincident sensory input by resetting the phase of spontaneous Golgi cell firing. This is consistent with *in vivo* studies which show that Golgi cells are spontaneously active (Edgley & Lidierth, 1987) and can exhibit a spike timing precision in the sub-millisecond range at the onset of a

sensory stimulus (Vos *et al.*, 1999b; Holtzman *et al.*, 2006). Such a response will evoke precisely timed phasic inhibition in a large population (>1000) of surrounding granule cells. My anatomical characterization of the circuitry suggests that interneuron and granule cell do not normally share the same excitatory input. However, the mossy fibre input train is likely to be spatially correlated due to the fractured somatotopic organization of the fibre input into the granule cell layer (Shambes *et al.*, 1978; Garwicz *et al.*, 1998) and highly spatiotemporally correlated mossy fibre input has been observed in granule cells *in vivo* during tactile stimulation of the forelimbs (Jorntell & Ekerot, 2006). This suggests that the circuitry is able to act as a classical feed-forward inhibitory loop given appropriate sensory stimuli. Since granule cells need to integrate multiple quanta to reach threshold and disynaptic IPSCs cancel slow granule cell EPSC components, Golgi cell mediated feed-forward inhibition is likely reduce the time window for synaptic integration (Pouille & Scanziani, 2001). This is likely to shape the latency and precision of the first spike in the granule cell response. In fact, such precise firing of GrCs has been observed *in vivo* following both mechanical and electrical stimulation of the upper lip (Bower & Woolston, 1983). Following the initial spike, Golgi cells will be insensitive to further mossy fibre input for 10's of milliseconds due to the pronounced Golgi cell after-hyperpolarisation. This transient relief from phasic inhibition, the presence of metabotropic glutamate receptor-mediated local inhibition of GABA release (Mitchell & Silver, 2000b) and summation of slow, spillover mediated components of the mossy fibre-granule cell EPSC (Saviane & Silver, 2006) is likely to make mossy fibre input more effective at activating granule cells during the remainder of EPSP barrage and result in increased granule cell firing as

observed *in vivo* (Jaeger & Bower, 1994; Chadderton *et al.*, 2004; Rancz *et al.*, 2007). However, the timing of subsequent action potentials is likely to be less precise, and may convey rate-coded rather than timing-based information. Therefore differences in synaptic transmission and spike generation in Golgi cell and granule cell result in the selective routing of timing- and rate-coded information contained in the mossy fibre train (see **Figure 8-1**).

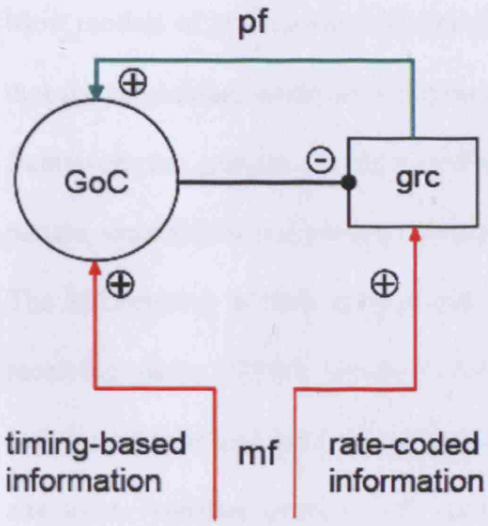

Figure 8-1 Proposed schematic diagram of the granule cell layer circuitry. Rate-coded information carried by mossy fibres (mf) is transmitted via granule cells (grc), whereas spike-timing based information contained in the spike train is routed via the Golgi cell (GoC), which can control granule cell spike timing via feed-forward inhibition at the onset of a stimulus train.

Evaluation of models of cerebellar processing in the light of new experimental evidence

Most models of granule cell layer processing are based on the underlying notion that the cerebellum works as a pattern recognition machine (Marr, 1969). In this framework the granule cell layer performs an input transformation that increases pattern separability and prevents overexcitation of subsequent processing stages. The information is then relayed via parallel fibres onto Purkinje cells, each receiving over 150000 parallel fibre inputs, which subsequently recognize activity patterns and produce adequate spike output. Golgi cells are thought to adaptively regulate granule cell excitability, so that parallel fibre activity is maintained within a narrow range in response to variable mossy fibre activity. Albus (Albus, 1971) specified that the optimal amount of parallel fibre activity for pattern storage and retrieval is 1% and proposed that Golgi cells regulate granule cell excitability to maintain this level of activation. Instead, Eccles (Eccles *et al.*, 1967) suggested that "Golgi cell inhibition suppresses discharges from weakly excited granule cells and thus serves to focus the response to those granule cells strongly excited by mossy fibre input" - a role similar to lateral inhibition sharpening spatial patterns.

Neither of these models incorporated the need to represent the timing of inputs and dynamic input integration in cerebellar processing. Braitenberg (Braitenberg, 1967) proposed that timing information is retained in delay lines along the parallel fibre beam. However, subsequent experimental results showed that Purkinje cells are predominantly responsive to parallel fibre activity originating in the underlying granule cell layer and invalidated the delay line hypothesis

(Bower & Woolston, 1983; Ekerot & Jorntell, 2003). More recent models of granule cell layer processing are designed to convert mossy fibre activity to firing of varying populations of granule cells, thus retaining the information conveyed over a period of hundreds of milliseconds (Fujita, 1982; Medina & Mauk, 2000) or, as a variation, generate network dynamics that represents a stimulus with constantly changing ensemble of firing neurons (Karmarkar & Buonomano, 2007; Yamazaki & Tanaka, 2007a). In this way the spatiotemporal properties of sensory stimuli can be encoded in a specific non-recurring dynamic pattern in the granule cell population activity.

Motivated by the observation of local field potential oscillations in the cerebellum (Adrian, 1935; Hartmann & Bower, 1998; Courtemanche *et al.*, 2002; Courtemanche & Lamarre, 2005) other models emphasize the importance of spike timing and synchronization in cerebellar processing (Isope *et al.*, 2002). Local field potential oscillations in the theta-rhythm range have been observed in the granule cell layer of the paramedian cerebellum of rats (Hartmann & Bower, 1998) and monkeys (Courtemanche & Lamarre, 1997, 2005). They occur when the animal is at rest or expecting a stimulus and disappear in response to sensory stimulation (Courtemanche & Lamarre, 2005). Local field potential oscillations were correlated with synchronized granule cell firing (Courtemanche *et al.*, 2002). Spike timing of granule cells in respect to ongoing theta-rhythm oscillations could be used by the cerebellum to represent stimulus parameters (Hopfield, 1995), similarly to coding schemes proposed for spatial navigation by hippocampal place cells (O'Keefe & Recce, 1993) and mitral cells in olfactory processing (Brody & Hopfield, 2003). But oscillation in hippocampus and

olfactory bulb persists during sensory stimulation, whereas cerebellar oscillations are greatly reduced.

In the following I will summarize my experimental findings and discuss the presented models of granule cell layer computation.

(1) The anatomical connectivity in the granule cell layer suggests granule cells are not excited by the same mossy fibres as the interneurons they receive inhibition from. This indicates that granule cells, depending on the spatiotemporal properties of mossy fibre input, receive either lateral or classical feed-forward inhibition.

(2) Golgi cells perform a highly non-linear input integration due to pacemaker conductances underlying rhythmic firing which effectively decouples mean firing rate from mossy fibre input.

(3) Golgi cell spontaneous rhythmic firing can be reset by mossy fibre input with high temporal precision.

(4) The long after-hyperpolarisation after an action potential makes Golgi cells insensitive to subsequent synaptic input, thereby creating a time window of disinhibition in granule cells after the initial IPSC. Thus the timing of excitatory input in respect to the ongoing Golgi firing is important for its synaptic efficacy.

(5) The amplitude of the phasic inhibitory conductance in comparison to the excitatory drive in granule cells via mossy fibres is small. But amplitude and timing of feed-forward IPSCs are tuned to cancel slow mossy fibre – granule cell EPSC components.

(6) The synergy of synaptic and cellular mechanisms in the mossy fibre – Golgi cell - granule cell circuitry ensures inhibitory signaling with high temporal precision.

Marr and Albus suggested that parallel fibre input allowed Golgi cells slow global sampling of the network population whereas mossy fibre input provided local fast sampling of the input activity. The estimate of present and predicted network activity can then be used to regulate granule cell excitability via feed-forward and feedback inhibition. In support of this theory tonic inhibition mediated by Golgi cells has been shown to alter the input-output relationship of granule cells (Brickley *et al.*, 1996; Rossi & Hamann, 1998; Mitchell & Silver, 2003) and GABA spillover onto extrasynaptic α_6-containing GABA receptors could potentially dynamically alter tonic inhibition with Golgi cell firing rate (Rossi & Hamann, 1998). However, the findings presented in this thesis show that Golgi cells are poor predictors of mean mossy fibre activity. Furthermore the model assumes that granule cell and Golgi cell receive common mossy fibre input but analysis of the anatomical arrangement suggests that this is not the case, unless mossy fibre input is spatiotemporally correlated. The predicted granule cell layer connectivity, suggesting lateral inhibition, favors a role of inhibition in shaping granule cell receptive fields as proposed by Eccles. However, the phasic inhibitory conductance is relatively small compared to the excitatory drive granule cells experience during sensory stimulation (Chadderton *et al.*, 2004; Jorntell & Ekerot, 2006; Rancz *et al.*, 2007). Therefore it is unlikely to affect the mean granule cell firing rate as would be expected for classical lateral inhibition.

To generate network dynamics that can represent the timing of a stimulus with constantly changing ensemble of firing neurons a randomly connected recurrent inhibitory network with long integration time constants for input signals is required (Yamazaki & Tanaka, 2007b). The connectivity and synaptic properties between mossy fibres, granule cell and Golgi cells seems appropriate for such an encoding scheme. Particularly, in the absence of correlated mossy fibre input, Golgi cell inhibition of granule cell is unlikely to entrain with sensory mossy fibre input. Therefore the ongoing Golgi cell mediated phasic inhibition will partly decorrelate granule cell activity from mossy fibre input and diversify the granule cell population activity in response to similar stimuli. However, in such a regime, it is unclear how reproducibility of network dynamics in response to a repetition of the same stimulus is achieved. The concerted action of a group of Golgi cells via feed-forward inhibition of granule cells on the onset of sensory stimulation may act as a reset mechanism to constrain network dynamics and increase reproducibility (Knusel *et al.*, 2004).

Synchronized granule cell activity, which underlies theta-frequency oscillations in the granule cell layer in cerebellar areas CrusI-II (Hartmann & Bower, 1998; Courtemanche *et al.*, 2002) is important for synaptic input integration in Purkinje cell, because feed-forward inhibition by molecular layer interneurons powerfully reduces the integration time window for parallel fibre events (Mittmann *et al.*, 2005). Furthermore synchronous granule cell population activity induces in combination with a climbing fibre input long term depression at parallel fibre - Purkinje cell synapses, which is thought to be essential for storage and recall of

sensory input patterns in form of a parallel fibre synaptic weight matrix onto Purkinje cells (Albus, 1971; Wang *et al.*, 2000; Jorntell & Ekerot, 2002; Brunel *et al.*, 2004; Ito, 2006; Steuber *et al.*, 2007). A likely candidate mechanism for the synchronization of granule cell firing is the inhibition by Golgi cells. Spontaneous Golgi cell firing has been shown to synchronize due to common parallel fibre input (Vos *et al.*, 1999a) which is likely to entrain granule cell firing along the parallel fibre axis (Maex & De Schutter, 1998). Local groups of Golgi cells could synchronize due to correlated mossy and parallel fibre input or common inhibition and synchronize several thousand granule cells. This may be responsible for the network oscillations observed *in vivo*. However, oscillations have only been observed in the paramedian cerebellum and no other part of the cerebellar cortex (Courtemanche *et al.*, 2002).

This discussion shows that the properties of phasic feed-forward inhibition of granule cells do not comply with the mechanistic requirements of a number of proposed models of granule cell layer processing. Instead, they highlight the need to understand the interaction of intrinsic network activity with evoked sensory input as well as the spatiotemporal properties of mossy fibre input to fully grasp granule cell layer processing.

The cerebellar cortex coordinates movements by computing, in 10s of milliseconds (Orlovsky, 1972; Rosen & Scheid, 1972), precisely timed (Ivry & Keele, 1989; Medina & Mauk, 2000) motor sequences based on sensory information. In such short processing time spike-time dependent coding seems attractive. In fact, impairment of spike timing in Purkinje cells (Walter *et al.*,

2006) and ablation of Golgi cells (Watanabe *et al.*, 1998) cause ataxia. But whether and how sensory events are represented with high temporal precision is unknown. My findings provide evidence for the likely synaptic basis of precise sensory evoked Golgi cell responses on the onset of certain (e.g. trigeminal) sensory stimulation *in vivo* (Vos *et al.*, 1999b; Holtzman *et al.*, 2006), and suggest that the synaptic and cellular properties of mossy fibre – Golgi cell – granule cell circuitry are tuned to allow timing and rate information to be routed through separate synaptic 'channels' at the input layer of the cerebellar cortex.

Bibliography

Adrian ED. (1935). Discharge frequencies in the cerebral and cerebellar cortex. *J Physiol* **83,** 33.

Albus JS. (1971). A theory of cerebellar function. *Math Biosci* **10,** 25-61.

Alonso A & Llinas RR. (1989). Subthreshold Na+-dependent theta-like rhythmicity in stellate cells of entorhinal cortex layer II. *Nature* **342,** 175-177.

Arieli A, Sterkin A, Grinvald A & Aertsen A. (1996). Dynamics of ongoing activity: explanation of the large variability in evoked cortical responses. *Science* **273,** 1868-1871.

Armano S, Rossi P, Taglietti V & D'Angelo E. (2000). Long-term potentiation of intrinsic excitability at the mossy fiber-granule cell synapse of rat cerebellum. *J Neurosci* **20,** 5208-5216.

Arthur RM, Pfeiffer RR & Suga N. (1971). Properties of 'two-tone inhibition' in primary auditory neurones. *J Physiol* **212,** 593-609.

Barmack NH & Yakhnitsa V. (2008). Functions of interneurons in mouse cerebellum. *J Neurosci* **28,** 1140-1152.

Barrett EF & Stevens CF. (1972). The kinetics of transmitter release at the frog neuromuscular junction. *J Physiol* **227,** 691-708.

Bartos M, Vida I, Frotscher M, Geiger JR & Jonas P. (2001). Rapid signaling at inhibitory synapses in a dentate gyrus interneuron network. *J Neurosci* **21,** 2687-2698.

Batchelor AM & Garthwaite J. (1992). GABAB receptors in the parallel fiber pathway of rat cerebellum. *Eur J Neurosci* **4,** 1059-1064

Beierlein M, Fioravante D & Regehr WG. (2007). Differential expression of posttetanic potentiation and retrograde signaling mediate target-dependent short-term synaptic plasticity. *Neuron* **54,** 949-959.

Ben-Ari Y. (2002). Excitatory actions of gaba during development: the nature of the nurture. *Nat Rev Neurosci* **3,** 728-739.

Berry MJ, 2nd & Meister M. (1998). Refractoriness and neural precision. *J Neurosci* **18,** 2200-2211.

Botta P, Radcliffe RA, Carta M, Mameli M, Daly E, Floyd KL, Deitrich RA & Valenzuela CF. (2007). Modulation of GABAA receptors in cerebellar

granule neurons by ethanol: a review of genetic and electrophysiological studies. *Alcohol* **41,** 187-199.

Bower JM & Kassel J. (1990). Variability in tactile projection patterns to cerebellar folia crus IIA of the Norway rat. *J Comp Neurol* **302,** 768-778.

Bower JM & Woolston DC. (1983). Congruence of spatial organization of tactile projections to granule cell and Purkinje cell layers of cerebellar hemispheres of the albino rat: vertical organization of cerebellar cortex. *J Neurophysiol* **49,** 745-766.

Braitenberg V. (1967). Is the cerebellar cortex a biological clock in the millisecond range? *Prog Brain Res* **1967,** 334-346.

Brickley SG, Cull-Candy SG & Farrant M. (1996). Development of a tonic form of synaptic inhibition in rat cerebellar granule cells resulting from persistent activation of GABAA receptors. *J Physiol* **497,** 753-759.

Brickley SG, Revilla V, Cull-Candy SG, Wisden W & Farrant M. (2001). Adaptive regulation of neuronal excitability by a voltage-independent potassium conductance. *Nature* **409,** 88-92.

Brody CD & Hopfield JJ. (2003). Simple networks for spike-timing-based computation, with application to olfactory processing. *Neuron* **37,** 843-852.

Brunel N, Hakim V, Isope P, Nadal JP & Barbour B. (2004). Optimal information storage and the distribution of synaptic weights: perceptron versus Purkinje cell. *Neuron* **43,** 745-757.

Bureau I, Dieudonne S, Coussen F & Mulle C. (2000). Kainate receptor-mediated synaptic currents in cerebellar Golgi cells are not shaped by diffusion of glutamate. *Proc Natl Acad Sci U S A* **97,** 6838-6843.

Cajal R. (1911). *Histologie du système nerveux de l'homme et des vertebrés*, vol. II. Maloine, Paris.

Carta M, Mameli M & Valenzuela CF. (2004). Alcohol enhances GABAergic transmission to cerebellar granule cells via an increase in Golgi cell excitability. *J Neurosci* **24,** 3746-3751.

Carter AG & Regehr WG. (2002). Quantal events shape cerebellar interneuron firing. *Nat Neurosci* **5,** 1309-1318.

Cathala L, Brickley S, Cull-Candy S & Farrant M. (2003). Maturation of EPSCs and intrinsic membrane properties enhances precision at a cerebellar synapse. *J Neurosci* **23,** 6074-6085.

Cathala L, Holderith NB, Nusser Z, DiGregorio DA & Cull-Candy SG. (2005). Changes in synaptic structure underlie the developmental speeding of AMPA receptor-mediated EPSCs. *Nat Neurosci* **8,** 1310-1318.

Cathala L, Misra C & Cull-Candy S. (2000). Developmental profile of the changing properties of NMDA receptors at cerebellar mossy fiber-granule cell synapses. *J Neurosci* **20,** 5899-5905.

Chadderton P, Margrie TW & Hausser M. (2004). Integration of quanta in cerebellar granule cells during sensory processing. *Nature* **428,** 856-860.

Chen C & Regehr WG. (1999). Contributions of residual calcium to fast synaptic transmission. *J Neurosci* **19,** 6257-6266.

Clements JD & Silver RA. (2000). Unveiling synaptic plasticity: a new graphical and analytical approach. *Trends Neurosci* **23,** 105-113.

Cobb SR, Buhl EH, Halasy K, Paulsen O & Somogyi P. (1995). Synchronization of neuronal activity in hippocampus by individual GABAergic interneurons. *Nature* **378,** 75-78.

Cobb SR, Halasy K, Vida I, Nyiri G, Tamas G, Buhl EH & Somogyi P. (1997). Synaptic effects of identified interneurons innervating both interneurons and pyramidal cells in the rat hippocampus. *Neuroscience* **79,** 629-648.

Courtemanche R & Lamarre Y. (1997). Localization of cerebellar oscillatory activity of the awake monkey and relation with cortical rhythms. *Abstracts Society for Neuroscience* **23,** 1286.

Courtemanche R & Lamarre Y. (2005). Local field potential oscillations in primate cerebellar cortex: synchronization with cerebral cortex during active and passive expectancy. *J Neurophysiol* **93,** 2039-2052.

Courtemanche R, Pellerin JP & Lamarre Y. (2002). Local field potential oscillations in primate cerebellar cortex: modulation during active and passive expectancy. *J Neurophysiol* **88,** 771-782.

Crepel F, Delhaye-Bouchaud N, Guastavino JM & Sampaio I. (1980). Multiple innervation of cerebellar Purkinje cells by climbing fibres in staggerer mutant mouse. *Nature* **283,** 483-484.

D'Angelo E, De Filippi G, Rossi P & Taglietti V. (1995). Synaptic excitation of individual rat cerebellar granule cells in situ: evidence for the role of NMDA receptors. *J Physiol* **484,** 397-413.

D'Angelo E, Rossi P, Armano S & Taglietti V. (1999). Evidence for NMDA and mGlu receptor-dependent long-term potentiation of mossy fiber-granule cell transmission in rat cerebellum. *J Neurophysiol* **81,** 277-287.

De Schutter E, Vos B & Maex R. (2000). The function of cerebellar Golgi cells revisited. *Prog Brain Res* **124,** 81-93.

De Schutter E, Vos BP & Maex R. (2000). The function of cerebellar Golgi cells revisited. *Prog Brain Res* **124,** 81-93.

Desmaisons D, Vincent JD & Lledo PM. (1999). Control of action potential timing by intrinsic subthreshold oscillations in olfactory bulb output neurons. *J Neurosci* **19,** 10727-10737.

Dickson CT, Magistretti J, Shalinsky M, Hamam B & Alonso A. (2000). Oscillatory activity in entorhinal neurons and circuits. Mechanisms and function. *Ann N Y Acad Sci* **911,** 127-150.

Dieudonne S. (1998). Submillisecond kinetics and low efficacy of parallel fibre-Golgi cell synaptic currents in the rat cerebellum. *J Physiol* **510,** 845-866.

Dieudonne S & Dumoulin A. (2000). Serotonin-driven long-range inhibitory connections in the cerebellar cortex. *J Neurosci* **20,** 1837-1848.

DiGregorio DA, Nusser Z & Silver RA. (2002). Spillover of glutamate onto synaptic AMPA receptors enhances fast transmission at a cerebellar synapse. *Neuron* **35,** 521-533.

DiGregorio DA, Rothman JS, Nielsen TA & Silver RA. (2007). Desensitization properties of AMPA receptors at the cerebellar mossy fiber granule cell synapse. *J Neurosci* **27,** 8344-8357.

Dino MR, Nunzi MG, Anelli R & Mugnaini E. (2000). Unipolar brush cells of the vestibulocerebellum: afferents and targets. *Prog Brain Res* **124,** 123-137.

Dugue GP, Dumoulin A, Triller A & Dieudonne S. (2005). Target-dependent use of co-released inhibitory transmitters at central synapses. *J Neurosci* **25,** 6490-6498.

Dumoulin A, Triller A & Dieudonne S. (2001). IPSC kinetics at identified GABAergic and mixed GABAergic and glycinergic synapses onto cerebellar Golgi cells. *J Neurosci* **21,** 6045-6057.

Eccles JC, Ito M & Szentagothai J. (1967). *The cerebellum as a neuronal machine*. Springer-Verlag, Berlin.

Edgley SA & Lidierth M. (1987). The discharges of cerebellar Golgi cells during locomotion in the cat. *J Physiol* **392,** 315-332.

Ekerot CF & Jorntell H. (2001). Parallel fibre receptive fields of Purkinje cells and interneurons are climbing fibre-specific. *Eur J Neurosci* **13,** 1303-1310.

Ekerot CF & Jorntell H. (2003). Parallel fiber receptive fields: a key to understanding cerebellar operation and learning. *Cerebellum* **2,** 101-109.

Emson PC. (2007). GABA(B) receptors: structure and function. *Prog Brain Res* **160,** 43-57.

Fetz EE & Gustafsson B. (1983). Relation between shapes of post-synaptic potentials and changes in firing probability of cat motoneurones. *J Physiol* **341,** 387-410.

Fiser J, Chiu C & Weliky M. (2004). Small modulation of ongoing cortical dynamics by sensory input during natural vision. *Nature* **431,** 573-578.

Forti L, Cesana E, Mapelli J & D'Angelo E. (2006). Ionic mechanisms of autorhythmic firing in rat cerebellar Golgi cells. *J Physiol* **574,** 711-729.

Fox CA, D. E. Hillmann, K. A. Siegesmund, and C. R. Dutta (1967). The primate cerebellar cortex: A Golgi and electron microscopic study. *Prog Brain Res: The Cerebellum,* 174-225.

Fricker D & Miles R. (2000). EPSP amplification and the precision of spike timing in hippocampal neurons. *Neuron* **28,** 559-569.

Fujita M. (1982). Adaptive filter model of the cerebellum. *Biological Cybernetics* **45,** 195-206.

Gabbiani F, Midtgaard J & Knopfel T. (1994). Synaptic integration in a model of cerebellar granule cells. *J Neurophysiol* **72,** 999-1009.

Gabernet L, Jadhav SP, Feldman DE, Carandini M & Scanziani M. (2005). Somatosensory integration controlled by dynamic thalamocortical feed-forward inhibition. *Neuron* **48,** 315-327.

Galarreta M & Hestrin S. (2001). Spike transmission and synchrony detection in networks of GABAergic interneurons. *Science* **292,** 2295-2299.

Gall D, Prestori F, Sola E, D'Errico A, Roussel C, Forti L, Rossi P & D'Angelo E. (2005). Intracellular calcium regulation by burst discharge determines bidirectional long-term synaptic plasticity at the cerebellum input stage. *J Neurosci* **25,** 4813-4822.

Garwicz M, Jorntell H & Ekerot CF. (1998). Cutaneous receptive fields and topography of mossy fibres and climbing fibres projecting to cat cerebellar C3 zone. *J Physiol* **512,** 277-293.

Geiger JR, Lubke J, Roth A, Frotscher M & Jonas P. (1997). Submillisecond AMPA receptor-mediated signaling at a principal neuron- interneuron synapse. *Neuron* **18,** 1009-1023.

Geurts FJ, De Schutter E & Dieudonne S. (2003). Unraveling the cerebellar cortex: cytology and cellular physiology of large-sized interneurons in the granular layer. *Cerebellum* **2,** 290-299.

Glickfeld LL & Scanziani M. (2006). Distinct timing in the activity of cannabinoid-sensitive and cannabinoid-insensitive basket cells. *Nat Neurosci* **9,** 807-815.

Golgi C. (1886). *Studii sulla fina anatomia degli organi centrali del sistema nervoso.* U. Hoepli, Milano.

Gray CM, König P, Engel AK & Singer W. (1989). Oscillatory responses in cat visual cortex exhibit inter-columnar synchronization which reflects global stimulus properties. *Nature* **338,** 334-337.

Gulyas AI, Miles R, Sik A, Toth K, Tamamaki N & Freund TF. (1993). Hippocampal pyramidal cells excite inhibitory neurons through a single release site. *Nature* **366,** 683-687.

Hamori J & Somogyi J. (1983). Differentiation of cerebellar mossy fiber synapses in the rat: a quantitative electron microscope study. *J Comp Neurol* **220,** 365-377.

Hamori J & Szentagothai J. (1966). Participation of Golgi neuron processes in the cerebellar glomeruli: an electron microscope study. *Exp Brain Res* **2,** 35-48.

Hanchar HJ, Dodson PD, Olsen RW, Otis TS & Wallner M. (2005). Alcohol-induced motor impairment caused by increased extrasynaptic GABA(A) receptor activity. *Nat Neurosci* **8,** 339-345.

Hansel C, Linden DJ & D'Angelo E. (2001). Beyond parallel fiber LTD: the diversity of synaptic and non-synaptic plasticity in the cerebellum. *Nat Neurosci* **4,** 467-475.

Hartmann MJ & Bower JM. (1998). Oscillatory activity in the cerebellar hemispheres of unrestrained rats. *J Neurophysiol* **80,** 1598-1604.

Hashimoto K & Kano M. (1998). Presynaptic origin of paired-pulse depression at climbing fibre-Purkinje cell synapses in the rat cerebellum. *J Physiol* **506,** 391-405.

Henze DA & Buzsaki G. (2001). Action potential threshold of hippocampal pyramidal cells in vivo is increased by recent spiking activity. *Neuroscience* **105,** 121-130.

Hisano S, Sawada K, Kawano M, Kanemoto M, Xiong G, Mogi K, Sakata-Haga H, Takeda J, Fukui Y & Nogami H. (2002). Expression of inorganic phosphate/vesicular glutamate transporters (BNPI/VGLUT1 and

DNPI/VGLUT2) in the cerebellum and precerebellar nuclei of the rat. *Brain Res Mol Brain Res* **107,** 23-31.

Hodgkin AL & Huxley AF. (1952). A quantitative description of membrane current and its application to conduction and excitation in nerve. *J Physiol* **117,** 500-544.

Holtzman T, Rajapaksa T, Mostofi A & Edgley SA. (2006). Different responses of rat cerebellar Purkinje cells and Golgi cells evoked by widespread convergent sensory inputs. *J Physiol* **574,** 491-507.

Hopfield JJ. (1995). Pattern recognition computation using action potential timing for stimulus representation. *Nature* **376,** 33-36.

Isaacson JS & Walmsley B. (1995). Counting quanta: direct measurements of transmitter release at a central synapse. *Neuron* **15,** 875-884.

Isope P, Dieudonne S & Barbour B. (2002). Temporal organization of activity in the cerebellar cortex: a manifesto for synchrony. *Ann N Y Acad Sci* **978,** 164-174.

Ito M. (2006). Cerebellar circuitry as a neuronal machine. *Prog Neurobiol* **78,** 272-303.

Ivry RB & Keele SW. (1989). Timing functions of the cerebellum. *Journal of Cognitive Neuroscience* **1,** 136-152.

Jack JJB, Noble D & Tsien RW. (1975). *Electric current flow in excitable cells.* Clarendon Press, Oxford.

Jaeger D & Bower JM. (1994). Prolonged responses in rat cerebellar Purkinje cells following activation of the granule cell layer: an intracellular in vitro and in vivo investigation. *Exp Brain Res* **100,** 200-214.

Jakab RI & Hámori J. (1988). Quantitative morphology and synaptology of cerebellar glomeruli in the rat. *Anatomy and Embryology* **179,** 81-88.

Johnston D & Wu SM-S. (1995). *Foundations of cellular neurophysiology.* MIT Press, Cambridge, MA.

Jonas P, Bischofberger J, Fricker D & Miles R. (2004). Interneuron Diversity series: Fast in, fast out--temporal and spatial signal processing in hippocampal interneurons. *Trends Neurosci* **27,** 30-40.

Jorntell H & Ekerot CF. (2002). Reciprocal bidirectional plasticity of parallel fiber receptive fields in cerebellar Purkinje cells and their afferent interneurons. *Neuron* **34,** 797-806.

Jorntell H & Ekerot CF. (2006). Properties of somatosensory synaptic integration in cerebellar granule cells in vivo. *J Neurosci* **26,** 11786-11797.

Karmarkar UR & Buonomano DV. (2007). Timing in the absence of clocks: encoding time in neural network states. *Neuron* **53,** 427-438.

Kenet T, Bibitchkov D, Tsodyks M, Grinvald A & Arieli A. (2003). Spontaneously emerging cortical representations of visual attributes. *Nature* **425,** 954-956.

Knusel P, Wyss R, Konig P & Verschure PF. (2004). Decoding a temporal population code. *Neural Comput* **16,** 2079-2100.

Kole MH, Letzkus JJ & Stuart GJ. (2007). Axon initial segment Kv1 channels control axonal action potential waveform and synaptic efficacy. *Neuron* **55,** 633-647.

Korpi ER & Sinkkonen ST. (2006). GABA(A) receptor subtypes as targets for neuropsychiatric drug development. *Pharmacol Ther* **109,** 12-32.

Laine J & Axelrad H. (2002). Extending the cerebellar Lugaro cell class. *Neuroscience* **115,** 363-374.

Larramendi LM & Lemkey-Johnston N. (1970). The distribution of recurrent Purkinje collateral synapses in the mouse cerebellar cortex: an electron microscopic study. *J Comp Neurol* **138,** 451-459.

Lawrence JJ & McBain CJ. (2003). Interneuron diversity series: containing the detonation--feedforward inhibition in the CA3 hippocampus. *Trends Neurosci* **26,** 631-640.

Lisberger SG & Fuchs AF. (1978). Role of primate flocculus during rapid behavioral modification of vestibuloocular reflex. I. Purkinje cell activity during visually guided horizontal smooth-pursuit eye movements and passive head rotation. *J Neurophysiol* **41,** 733-763.

Llano I, Marty A, Armstrong CM & Konnerth A. (1991). Synaptic- and agonist-induced excitatory currents of Purkinje cells in rat cerebellar slices. *J Physiol* **434,** 183-213.

Llinas R & Muhlethaler M. (1988). Electrophysiology of guinea-pig cerebellar nuclear cells in the in vitro brain stem-cerebellar preparation. *J Physiol* **404,** 241-258.

Llinas R & Yarom Y. (1986). Oscillatory properties of guinea-pig inferior olivary neurones and their pharmacological modulation: an in vitro study. *J Physiol* **376,** 163-182.

Losonczy A, Zhang L, Shigemoto R, Somogyi P & Nusser Z. (2002). Cell type dependence and variability in the short-term plasticity of EPSCs in identified mouse hippocampal interneurones. *J Physiol* **542,** 193-210.

Lytton WW & Sejnowski TJ. (1991). Simulations of cortical pyramidal neurons synchronized by inhibitory interneurons. *J Neurophysiol* **66,** 1059-1079.

Maex R & De Schutter E. (1998). Synchronization of Golgi and granule cell firing in a detailed network model of the cerebellar granule cell layer. *J Neurophysiol* **80,** 2521-2537.

Maffei A, Prestori F, Shibuki K, Rossi P, Taglietti V & D'Angelo E. (2003). NO enhances presynaptic currents during cerebellar mossy fiber-granule cell LTP. *J Neurophysiol* **90,** 2478-2483.

Mann EO & Paulsen O. (2007). Role of GABAergic inhibition in hippocampal network oscillations. *Trends Neurosci* **30,** 343-349.

Marr D. (1969). A theory of cerebellar cortex. *J Physiol* **202,** 437-470.

Marty A & Llano I. (2005). Excitatory effects of GABA in established brain networks. *Trends Neurosci* **28,** 284-289.

Medina JF & Mauk MD. (2000). Computer simulation of cerebellar information processing. *Nat Neurosci* **3,** 1205-1211.

Miles R. (1990). Synaptic excitation of inhibitory cells by single CA3 hippocampal pyramidal cells of the guinea-pig in vitro. *J Physiol* **428,** 61-77.

Misra C, Brickley SG, Farrant M & Cull-Candy SG. (2000). Identification of subunits contributing to synaptic and extrasynaptic NMDA receptors in Golgi cells of the rat cerebellum. *J Physiol* **524,** 147-162.

Mitchell SJ & Silver RA. (2000a). GABA Spillover from Single Inhibitory Axons Suppresses Low-Frequency Excitatory Transmission at the Cerebellar Glomerulus. *J Neurosci* **20,** 8651-8658.

Mitchell SJ & Silver RA. (2000b). Glutamate spillover suppresses inhibition by activating presynaptic mGluRs. *Nature* **404,** 498-502.

Mitchell SJ & Silver RA. (2003). Shunting inhibition modulates neuronal gain during synaptic excitation. *Neuron* **38,** 433-445.

Mittmann W, Koch U & Hausser M. (2005). Feed-forward inhibition shapes the spike output of cerebellar Purkinje cells. *J Physiol* **563,** 369-378.

Miyazaki T, Fukaya M, Shimizu H & Watanabe M. (2003). Subtype switching of vesicular glutamate transporters at parallel fibre-Purkinje cell synapses in developing mouse cerebellum. *Eur J Neurosci* **17,** 2563-2572.

Mody I & Pearce RA. (2004). Diversity of inhibitory neurotransmission through GABA(A) receptors. *Trends Neurosci* **27,** 569-575.

Mountcastle VB & Powell TP. (1959a). Central nervous mechanisms subserving position sense and kinesthesis. *Bull Johns Hopkins Hosp* **105,** 173-200.

Mountcastle VB & Powell TP. (1959b). Neural mechanisms subserving cutaneous sensibility, with special reference to the role of afferent inhibition in sensory perception and discrimination. *Bull Johns Hopkins Hosp* **105,** 201-232.

Mugnaini E & Floris A. (1994). The unipolar brush cell: a neglected neuron of the mammalian cerebellar cortex. *J Comp Neurology* **339,** 174-180.

Nicholls JG. (2001). *From neuron to brain.* Sinauer, Sunderland, Mass.

Nielsen TA, DiGregorio DA & Silver RA. (2004). Modulation of Glutamate Mobility Reveals the Mechanism Underlying Slow-Rising AMPAR EPSCs and the Diffusion Coefficient in the Synaptic Cleft. *Neuron* **42,** 757-771.

Nusser Z, Sieghart W & Somogyi P. (1998). Segregation of different GABAA receptors to synaptic and extrasynaptic membranes of cerebellar granule cells. *J Neurosci* **18,** 1693-1703.

O'Keefe J & Recce ML. (1993). Phase relationship between hippocampal place units and the EEG theta rhythm. *Hippocampus* **3,** 317-330.

Orlovsky GN. (1972). Activity of rubrospinal neurons during locomotion. *Brain Res* **46,** 99-112.

Palay SL & Chan-Palay V. (1974). *Cerebellar Cortex: Cortex and Organization.* Springer-Verlag, Germany.

Palkovits M, Magyar P & Szentagothai J. (1972). Quantitative histological analysis of the cerebellar cortex in the cat. IV. Mossy fiber-Purkinje cell numerical transfer. *Brain Res* **45,** 15-29.

Pellionisz A & Szentagothai J. (1973). Dynamic single unit simulation of a realistic cerebellar network model. *Brain Res* **49,** 83-99.

Petersen CC, Hahn TT, Mehta M, Grinvald A & Sakmann B. (2003). Interaction of sensory responses with spontaneous depolarization in layer 2/3 barrel cortex. *Proc Natl Acad Sci U S A* **100,** 13638-13643.

Pouille F & Scanziani M. (2001). Enforcement of temporal fidelity in pyramidal cells by somatic feed- forward inhibition. *Science* **293,** 1159-1163.

Pouille F & Scanziani M. (2004). Routing of spike series by dynamic circuits in the hippocampus. *Nature* **429,** 717-723.

Rancz EA, Ishikawa T, Duguid I, Chadderton P, Mahon S & Hausser M. (2007). High-fidelity transmission of sensory information by single cerebellar mossy fibre boutons. *Nature* **450,** 1245-1248.

Rieke F, Warland D, de Ruyter van Steveninck RR & Bialek W. (1997). *Spikes. Exploring the neural code*. The MIT Press, Cambridge, MA.

Rinzel J & Ermentrout B. (1998). Analysis of neural excitability and oscillations. In *Methods in neuronal modeling: from ions to networks*, 2nd edn, ed. Koch C & Segev I, pp. 251-291. MIT Press, Cambridge, MA.

Rosen I & Scheid P. (1972). Cerebellar surface cooling influencing evoked activity in cortex and in interpositus nucleus. *Brain Res* **45,** 580-584.

Rossi DJ, Alford S, Mugnaini E & Slater NT. (1995). Properties of transmission at a giant glutamatergic synapse in cerebellum: the mossy fiber-unipolar brush cell synapse. *J Neurophysiol* **74,** 24-42.

Rossi DJ & Hamann M. (1998). Spillover-mediated transmission at inhibitory synapses promoted by high affinity alpha6 subunit GABA(A) receptors and glomerular geometry. *Neuron* **20,** 783-795.

Rossi DJ, Hamann M & Attwell D. (2003). Multiple modes of GABAergic inhibition of rat cerebellar granule cells. *J Physiol* **548,** 97-110.

Salazar G, Craige B, Love R, Kalman D & Faundez V. (2005). Vglut1 and ZnT3 co-targeting mechanisms regulate vesicular zinc stores in PC12 cells. *J Cell Sci* **118,** 1911-1921.

Sargent PB, Saviane C, Nielsen TA, DiGregorio DA & Silver RA. (2005). Rapid vesicular release, quantal variability and spillover contribute to the precision and reliability of transmission at a glomerular synapse. *Journal of Neuroscience* **25,** 8173-8187.

Saviane C & Silver RA. (2006). Fast vesicle reloading and a large pool sustain high bandwidth transmission at a central synapse. *Nature* **439,** 983-987.

Schaefer AT, Angelo K, Spors H & Margrie TW. (2006). Neuronal oscillations enhance stimulus discrimination by ensuring action potential precision. *PLoS Biol* **4,** e163.

Scheuss V, Taschenberger H & Neher E. (2007). Kinetics of both synchronous and asynchronous quantal release during trains of action potential-evoked EPSCs at the rat calyx of Held. *J Physiol* **585,** 361-381.

Schiffmann SN, Cheron G, Lohof A, d'Alcantara P, Meyer M, Parmentier M & Schurmans S. (1999). Impaired motor coordination and Purkinje cell excitability in mice lacking calretinin. *Proc Natl Acad Sci U S A* **96,** 5257-5262.

Schneggenburger R, Sakaba T & Neher E. (2002). Vesicle pools and short-term synaptic depression: lessons from a large synapse. *Trends Neurosci* **25,** 206-212.

Shambes GM, Gibson JM & Welker W. (1978). Fractured somatotopy in granule cell tactile areas of rat cerebellar hemispheres revealed by micromapping. *Brain Behavior and Evolution* **15,** 94-140.

Silver RA. (2003). Estimation of nonuniform quantal parameters with multiple-probability fluctuation analysis: theory, application and limitations. *J Neurosci Methods* **130,** 127-141.

Silver RA, Colquhoun D, Cull-Candy SG & Edmonds B. (1996a). Deactivation and desensitization of non-NMDA receptors in patches and the time course of EPSCs in rat cerebellar granule cells. *J Physiol* **493,** 167-173.

Silver RA, Cull-Candy SG & Takahashi T. (1996b). Non-NMDA glutamate receptor occupancy and open probability at a rat cerebellar synapse with single and multiple release sites. *J Physiol* **494,** 231-250.

Silver RA, Momiyama A & Cull-Candy SG. (1998). Locus of frequency-dependent depression identified with multiple- probability fluctuation analysis at rat climbing fibre-Purkinje cell synapses. *J Physiol* **510,** 881-902.

Silver RA, Traynelis SF & Cull-Candy SG. (1992). Rapid-time-course miniature and evoked excitatory currents at cerebellar synapses in situ. *Nature* **355,** 163-166.

Simat M, Parpan F & Fritschy JM. (2007). Heterogeneity of glycinergic and gabaergic interneurons in the granule cell layer of mouse cerebellum. *J Comp Neurol* **500,** 71-83.

Somogyi P & Klausberger T. (2005). Defined types of cortical interneurone structure space and spike timing in the hippocampus. *J Physiol* **562,** 9-26.

Stell BM, Brickley SG, Tang CY, Farrant M & Mody I. (2003). Neuroactive steroids reduce neuronal excitability by selectively enhancing tonic inhibition mediated by delta subunit-containing GABAA receptors. *Proc Natl Acad Sci U S A* **100,** 14439-14444.

Steuber V, Mittmann W, Hoebeek FE, Silver RA, De Zeeuw CI, Hausser M & De Schutter E. (2007). Cerebellar LTD and Pattern Recognition by Purkinje Cells. *Neuron* **54,** 121-136.

Tamas G, Buhl EH, Lorincz A & Somogyi P. (2000). Proximally targeted GABAergic synapses and gap junctions synchronize cortical interneurons. *Nat Neurosci* **3,** 366-371.

Taschenberger H, Scheuss V & Neher E. (2005). Release kinetics, quantal parameters and their modulation during short-term depression at a developing synapse in the rat CNS. *J Physiol* **568,** 513-537.

Taschenberger H & von Gersdorff H. (2000). Fine-tuning an auditory synapse for speed and fidelity: developmental changes in presynaptic waveform, EPSC kinetics, and synaptic plasticity. *J Neurosci* **20,** 9162-9173.

Trussell LO. (1999). Synaptic mechanisms for coding timing in auditory neurons. *Annu Rev Physiol* **61,** 477-496.

Tsodyks M, Kenet T, Grinvald A & Arieli A. (1999). Linking spontaneous activity of single cortical neurons and the underlying functional architecture. *Science* **286,** 1943-1946.

Tyrrell T & Willshaw D. (1992). Cerebellar cortex: its simulation and the relevance of Marr's theory. *Philos Trans R Soc Lond B Biol Sci* **336,** 239-257.

Uhlhaas PJ & Singer W. (2006). Neural synchrony in brain disorders: relevance for cognitive dysfunctions and pathophysiology. *Neuron* **52,** 155-168.

Van Kan PLE, Gibson AR & Houk JC. (1993). Movement-related inputs to intermediate cerebellum of the monkey. *J Neurophysiol* **69,** 74-94.

Vida I, Bartos M & Jonas P. (2006). Shunting inhibition improves robustness of gamma oscillations in hippocampal interneuron networks by homogenizing firing rates. *Neuron* **49,** 107-117.

Vos BP, Maex R, Volny-Luraghi A & De Schutter E. (1999a). Parallel fibers synchronize spontaneous activity in cerebellar Golgi cells. *J Neurosci* **19,** RC6: 1-5.

Vos BP, Volny-Luraghi A & De Schutter E. (1999b). Cerebellar Golgi cells in the rat: receptive fields and timing of responses to facial stimulation. *Eur J Neurosci* **11,** 2621-2634.

Wada N, Kishimoto Y, Watanabe D, Kano M, Hirano T, Funabiki K & Nakanishi S. (2007). Conditioned eyeblink learning is formed and stored without cerebellar granule cell transmission. *Proc Natl Acad Sci U S A* **104,** 16690-16695.

Wall MJ & Usowicz MM. (1996). Postnatal development of spontaneous GABAergic transmission at the Golgi cell-granule cell synapse of rat cerebellum. *J Physiol* **494,** P83-P84.

Wall MJ & Usowicz MM. (1997). Development of action potential-dependent and independent spontaneous GABAA receptor-mediated currents in granule cells of postnatal rat cerebellum. *Eur J Neurosci* **9,** 533-548.

Walter JT, Alvina K, Womack MD, Chevez C & Khodakhah K. (2006). Decreases in the precision of Purkinje cell pacemaking cause cerebellar dysfunction and ataxia. *Nat Neurosci* **9,** 389-397.

Wang SS-H, Denk W & Häusser M. (2000). Coincidence detection in single spines mediated by calcium release. *Nat Neurosci* **3,** 1266-1273.

Watanabe D, Inokawa H, Hashimoto K, Suzuki N, Kano M, Shigemoto R, Hirano T, Toyama K, Kaneko S, Yokoi M, Moriyoshi K, Suzuki M, Kobayashi K, Nagatsu T, Kreitman RJ, Pastan I & Nakanishi S. (1998). Ablation of cerebellar Golgi cells disrupts synaptic integration involving GABA inhibition and NMDA receptor activation in motor coordination. *Cell* **95,** 17-27.

Woolston DC, La Londe JR & Gibson JM. (1982). Comparison of response properties of cerebellar and thalamic-projecting interpolaris neurons. *J Neurophysiol* **48,** 160-173.

Wu HS, Sugihara I & Shinoda Y. (1999). Projection patterns of single mossy fibers originating from the lateral reticular nucleus in the rat cerebellar cortex and nuclei. *J Comp Neurol* **411,** 97-118.

Wulff P, Goetz T, Leppa E, Linden AM, Renzi M, Swinny JD, Vekovischeva OY, Sieghart W, Somogyi P, Korpi ER, Farrant M & Wisden W. (2007). From synapse to behavior: rapid modulation of defined neuronal types with engineered GABAA receptors. *Nat Neurosci* **10,** 923-929.

Yamada K, Fukaya M, Shimizu H, Sakimura K & Watanabe M. (2001). NMDA receptor subunits GluRepsilon1, GluRepsilon3 and GluRzeta1 are enriched at the mossy fibre-granule cell synapse in the adult mouse cerebellum. *Eur J Neurosci* **13,** 2025-2036.

Yamazaki T & Tanaka S. (2007a). The cerebellum as a liquid state machine. *Neural Netw* **20,** 290-297.

Yamazaki T & Tanaka S. (2007b). A spiking network model for passage-of-time representation in the cerebellum. *Eur J Neurosci* **26,** 2279-2292.

Zhang Q, Pangrsic T, Kreft M, Krzan M, Li N, Sul JY, Halassa M, Van Bockstaele E, Zorec R & Haydon PG. (2004). Fusion-related release of glutamate from astrocytes. *J Biol Chem* **279,** 12724-12733.

Zhang S & Trussell LO. (1994). A characterization of excitatory postsynaptic potentials in the avian nucleus magnocellularis. *J Neurophysiol* **72,** 705-718.